MATHEMATICAL MODELING AND ANALYSIS OF COVID-19 AND TUBERCULOSIS COINFECTION WITH OPTIMAL CONTROL

Kassahun Getnet Mekonen

A Dissertation Submitted to the Department of Applied Mathematics,
School of Applied Natural Science

Presented in Partial Fulfillment of the Requirements for the Degree of Doctor of Philosophy
in Applied Mathematics

Office of Graduate Studies
Adama Science and Technology University

June, 2022
Adama, Ethiopia

MATHEMATICAL MODELING AND ANALYSIS OF COVID-19 AND TUBERCULOSIS COINFECTION WITH OPTIMAL CONTROL

Kassahun Getnet Mekonen

Main Supervisor: Dr. Legesse Lemecha
Co-Supervisor: Dr. Tatek Getachew

A Dissertation Submitted to the Department of Applied Mathematics,
School of Applied Natural Science

Presented in Partial Fulfillment of the Requirements for the Degree of Doctor of Philosophy in Applied Mathematics

Office of Graduate Studies
Adama Science and Technology University

June, 2022
Adama, Ethiopia

Declaration

I hereby declare that this dissertation entitled "**Mathematical Modeling and Analysis of COVID-19 and Tuberculosis Coinfection with Optimal Control**" is my original work. That is, it has not been submitted for the award of any academic degree, diploma or certificate in any other university. All sources of materials used for this dissertation have been duly acknowledged through appropriate citations.

Kassahun Getnet Mekonen	_____	_____
Name of Student	Signature	Date

Recommendation

We, the supervisors of this dissertation, hereby certify that we have read and revised the dissertation entitled **"Mathematical Modeling and Analysis of COVID-19 and Tuberculosis Coinfection with Optimal Control"** prepared under our guidance by **Kassahun Getnet Mekonen** submitted in partial fulfillment of the requirements for the degree of Doctor of Philosophy in Applied Mathematics. Therefore, we recommend the submission of the dissertation to the department for further review and defense.

Dr. Legesse Lemecha Obsu	_____	_____
Major Supervisor	Signature	Date
Dr. Tatek Getachew Habtemichael	_____	_____
Co-supervisor	Signature	Date

Approval Page

We hereby certify that the recommendations and suggestions made by the board of examiners are appropriately incorporated into the final version of the dissertation entitled "**Mathematical Modeling and Analysis of COVID-19 and Tuberculosis Coinfection with Optimal Control**" by **Kassahun Getnet Mekonen**.

Dr. Legesse Lemecha Obsu	_____	_____
Major Supervisor	Signature	Date
Dr. Tatek Getachew Habtemichael	_____	_____
Co-supervisor	Signature	Date

We, the undersigned, members of the Board of Examiners of the dissertation open defense by **Kassahun Getnet Mekonen** have read and evaluated the dissertation entitled "**Mathematical Modeling and Analysis of COVID-19 and Tuberculosis Coinfection with Optimal Control**" and examined the candidate during open defense. This is, therefore, to certify that the dissertation is accepted for partial fulfillment of the requirement of the degree of Doctor of Philosophy in Applied Mathematics.

Dr. Belay Mitiku Damtew	_____	_____
Chairperson	Signature	Date
Dr. Mitiku Daba Firdi	_____	_____
Internal Examiner 1	Signature	Date
Dr. Tamirat Temesgen Dufera	_____	_____
Internal Examiner 2	Signature	Date
Prof. Semu Mitiku Kassa	_____	_____
External Examiner 1	Signature	Date
Dr. Chernet Tuge Deressa	_____	_____
External Examiner 2	Signature	Date

Finally, approval and acceptance of the dissertation is contingent upon submission of its final copy to the Office of Postgraduate Studies (OPGS) through the candidate's Department Graduate Council (DGC) and School Graduate Committee (SGC).

_____	_____	_____
Department Head	Signature	Date
_____	_____	_____
School Dean	Signature	Date
_____	_____	_____
Office of Postgraduate Studies, Dean	Signature	Date

ACKNOWLEDGMENT

First, I want to thank the almighty God and his Gracious Mother St. Mary for caring for my life and blessing my activities in advance of the completion of my dissertation.

My special and heart full gratitude and appreciation goes to my supervisor Dr. Legesse Lemecha for his great assistance, contribution, useful suggestion, and constructive criticism on this excellent advising and limitless effort in encouraging me in my work, correcting and providing comments by devoting his time from the beginning to the end of this dissertation work. I must admit that without him, this work would have been difficult to complete. I greatly appreciate him not only for his keen and unlimited constructive advises in every aspect of my work, but also for his professional and personal ethic, that should be an icon for others. I would also like to express my greatest thanks to my co-supervisor Dr. Tatek Getachew for his unwavering support and advice during the dissertation work, which would be over appreciated. I was not be in this step without his help.

I am pleased to thank my former co-supervisor Dr. Shiferaw Feyissa. He assisted my work from the development of my proposal to the preparation of my papers with a great contribution of his knowledge. Unfortunately we lost him suddenly, let his soul rest in peace.

My thanks also go to Hawassa University for sponsoring me with financial support for all educational and research expenses and for giving me a chance to pursue this education program.

My grateful thanks are given to the Department of Applied Mathematics of Adama Science and Technology University, and the Department's post Graduate committee because of their committed support and immediate change of the supervisors after the passing away of my first co-supervisor. I would also like to thank my colleagues, friends, and all Applied Mathematics postgraduate students who have helped me in all ways and shared different ideas and comments to complete this dissertation.

Finally, special thanks go to my family who prays with me all the time, in all circumstances by providing my educational career and building up my life foundations for the best achievements. Lastly, but certainly not least, I offer my regards, friends and blessings to all those who supported me in one way or another during my studies at the time of this work.

TABLE OF CONTENTS

LIST OF TABLES

LIST OF FIGURES

Acronyms

BCG	.....	Bacille Calmette-Guerin
BRR	.....	Basic Reproduction Ratio
BSEIR	.....	BCG Vaccinated Susceptible-Exposed-Infected-Recovered
COVID-19	.....	Corona Virus Disease 2019
DFEP	.....	Disease Free Equilibrium Point
EEP	.....	Endemic Equilibrium Point
IVP	.....	Initial Value Problem
MCMC	.....	Markov Chain Monte Carlo
MERS-CoV	.....	Middle Eastern Respiratory Syndrome virus
MDR-TB	.....	Multidrug Resistant Tuberculosis
NGM	.....	Next Generation Matrix
OCP	.....	Optimal Control Problem
ODE	.....	Ordinary Differential Equations
PMP	.....	Pontryagin's Minimum Principle
RK4	.....	Rung Kutta Method of Order Four
SARS-CoV	.....	Severe Acute Respiratory Syndrome virus
SEIR	.....	Susceptible-Exposed-Infected-Recovered
SEIRDM	.....	Susceptible-Educated-Infected-Recovered-Death-Material
SEQIAHR	.....	Susceptible-Exposed-Quarantined-Infected-Asymptomatic -Hospitalized-Recovered
SIR	.....	Susceptible-Infected-Recovered
TB	.....	Tuberculosis
WHO	.....	World Health Organization

Abstract

Coronavirus disease (COVID-19) continues to claim the lives of many people globally and controlling the disease has become the most challenging part of the modern health care system. Tuberculosis (TB) is also a major global health threat affecting millions of people every year. Both are infectious diseases that transmit mainly through close contact, and both primarily attack the respiratory system with similar symptoms such as cough, fever, and difficulty breathing. In this dissertation, we studied the dynamics of COVID-19, and the coinfection of TB and COVID-19 to forecast the possible features and establish mitigation strategies for their spread. We developed an extended SIR type compartmental model for the COVID-19 pandemic and analyzed the model with analytical methods and numerical simulations. The biological meaningfulness of the model was proved and the stability analysis was performed by obtaining the basic reproduction number. The parameter values of the proposed model are estimated with a modified combination of the Bayesian and least square estimation technique. The sensitivity analysis of the model parameters has also been performed using the normalized forward analysis. We have then proposed a deterministic mathematical model to give insight into the coinfection of COVID-19 and TB. The coinfection model is qualitatively studied by proving the properties such as the existence, boundedness, and positivity of the solutions. In each sub-model, the disease-free equilibrium points are proved to be both locally and globally stable if the reproduction numbers are less than unity. We computed the basic reproduction number of the coinfection, and the disease-free equilibrium point was proved to be conditionally stable. The analytical findings reveal that an increase in infected individuals with TB has a positive impact on the spread of COVID-19 while under some conditions, an increase in the number of COVID-19 cases has a positive impact on the spread of TB disease. Furthermore, the coinfection model is extended into an optimal control problem by adding four control measures as the prevention effort against TB, prevention techniques against COVID-19, treatments for TB infections, and medical care for COVID-19 infection to optimally manage the diseases. The optimal control problem was analyzed with Pontryagin's Minimum Principle. Different simulation cases were performed to supplement the analytical results and to identify the most appropriate control intervention strategies. The simulation results show that the prevalence of the coinfection was reduced when all the four control measures were concurrently implemented.

Keywords: COVID-19, TB, Coinfection, Mathematical Modeling, Stability Analysis, Sensitivity Analysis, Bifurcation, Optimal Control, Pontryagin's Minimum Principle, Parameter Estimation, Numerical Simulation.

List of Publications

P1) Kassahun Getnet Mekonen, Tatek Getachew Habtemicheal, and Shiferaw Feyissa Balcha, "Modeling the effect of contaminated objects for the transmission dynamics of covid-19 pandemic with self protection behavior changes", Results in Applied Mathematics, 9:100134, 2021; https://doi.org/10.1016/j.rinam.2020.100134.

P2) Kassahun Getnet Mekonen, Shiferaw Feyissa Balcha, Legesse Lemecha Obsu, Abdulkadir Hassen, "Mathematical Modeling and Analysis of TB and COVID-19 Coinfection", Journal of Applied Mathematics, Vol. 2022, ID 2449710, 2022; https://doi.org/10.1155/2022/2449710.

P3) Kassahun Getnet Mekonen, Legesse Lemecha Obsu, Tatek Getachew Habtemichael, "Optimal control analysis for the co-dynamics of COVID-19 and TB", Arab Journal of Basic and Applied Sciences, 2022, Vol. 29, No. 1, 175–192; https://doi.org/10.1080/25765299.2022.2085445.

CHAPTER 1

INTRODUCTION

1.1 Background of the Study

The emergence and spread of infectious diseases with pandemic potential occurred in different times throughout history. Major pandemics and epidemics such as flue, cholera, tuberculosis, human immunodeficiency virus, Ebola, coronavirus e.t.c. have already afflicted humanity. Many of these infectious diseases were caused by zoonotic pathogens, water-borne pathogens, and vector-borne diseases that were transmitted to humans due to increased contacts for different activities. During epidemics, implementation of public health measures such as isolation, quarantine and border control helped to contain the spread of infectious diseases. Emerging technologies for rapid diagnostic testing, contact tracing, biomarkers of disease severity, and new platforms for the development and production of vaccines are effective responses during the occurrence of pandemics (Piret and Boivin, 2021).

The pandemic of coronavirus disease (COVID-19) continued claiming the lives of many people globally and controlling the disease has became the most challenging aspect of the modern health care system. Tuberculosis (TB) is also a major global health threat affecting millions of people every year. TB and COVID-19 are both infectious diseases transmitted mainly via close contact. They primarily attack the respiratory system and show matching symptoms such as cough, fever, and difficulty breathing (Organization, 2020c, 2021), but differ in incubation periods. The relationship between COVID-19 and TB is a public health concern and the coinfection of the two diseases exist when individuals are infected with both diseases simultaneously. We discuss the basic backgrounds of the two diseases and their impacts in the following subsections.

1.1.1 COVID-19

COVID-19 is a communicable respiratory disease caused by a strain of coronavirus that causes illness in humans. The outbreak of the virus was first reported by World Health Organization (WHO) as pneumonia of unknown cause on December 31, 2019, observed in Wuhan, China. However, on the 10^{th} of January 2020, the virus was determined to be a new family of novel coronavirus with the same category as the Severe Acute Respiratory Syndrome virus (SARS-CoV) and the Middle Eastern Respiratory Syndrome virus (MERS-CoV) that occurred respectively in Asia and Saudi Arabia (Li et al., 2020). The rapid expansion of the virus forced the WHO to declare it as a pandemic on March 11, 2020

(Organization, 2020b).

COVID-19 is a respiratory virus that transmits mainly through contacts of tiny aerosol particles of respiratory droplets generated from an infected person through coughing or sneezing (Organization, 2020a). Respiratory droplets of the virus can land on surfaces and objects. The COVID-19 virus may land and survive on surfaces for long periods under the right environmental conditions. Hence, it is possible that a person could get the virus by touching such landed surfaces or objects and contacting with their mouth, nose, or eyes with the contaminated hands (Organization, 2020a). Most infected people develop mild to moderate illness and recover without hospitalization, and others have serious symptoms (difficulty breathing or shortness of breath, chest pain or pressure, and loss of speech or movement) that may lead to death.

As of March 2022, there is no known curing medicine to combat the COVID-19 pandemic. Standard recommendations by the WHO to prevent the spread of COVID-19 include frequent cleaning of hands using soap or alcohol-based sanitizer, use face-mask, covering the nose and mouth with a flexed elbow or disposable tissue when coughing and sneezing, avoiding close contact with anyone that has a fever and cough, and vaccination of individuals when available (Organization, 2020a).

Coronavirus, so named because they look like halos (known as coronas) when viewed under the electron microscope, and the structures of the coronavirus are given in Figures 1.1 and 1.2. The virus that causes COVID-19, known as SARS-CoV-2 has changing constantly since the beginning of the pandemic. Certain variants of the virus have garnered widespread attention because of their rapid emergence within populations and evidence of transmission or clinical implications. Several prominent variants of concerns by WHO have been designated, including Alpha, Beta, Gamma, Delta, and Omicron. Omicron is more transmissible than the Delta variant, though it appears less severe than previous variants. The Delta variant caused a more severe disease than other variants, It's estimated that Delta caused more than twice as many infections as previous variants, it was estimated to have been 40 to 60% more transmissible than the Alpha variant, with a higher risk of hospitalization (Prevention and Control, 2021).

The first case of COVID-19 from Africa was reported on 14^{th} February 2020, which was reported from Egypt and later from other three African countries: South Africa, Morocco, and Algeria. The first two cases from Ethiopia were reported on 13 March 2020, two days after the WHO declared the disease as a pandemic (Mohammed et al., 2020). As of the WHO COVID-19 weekly situation report on 07 March 2022, above 11.57 million people were infected with the virus, and 251,191 have died in Africa. At the time of writing this dissertation, the WHO report of COVID-19 indicated that on 07 March 2022, more than 447.9 million people were infected with the virus, and over 6.02 million have died.

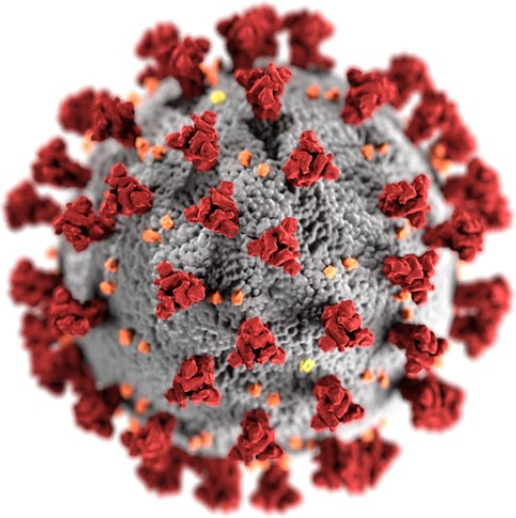

Figure 1.1: Illustration of the ultrastructure of the SARS-CoV-2 coronavirus (COVID-19). Source: https://www.cdc.gov/dotw/covid-19/index.html

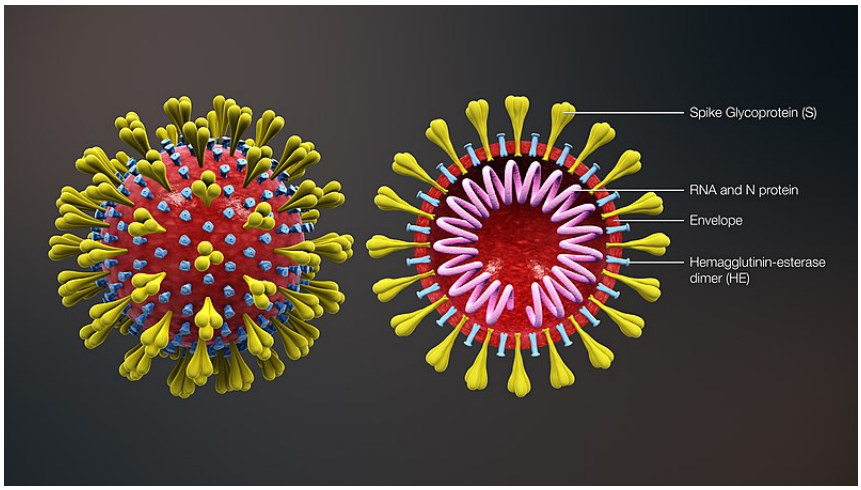

Figure 1.2: Diagram of coronavirus virion structure showing spikes. Source: https://commons.wikimedia.org/wiki/File:3D_medical_animation_corona_virus.jpg

1.1.2 Tuberculosis (TB)

Tuberculosis (TB) is potentially a serious infectious disease which is caused by *Mycobacterium tuberculosis*. It is a major cause of death from a single infectious agent, one of the top 10 causes of death worldwide, and the leading cause of death from a single infectious agent (Wang et al., 2021). The bacteria that cause TB usually spreads when an infected person coughs, sneezes, or any other forceful expiratory maneuver that shears respiratory secretions. It mostly affects the lungs but can also affect other organs such as bones, brain, kidneys, and glands (Awoke and Kassa, 2018). General symptoms of TB disease include unexplained weight loss, loss of appetite, night sweats, fever, fatigue, chills. WHO recommends the use of Bacille Calmette-Guerin (BCG) vaccination as a prevention act against the disease. In the case of TB infection, where the patient is infected with TB bacteria but not ill,

a short time TB preventive treatment can be given to stop the onset of disease (WHO, 2019).

About a quarter of the worldwide population is infected with *Mycobacterium tuberculosis* and thus at risk of developing TB disease. In some cases, TB infection can progress directly into active TB. However, in a large number of cases, TB infection initially enters a latent phase, in which the bacillus is made 'asleep' or inactive by the immune system of the infected individual. The development of TB infection into active TB is highly dependent on the immunity of the infected individual, which may progress to active TB if the infected individual experiences a decreased immunity. Globally, approximately 9.9 million people fell ill with TB and 1.5 million people died from TB in 2020 (Fund, 2021).

1.1.3 TB and COVID-19

Tuberculosis and COVID-19 are currently the main causes of death among infectious diseases. While experience on COVID-19 infection in TB patients remains limited, it is anticipated that people ill with both TB and COVID-19 may have poorer treatment outcomes. Coinfection of coronavirus and TB has a complex clinical entities such that the propagation of disease is faster in the coinfection compared to those of mono-infection. Other clinical reports have also shown that treatment of TB increase the risk of COVID-19 reactivation (Fatima and Zaman, 2020).

Some aspects of clinical evidence argue COVID-19 occurs in any time of TB occurrence before, during, or after an active TB detection (Visca et al., 2021), and studies described both latent and active TB are risk factors for COVID-19 infections (Chen et al., 2020). Patients with active or latent TB are more susceptible, and the symptom progression of the COVID-19 infection was more rapid and severe (Fund, 2021). Studies suggest that TB diseases are associated with COVID-19 outcomes, including an approximately two to three-fold increase in mortality and a 25% relative decrease in the possibility of recovery for COVID-19 coinfection with TB disease (Mcquaid et al., 2021). There was also concern on high mortality of about 12.3% in the cases with apparent coinfections, which is higher than that of COVID-19 alone (Khurana and Aggarwal, 2020; Tadolini et al., 2020).

1.1.4 Impacts of TB on COVID-19

People with TB are at higher risk of infection and deaths with COVID-19. Considering this, WHO recommended simultaneous testing for TB and COVID-19. TB is yet the most killer infectious diseases in sub-Saharan Africa, and the fact that COVID-19 and TB have some similarities in clinical features is a potential risk for misdiagnosing the two (Comella-del Barrio et al., 2021). The limited evidence on the TB-COVID-19 coinfection showed that having TB infection may contribute to developing severe forms of acute respiratory syndrome in patients co-infected with COVID-19.

1.1.5 Impacts of COVID-19 on TB

COVID-19 pandemic influenced many research activities as many scientists shifted their focus to COVID-19, including their laboratories. TB patients are not coming to health-care facilities for a fear of COVID-19, and on the other side, TB services are marginally delivered and some sites stopped their routine services (Beyne et al., 2021).

The impact of the COVID-19 pandemic on the fight against TB has been highly destructive worldwide. It affects the treatment and management of TB in many ways. For example, lock-downs and other measures introduced to slow transmission of COVID-19 have interrupted access to routine care and prevention services, thereby affecting the extent of case management such as testing and treatment (Cilloni et al., 2020; Beyne et al., 2021). In 2019 and 2020, the number of people treated for infected TB in countries where the invested Global Fund dropped by 19%, is decreased with that of 37% (Fund, 2021). While continued TB prevention and treatment initiatives is be vital to reducing pressure on public health during the COVID-19 pandemic, the presence of these two diseases could lead to a deadly coinfection cycle (Feldman and Anderson, 2021). In consequence, enhancing surveillance principles to investigate whether COVID-19 and TB are synergistic epidemics (syndemics), and determining the possible rates of coinfection could help to mitigate the potential impact of their coinfections (Fund, 2021).

In Ethiopia, the COVID-19 pandemic has reduced the routine TB diagnosis, care, and treatment significantly. TB cases detection rate has reduced considerably and directly observed therapy visits have been interrupted. After the first COVID case was identified in Ethiopia, there have been significant reductions in TB case detection. Some health facilities that have been providing TB care and treatment services have been committed as COVID-19 isolation and treatment centers. Human and material resources for TB have been shifted to COVID- 19, which also affected the TB case finding and care. To avoid interruption of TB care and minimize exposure of TB patients to COVID-19, a well organized intervention mechanism is needed (Mohammed et al., 2020).

1.1.6 Mathematical Modeling

A mathematical model is a description of a system using mathematical tools and equations. The process of developing mathematical models is called mathematical modeling. The modeling process typically begins with a description of the processes based on the scientist's understanding of the system. Mathematical models are developed to help explain a system, to study the effects of its various components, and to make predictions about their behavior. Epidemiology is the subject that studies the patterns of health and illness and associated factors at the population level. In our study, we focus on the mathematical epidemiology of the infectious diseases (COVID-19 and TB). An infectious disease is a clinically evident illness resulting from the presence of a pathogenic microbial agent. The microbial agent causing

the disease can be bacterial, viral, fungal, parasitic, or it can be toxic proteins, called prions.

Mathematical epidemiology is an emerging research area, where different types of models have been developed and studied to explore the disease dynamics and possible control measures. Modeling the transmission dynamics of diseases is a way to formulate what is known about the transmissions and explore all possible features of the disease with mathematical techniques. The dynamical model study is used to investigate the vital parameters, predict future trends, and evaluate control measures to provide decisive information for decision making. Mathematical models have become important tools in understanding and analyzing the spread and control of infectious diseases, which clarifies variables and parameters to obtain conceptual results such as basic reproduction numbers, and uses to control and understand the dynamics of such disease. The computer simulations of models are useful for determining sensitivities of parameter changes, and estimating key parameters from data which can contribute to identifying trends, make general forecasts, and estimate the future.

Understanding the viral dynamics and host response is essential in developing strategies for antiviral treatment, vaccination, and epidemiological control with COVID-19, and the coinfection of TB and COVID-19. On a wider scale, mathematical biologists have proposed mechanisms that can be used to control the spread of fatal infectious diseases and to ensure that limited resources allocated for this purpose are used as efficiently as possible.

In this dissertation, we have focused our study on a deterministic epidemic model with an optimal control mechanism. We have developed mathematical models in which the analysis from our models may assist decision-makers in identifying and estimating the risk and the potential future growth of the diseases in the population. For this, two mathematical models were developed to study the dynamics of COVID-19 and TB. The first model focuses on a mathematical study of the transmission dynamics of COVID-19 using a system of nonlinear ordinary differential equations by incorporating self protection behavior changes in the population considering the impact of the contaminated environment. The second model is developed to investigate the coinfection of TB and COVID-19, and to study their co-dynamics.

1.2 Statement of the Problem

The COVID-19 pandemic continues affecting millions and passing thousands of lives every day. Governments across the world designed a lot of strategic intervention measures such as immediate case identification, contact tracing, quarantine, isolation to eradicate the transmission of the novel coronavirus pandemic. TB is also a global disease that is the world's top killer among infectious diseases. Emerging evidence shows that patients with TB disease have an increased risk of the COVID-19 infection and susceptibility towards developing severe COVID-19 (Marimuthu et al., 2020). Despite this, it is vital to look for more scientific results that helps to mitigate the severity of the diseases. Therefore, it is interesting to model

and interpret the dynamics of COVID-19, and the coinfection of COVID-19 and TB mathematically with optimal control to reduce their prevalence and advice on strategic options for controlling of the diseases.

1.3 Objectives

1.3.1 General Objective

The general objective of this study is to develop a mathematical model and investigate the transmission dynamics of COVID-19, and the coinfection of COVID-19 and TB diseases with optimal control strategies.

1.3.2 Specific Objectives

The specific objectives of this study are to:

- develop and analyze a mathematical model for the transmission dynamics of COVID-19.
- estimate parameter values of the COVID-19 model using real data.
- formulate a mathematical model for TB-COVID-19 co-dynamics.
- analyze the COVID-19 and TB sub-models separately, as well as the coinfection model.
- develop a control induced model for the TB-COVID-19 coinfection model and determine optimal control strategies.

1.4 Significance of the Study

This study is motivated on the current problem of the spread of COVID-19 pandemic and tuberculosis disease. Epidemic mathematical models can provide decision support for planning interventions, and control practices to be imposed on the society. The analysis from mathematical models for TB and COVID-19 coinfection transmission dynamics could be used to predict the future spread of the disease. Our findings presented in this dissertation are significant to variety of stakeholders as follows:

i **To researchers:** It provide a platform for further research in the dynamics and co-dynamics of diseases like COVID-19, TB, HIV/AIDS, Malaria, Hepatitis, e.t.c.

ii **To policy makers:** provides a framework for designing control strategies of the diseases. Our analysis and interpretation of solutions of the models could help an insight

to medical administrators on focusing the possible intervention mechanisms for controlling the disease.

iii **To individuals:** Provide a chance of understanding the dynamics of COVID-19, and the co-dynamics of TB-COVID-19 coinfection, and how to prevent themselves against the diseases. Proposed models and results will also certainly improve the existing knowledge on the diseases dynamics and its implications in decreasing of the diseases.

1.5 Delimitation

This study is conducted for the analysis of a general mathematical model for the transmission dynamics of COVID-19, and co-dynamics of TB and COVID-19 diseases. Hence the theoretical analysis works for the problems without delimitation. For the numerical simulations in data fitting and parameter estimation parts, we use an Ethiopian COVID-19 data collected from different sources. When applying optimal control strategies on the mathematical model, we apply suitable control measures without being limited in a specified scope.

1.6 Organization of the Dissertation

This dissertation is organized as follows. In chapter 2, relevant and past related literature is briefly discussed. The methodologies used in conducting this dissertation is presented in Chapter 3. In chapter 4, a deterministic model is developed with a system of ordinary differential equations to study the dynamics of COVID-19 by applying self protection behavior changes in considering with impacts of contaminating objects. Stability analysis of the dynamics have been studied for the developed model. The parameters of the model are estimated using the experimental data collected from five countries. The obtained analytical results are assured by computing numerical simulations. Chapter 5 deals with a mathematical model for the coinfection of COVID-19 and tuberculosis. The detail analysis of the sub-models as well as the full coinfection model is studied, and the analytical findings of the deterministic model is supported by numerical results. In this chapter, we further extended the coinfection proposed model into an optimal control problem with the intervention of four control measures with the goal to minimize the number of infection with both diseases. The full analysis for the optimal control problem is presented in this chapter, and the numerical results by comparing the control interventions is discussed well. Finally, we end the dissertation with summary, conclusions and recommendations, as given in Chapter 6.

CHAPTER 2

LITERATURE REVIEW

Epidemiological and mathematical models play fundamental role in the study of the dynamics of diseases. The earliest account of mathematical modeling of the spread of a disease was carried out in 1766 by Daniel Bernoulli: he created a mathematical model to defend the practice of inoculating against smallpox, and showed that universal inoculation would increase the life expectancy from 26 to 29 years. The Kermack–McKendrick epidemic model (1927) and the Reed–Frost epidemic model (1928), both describe the relationship between susceptible, infected and immune individuals in a population. The special case of the model proposed by Kermack and McKendrick in 1927, which was the starting point for the study of epidemic models is given by (Kermack and McKendrick, 1927)

$$\begin{cases} \frac{dS}{dt} = -\beta SI, \\ \frac{dI}{dt} = \beta SI - \alpha I, \\ \frac{dR}{dt} = \alpha I. \end{cases} \tag{2.1}$$

The Kermack and McKendrick model (2.1) was a compartmental model based on relatively simple assumptions on the rates of flow between different classes and defined as follows. The transmission process between infectious and susceptible individuals is described in terms of incidence βSI. In this case, the incidence rate assumed that the transmission follows the law of mass action. Individuals are represented as interacting particles and from a random encounter between a susceptible and an infectious, the infection may be transmitted with a probability of β. The transfer from I to R is with a constant positive coefficient α (the recovery rate). The epidemiological meaning of $1/\alpha$ is the average residence time in I (average infectious period).

For the last three decades, various models have been developed and studied to investigate the transmission dynamics and treatment strategy of different infectious diseases by mathematicians. In this chapter, we review some of the mathematical models and extensions to optimal control problems for each of TB, COVID-19 and TB-COVID-19 coinfection diseases.

2.1 Reviews on Mathematical Modeling of the Diseases

The commonly used epidemic models in dynamics of COVID-19 and TB are the susceptible, infected, and recovered (SIR) model and susceptible, exposed, infected, and recovered (SEIR). Various mathematical models have been proposed for TB and COVID-19 disease dynamics by different researchers and here we review some of them.

2.1.1 Mathematical Modeling of COVID-19

Studies have adapted dynamic mathematical models to investigate the crucial epidemiological parameters, predict the trend, estimate the peak, and evaluate control measures, so as to provide critical information for decision making (Park et al., 2020). As epidemiological models play a fundamental role in the study of the dynamics of disease, numerous mathematical models have been used to investigate the transmission dynamics of COVID-19 (Cao et al., 2020; Jewell et al., 2020; Sameni, 2020; Peng et al., 2020; Giordano et al., 2020; Tuite et al., 2020; Obsu and Balcha, 2020; Mamo, 2020; Ega et al., 2020; Kifle and Obsu, 2022). The studies in (Ndii et al., 2020) described the effect of speeding the detection time of COVID-19 infected individuals and reducing the transmission rate using both deterministic and stochastic models. In (Hattaf et al., 2021), the authors developed a mathematical model to describe the dynamics of COVID-19 by taking into account all modes of transmission and prosocial awareness.

Peng et al. (2020) constructed an epidemic model for COVID-19 with media coverage and quarantine. The model allows for the susceptible to the unconscious and conscious susceptible compartment. They established with the mathematical analyses that the global dynamics of the spread of the COVID-19 infectious disease are completely determined by the basic reproduction number. The unknown parameters of model were estimated by the MCMC algorithm on the basis of the total confirmed new cases from February 1, 2020 to March 23, 2020 in the UK, and estimated that the basic reproduction number is 4.2816. Without the most restrictive measures, they forecasted that the COVID-19 pandemic will peak on June 2, 2020. In order to determine the key parameters of the model, sensitivity analysis were also explored and their results showed that reducing close contact is effective against the spread of the disease.

Kassa et al. (2020) formulated and analyzed a mathematical model for the transmission of COVID-19 disease. Bifurcation analysis of their model exhibits a backward bifurcation will occur at $R_0 = 1$ when recovered individuals do not develop a permanent immunity for the disease. In the absence of reinfection, it is proved that the model is without backward bifurcation and the disease free equilibrium is globally asymptotically stable for $R_0 < 1$. Various mitigation strategies were investigated using the proposed model and it was observed that the asymptomatic infectious group of individuals may play the major role in the re-emergence

of the disease in the future. They recommended that in the absence of vaccination, countries need to develop capacities to detect and isolate at least 30% of the asymptomatic infectious group of individuals while treating in isolation at least 50% of symptomatic patients to control the disease.

Silva et al. (2021) proposed a mathematical model for forecasting and anticipating the consequences of political decisions. With a deterministic mathematical model, described by a system of ordinary differential equations, they fitted the model with Portugal cases of COVID-19 data. After identification of the population readiness to follow social restrictions, they incorporated the effect in a version of the model that allow them to check different scenarios. Thy also applied an optimal control theory to maximize the number of people returning to normal life and minimizing the number of active infected individuals with minimal economical costs while warranting a low level of hospitalizations.

Kifle and Obsu (2022) formulated a nonlinear deterministic model for the transmission dynamics of COVID-19 and studied its dynamics. Local and global stability of the disease-free equilibrium point is proved by using the method of Castillo-Chavez and Song. Existence of the forward bifurcation using the center manifold theory, and global stability of the endemic equilibrium point is studied. The model parameters are estimated with the Ethiopian COVID-19 infected cases reported from March, 2020, to July, 2021 using the least square method. They computed the basic reproduction number and studied its sensitivity analysis to pick out the most influencing parameter. Their analysis suggest that the virus will be managed via minimizing the contact rate of infected individuals and increasing the quarantine of exposed individuals.

However, the extent of immunity, the transmission rate of people with no or minimal symptoms and varied contact rates during rapidly changing intervention and control measures remain uncertain, which could have limited the model's ability to predict the future of the COVID-19 pandemic (Holmdahl and Buckee, 2020; Siegenfeld et al., 2020).

2.1.2 Mathematical Modeling of TB

Mathematical models for TB are largely studied in (Trauer et al., 2014; Egonmwan and Okuonghae, 2019; Ullah et al., 2020; Ucakan et al., 2021).

Trauer et al. (2014) formulated a ten compartment mathematical model to simulate tuberculosis (TB) transmission in a highly endemic regions of the Asia-Pacific. Their deterministic model captures many of the observed phenomena important to disease dynamics, including partial and temporary vaccine efficacy, declining risk of active disease following infection, the possibility of reinfection both during the infection latent period and after treatment, multidrug resistant TB (MDR-TB) and de novo (initial) resistance during treatment. They found that the rate of detection and treatment was the most important determinant of disease dynamics with each respective strain, while vaccination rates were less important.

Egonmwan and Okuonghae (2019) also formulated a mathematical model to investigate the impact of diagnosis and treatment of both latent TB infections and active cases on the transmission dynamics of the disease. Mathematical analysis reveal that the model undergoes the phenomenon of backward bifurcation where a stable disease-free equilibrium coexist with a stable endemic equilibrium when the associated reproduction number is less than unity. It was further shown that a special case of the model has a unique endemic equilibrium point, which is globally asymptotically stable when the associated reproduction number exceeds unity. Sensitivity analysis of their model showed that the top three parameters that have the most influence on its reproduction number are the transmission rate, the fraction of fast disease progression and the rate of detection of active TB cases. Numerical simulations suggested that, with availability of treatment for both latent and active TB cases, increasing the fraction of latent TB cases that were diagnosed and treated (even with a small fraction of active TB cases promptly receiving treatment) will result in a reduction of the TB burden in the population.

Ullah et al. (2020) studies a deterministic epidemic model for TB by investigating the impact of effective contact rate, treatment rate, and incomplete treatment versus efficient treatment. They also analyze the asymptotic behavior, spread, and possible eradication of the TB infection characterized by the basic reproduction number. It is obtained that incomplete treatment of TB causes increase in disease infection while efficient treatment results in a reduction in TB. Some numerical simulations are performed and the results indicate that decrease in the effective contact rate and increase in the treatment rate play a significant role in the control of TB infection.

Ucakan et al. (2021) studies the dynamics of TB to determine how much it will affect the future and the impact of vaccine therapy on the disease. For this purpose, three mathematical models (SIR, SEIR and BSEIR) in the literature are considered. The model parameters are obtained with TB reported data in of Turkey from 2005 to 2015 by using the least square method. The obtained results revealed that the basic reproduction ratio for all three models is less than 1. Moreover, the stability analysis of the models and sensitivity analysis of the model parameters are presented and discussed. Finally, the accuracy of results for all three models is compared and the effect of the vaccination rate is discussed.

2.1.3 Reviews on Mathematical Modeling of the Coinfection

The coinfection of various diseases is studied in mathematical literature's. For instance, the co-dynamics of TB and HIV/AIDS is studied in (Awoke and Kassa, 2018; Silva and Torres, 2014), Hepatitis E and HIV (Alzahrani and Khan, 2020), Cholera-schistosomiasis coinfection in (Okosun et al., 2019), pneumonia and meningitis (Tilahun, 2019), Pneumonia and Typhoid fever (Tilahun et al., 2018), HIV-visceral leishmaniasis (VL) (Melese and Alemneh, 2021), measles and dysentery diarrhea in (Berhe et al., 2019).

On the contrary, the study on coinfection of COVID-19 and other diseases are at its infant stage and related mathematical literature is scant. For instance, COVID-19 and malaria coinfection are discussed in (Attiq et al., 2021; Tchoumi et al., 2021), COVID-19 with co-morbidity (diabetes) (Omame et al., 2021b, 2022b), COVID-19 and cholera in (Hezam et al., 2021), HIV and COVID-19 in (Ahmed et al., 2021; Omame et al., 2022a). Omame et al. (2021b) developed a model for COVID-19 and co-morbidity coinfection with optimal control. They showed that COVID-19 re-infection and modification parameter for susceptibility of co-morbid individuals induced the phenomenon of backward bifurcation in the model. Simulations of the model revealed that the strategy that prevents COVID-19 infection by co-morbid susceptibles is the most cost-effective of all the control strategies for the prevention of COVID-19. The authors in (Tchoumi et al., 2021) considered a coinfection model for COVID-19 and Malaria with optimal control. They showed that applying both COVID-19 and malaria protective strategies could help reduce their spread in comparison to applying each preventive measures singly. Furthermore, in a related research, the authors in (Hezam et al., 2021) showed that the policy of providing resources for the distribution of chlorine water tablets, sufficient equipments for testing with adequate compliance on social distancing rules as well as quarantining infected individuals has significant impact in reducing COVID-19 and cholera coinfections in Yemen.

Tuberculosis and COVID-19 are among the diseases with major global public health concern and great socio-economic impacts. Coinfection of the diseases is inevitable due to their spatial overlap, a potential double blow as their clinical similarities could hamper strategies to mitigate their spread and transmission dynamics. Some mathematical models for the coinfection of TB and COVID-19 are described, and optimal control strategies to decrease the risk from the dynamics of the coinfection are also studied. The mathematical perspective study of TB and COVID-19 coinfection is at an infant stage and these few studies can be found in (Fatima and Zaman, 2020; Marimuthu et al., 2020; Omame et al., 2021a).

The studies in (Marimuthu et al., 2020) attempted to estimate the number of TB patients infected with SARS-CoV-2 and have severe disease during the COVID-19 epidemic in Delhi, India. The SEIR model was used to estimate the number of COVID-19 cases, and R_0 was estimated for two scenarios, without any intervention and with public health interventions. Their study showed that the peak of COVID-19 and TB co-infected patients would occur on the 94^{th} day in the absence of public health interventions and on the 138^{th} day with interventions.

Fatima and Zaman (2020) proposed an epidemic model to represents the Middle East respiratory syndrome coronavirus (MERS-CoV) and TB coinfection. They first obtained the basic reproductive number and analyzed the stability of the model. The stability conditions are obtained in term of the basic reproductive number. They also studied the bifurcation analysis of the model, using the central manifold theory. Sensitivity of the basic reproductive number was performed to understand the most sensitive parameters. The study concluded

that the primary prevention measures would be emphasized especially for the TB patients and TB treatment centers need to be arranged for early diagnosis of COVID-19 in TB patients.

Omame et al. (2021a) proposed a fractional order mathematical model for the coinfection of COVID-19 and TB. The result of their study reveals that reducing the risk of COVID-19 infection particularly with latent TB infected individuals significantly halter the co-dynamics in the population. The model was simulated using the cumulative confirmed COVID-19 cases for New Delhi from March 2021 to June 2021, COVID-19 and TB contact rates and some other important parameters of the model are estimated. Simulations of their model revealed that reducing the risk of COVID-19 infection by latently-infected TB individuals will not only bring down the burden of COVID-19, but will also reduce the coinfection of both diseases in the population. Lowering COVID-19 and TB contact rates as well as increasing COVID-19 treatment rate are established for the elimination of both diseases from the population.

2.2 Reviews on Optimal Control Analysis of the Diseases

Optimal control problem for the mathematical models of infectious disease has a successful method in indicating ways to decrease the spread of the diseases by developing optimal intervention strategies (Sharomi and Malik, 2017). The method is applied to suggest the most effective mitigation strategies to minimize the number of individuals who become infected while efficiently balancing for prevention, and treatment applied to the models with various cost scenarios (Gaff and Schaefer, 2009; Obsu and Balcha, 2020). Optimal control can be of help to test and compare different strategies of mitigating a certain disease. The usefulness of optimal control theory in epidemiology is nowadays well recognized (Biswas et al., 2014; Ledzewicz and Schättler, 2011; Lenhart and Workman, 2007), and have been applied to many epidemic models. In this sub-section, we review some of the optimal control analysis of disease applied to COVID-19, TB and their coinfection.

2.2.1 Optimal Control Analysis for COVID-19

The problem of optimal control for the transmission of disease dynamics are studied and applied for COVID-19 models in (Obsu and Balcha, 2020; Silva et al., 2021; Deressa and Duressa, 2021; Grigorieva et al., 2021; Nana-Kyere et al., 2022a; Treesatayapun, 2022; Asamoah et al., 2022; Nana-Kyere et al., 2022b) using different intervention measures. Some of the measures for reducing the spread of COVID-19 includes keeping physical distancing, vaccination, keeping rooms well ventilated, wearing face masks, and handwashing with soap (Organization et al., 2020; Organization, 2020a; Obsu and Balcha, 2020). To suppress the epidemics caused by COVID-19, three effective strategies listing vaccination, quarantine and medical treatments, are employed under suitable policies. Quarantine motions may affect

the economic systems and pharmaceutical medications may be recently in the developing phase. Thus, vaccination seems the best hope of the current situation to control COVID-19 epidemics (Treesatayapun, 2022).

Obsu and Balcha (2020) applied optimal control theory to a COVID-19 transmission model given by a system of non-linear ordinary differential equations. The optimal control strategies were obtained by minimizing the number of exposed and infected population considering the cost of implementation. The existence of optimal controls and characterization was established using Pontryagin's Minimum Principle. An expression for the basic reproduction number was derived in terms of control variables, and the sensitivity of basic reproduction number with model parameters was analysed. The findings of their study showed that comprehensive impacts of prevention, intensive medical care and surface disinfection strategies outperform in reducing the disease epidemic with optimum implementation cost.

Tsay et al. (2020) introduced an optimization-based decision-making framework for managing the COVID-19 outbreak in the US, by modeling the dynamics of affected populations, estimating the model parameters and hidden states from data, and an optimal control strategy for sequencing social distancing and testing events such that the number of infections is minimized. The analysis of their computational efforts reveals that social distancing and quarantining are most effective when implemented early, with quarantining of confirmed infected subjects having a much higher impact. Further, they found that on-off policies alternating between strict social distancing and relaxing such restrictions can be effective at flattening the curve while likely minimizing social and economic cost.

Deressa and Duressa (2021) developed a mathematical model to estimate transmission dynamics of COVID-19 for the case of Ethiopia. The parameter values are estimated and the basic reproduction number is obtained as $R_0 = 1.51$. Their optimal control analysis also showed that, a combination of optimal preventive strategies such as public health education, personal protective measures and treatment of hospitalized cases are effective to significantly decrease the number of COVID-19 cases.

Asamoah et al. (2022) formulated a deterministic model to study the control of COVID-19 to unravel the cost and economic health outcomes. An optimal control problem is proposed by capturing four control functions as; practicing physical distancing protocols, practicing personal hygiene, practicing proper and safety measures by exposed, asymptomatic and symptomatic infected individuals, and fumigating schools, sports, commercial, and religious centers. Comparing the control strategies, they noticed that practicing physical protocols is the most cost-saving and most effective control intervention in the absence of vaccination.

Nana-Kyere et al. (2022a) studies a COVID-19 SEQIAHR compartmental model to provide insight into the dynamics of the disease by underlying tailored strategies designed to minimize the pandemic. They first studied the non-control model dynamic behaviors by examining the equilibrium points with their stability analysis, and the parameter sensitiv-

ity analysis of its basic reproduction number. Extension of the compartmental model to an optimal control problem is studied by implementing two time-dependent controls: personal protection and vaccination of the susceptible individuals. The combined effect of the strategies had a significant impact on the disease by emphatically minimizing the exposed, symptomatic, and asymptomatic infectious individuals.

2.2.2 Optimal Control Analysis for TB

Optimal control strategies on the dynamic of TB is applied in (Hattaf et al., 2009; Liu et al., 2017; Gao and Huang, 2018; Shi et al., 2020). Implementations used to mitigate the spread of TB includes Bacille Calmette-Guérin (BCG) vaccination, infection control with personal protection measures, and contact tracing (Visca et al., 2021).

The application of optimal control for the system of ordinary differential equations which describe the dynamics of a tuberculosis disease with exogenous reinfection were done in (Hattaf et al., 2009). Seeking to reduce the infectious group by reducing the contact between infectious and exposed individuals, they used control measures to represent the prevention of exogenous reinfection. They applied the Pontryagin's maximum principle to characterize the optimal control and the optimality system was derived and solved numerically.

Yang et al. (2016) formulated a mathematical model to explore the impact of vaccination and treatment on the transmission dynamics of tuberculosis (TB). They included a control term and evaluate the cost of control strategies, and then performed an optimal control analysis by Pontryagin's maximum principle. Their numerical simulations suggested that the maximum vaccination strategy should be enforced regardless of its efficacy.

Liu et al. (2017) studied a mathematical model of TB transmission considering BCG vaccination compartment to investigate the transmission dynamics. Based on data reported by the National Bureau of Statistics of China, they estimated the basic reproduction number approximately as $R_0 = 1.1892$. Theoretical analysis indicates that the infectious population asymptotically tends to zero with the new vaccination strategy which is the combination of constant vaccination and pulse vaccination. The new strategy can make the best of current constant vaccination, and the periodic routine health examination provides an operable environment for implementing pulse vaccination in China. Numerical simulations are provided to illustrate the theoretical results and help to design the final mixed vaccination strategy, they obtain control of TB is quicker to achieve with the mixed vaccination.

Gao and Huang (2018) extended the spread of tuberculosis model on effects of vaccination and treatment given in (Liu and Zhang, 2011) by incorporating three control terms and applying optimal control theory to the resulting model. They considered the control terms as constant vaccination of the susceptible individuals, successful treatment of TB latent individuals and treatment of the infected class. The optimal control strategies were proposed to minimize both the disease burden and the intervention cost. They proved the existence

and uniqueness of optimal control paths and obtain these optimal paths analytically using Pontryagin's Maximum Principle. The results were analyzed numerically to compare various strategies of proposed controls, and they observed the implementation of three controls is most effective and less expensive among all the strategies.

Shi et al. (2020) construct a fractional-order mathematical model with control to describe the transmission of tuberculosis. Two cases are considered: the constant control and the optimal control. In the former case, the stability conditions of the disease-free equilibrium and the endemic equilibrium are obtained. In the second case, optimal control theory is applied to the corresponding model. The optimal control formula is derived by use of the Hamiltonian function and the Pontryagin's Maximum Principle. In addition, some numerical simulations are performed to support their analytic results.

Despite the above few literature's on mathematical model of TB and COVID-19 transmission dynamics, there are lack of sufficient studies done for the coinfection of the two diseases. To the best of our knowledge, mathematical models considering the coinfection of TB and COVID-19 are rare and they prompt us for further investigation.

In this work, we propose a deterministic model for the dynamics of COVID-19, and the co-dynamics of TB and COVID-19. The qualitative analysis of the proposed models have been studied and the COVID-19 model parameters are estimated using real data. We then apply an optimal control analysis to the TB and COVID-19 coinfection model and study optimal strategies for the minimization of individuals co-infected with TB and COVID-19, taking into account the costs associated to the proposed control measures. We had also estimated the parameter values of the model. So, our work had indicated the strategies for the public health policymakers to control the disease. It will also serve as a groundsheet for conducting researches related to this problems.

CHAPTER 3

MATERIALS AND RESEARCH METHODOLOGY

In this chapter, we present the methods and materials that are used to attain the general and specific objectives of this dissertation. For this, we briefly discuss the approach of study and mathematical procedures, methods of parameter estimations, and the source of data with analysis.

3.1 Formulation of Mathematical Models

We developed a SEIR-type mathematical model for the transmission dynamics of COVID-19, and the co-dynamics of TB and COVID-19 in a population. Indeed, we formulated two mathematical models; the first is to examine the dynamics of COVID-19, and the second is to study the co-dynamics of TB and COVID-19. The model is formulated based on stratifying the total human population at time t, denoted by N(t), into the mutually-exclusive compartments. In both models, we consider some basic assumptions.

For the dynamics of COVID-19, we subdivide the human population into five compartments; named Susceptible (S), Educated (E), Infected (I), Recovered (R), Died with the virus (D); and one compartment, which is the contaminated material or surface (M).

For the co-dynamics of TB and COVID-19, we subdivide the total human population into eight mutually-exclusive compartments, namely susceptible individuals (S), TB-latent infected individuals who have no symptoms of TB disease and are not infectious (L_T), TB-infected individuals who have active TB disease and are infectious (I_T), COVID-19 infected individuals with no symptoms but are infectious (E_C), COVID-19 infected individuals with symptoms and under treatment for the infection (I_C), TB-latent individuals co-infected with COVID-19 (L_{TC}), COVID-19 infected individuals co-infected with active TB disease (I_{TC}), Recovered individuals from both TB and COVID-19 (R).

3.2 Description of Mathematical Procedures

To achieve the objectives of this study, we first developed the model by defining the problem. We then studied both the qualitative analysis and numerical simulations of the models. In analytical methods, we showed the well-posedness of the models in a biologically feasible domain. We then performed the qualitative analysis of the models equilibrium points based on the basic reproduction numbers. The local and global stabilities are analyzed using

stability theory. The sensitivity analysis of the model parameters is investigated to determine and identify the key factors for the spread of disease dynamics. We used the normalized forward sensitivity analysis to identify the most sensitive parameters. We extended the TB and COVID-19 coinfection model into an optimal control problem to examine possible control strategies for decreasing the prevalence of diseases.

To supplement the analytical solution of the proposed mathematical models, we performed numerical simulations using MATLAB software. The numerical solutions of mathematical models with the initial conditions of the state system without control are solved with a fourth-order rung kutta method. The optimality system in the model with control is solved using the forward-backward sweep numerical method.

3.3 Source of Data

The data required for the analysis of this study were obtained from secondary sources of information. A secondary source of information is collected from online and published documents. That is, the source of information used in this study are online data centers, books, journals and related studies from the internet.

For the COVID-19 mathematical model, the online COVID-19 data were collected from WHO situation reports, Johns Hopkins University data center, and worldometers COVID-19 information for five countries such as Ethiopia, China, Brazil, South Africa, and Italy. The data are collected as the number of hospitalized persons who are actively infected, recovered and died with COVID-19 infections on a daily basis time-scale.

To estimate the parameter values of the coinfection mathematical model, we use an Ethiopian data collected on online sources. The COVID-19 data was obtained from the Johns Hopkins University data center (J.H.University, 2022) in a monthly time basis. While, the TB data are obtained from the stop TB partnership online source on a yearly time basis (Stop-TB-Partnership, 2020).

3.4 Method of Data Analysis

The data are collected in a sequence of data points that measure the same variable at different points in time. As the ability to make predictions about the future has immense value, we fed our data into the dynamical model and estimated the parameter values. The parameter values obtained are used in the numerical simulations of the models. The simulation is used to find critical patterns, and to make predictions on how the dynamical state variables of interest may fluctuate in the future. The numerical simulation is conducted using MATLAB software and the results are displayed in the form of figures.

3.5 Parameter Estimation Methods

To get better predictions and to design and analyze various intervention strategies, we should estimate the model parameters from existing epidemiological data. Various methods such as least square, maximum likelihood, Bayesian methods have been previously investigated for handling this problem. Simulations of a model with real data involves the process of creating and analyzing substantial changes in the model parameters to get an optimal agreement between simulations and data.

We estimate and calculate the model parameters from observed data with a modified Bayesian approach combined with least square techniques. In the least square estimator, first the dynamical system is simulated using initial guesses for parameters. Then, model predictions are compared with measured data and the optimization algorithm updates the parameters. Using the initialized parameters in their parameter space, the Bayesian technique proposes the next parameter value by sampling from the proposal density. In the proposal density, we assign $\phi_i^{prop} = \phi_i \ \pm \ U[\phi_i - c_1, \phi_i + c_1]$, where c_1 is a tuning value, which is a small number and helps to move the parameter ϕ_i up and down through the parameter estimation process.

CHAPTER 4

MODELING THE IMPACT OF CONTAMINATED OBJECTS FOR THE DYNAMICS OF COVID-19 WITH BEHAVIOR CHANGE

In this chapter, a mathematical model for the transmission dynamics of Coronavirus diseases (COVID-19) is proposed using a system of nonlinear ordinary differential equations by incorporating self protection behavior changes in combination with the effect of indirect transmission. The disease free equilibrium point is computed, and both the local and global stability analysis is performed. The basic reproduction number(R_0) of the model is computed using the method of next generation matrix. Based on the available data, the unknown model parameters are estimated using a combination of least square and Bayesian estimation methods for different countries. The forward sensitivity index is applied to determine and identify the key model parameters for the spread of disease dynamics.

4.1 Introduction:

The COVID-19 virus may survive on surfaces for long periods with the right environmental conditions (Organization, 2020a). As a result, COVID-19 infection can spread from such contaminated surfaces to uninfected humans. Individuals are infected by contacting surfaces contaminated with the virus and touching their eyes, nose and mouth. We develop a SEIRDM mathematical model in combination with the effect of indirect transmission due to contaminated objects in the environment for the spread of COVID-19 dynamics. The analysis from mathematical models may assist decision-makers to estimate the risk and the potential future growth of the disease, to formulate strategies for antiviral treatment, vaccination, and epidemiological control of COVID-19 (Chen et al., 2020).

Behavior change towards using preventive mechanisms by the population to protect themselves from an infectious disease is assumed to be dependent on the way that the disease is transmitted and its fatality (Kassa and Ouhinou, 2011). Individuals who have awareness about the disease and decided to use preventive mechanisms have less susceptibility than those without awareness and demonstrating the usual risky behavior (Kassa et al., 2020; Berge et al., 2018). We study the populations awareness by introducing a behavior change function in the proposed model.

4.2 Model Formulation

The model subdivides the human population into five disjoint compartments; Susceptible, Educated, Infected, Recovered, Died; and one compartment, which is the contaminated material or surface. We consider the following basic assumptions to formulate the model.

1. The transmission dynamics of COVID-19 is assumed similar with the SIR model.
2. We consider the contribution of the awareness of individuals about the virus in the transmission dynamics of the disease.
3. We add the death compartment for which individuals die via the virus.
4. The effect of indirect transmission through virus concentration in the environment due to shedding by infectious is considered.
5. We apply behavior change towards self-protective measures by the population to protect themselves from the virus.
6. We assumed that each of the rates are constant (transmission, recovery, death, etc rates)

We then proposed a mathematical model and analyze the effect of these factors to investigate in terms of their contribution to preventing the spread of disease.

The model state variables and parameters with their meanings are given in Table 4.1 and Table 4.2 respectively.

Table 4.1: The subdivided compartments and their description of our model

Symbol	Biological Description of the State Variables
S	Susceptible individuals
E	Educated or was aware individuals to apply self protection mechanisms
I	Individuals infected with COVID-19
R	Recovered individuals
D	Individuals who died of COVID-19
M	COVID-19 infected environment (pathogens concentration in the environment)

The total population at time t, denoted by $N(t)$, is given by

$$N(t) = S(t) + E(t) + I(t) + R(t) + D(t).$$

The flow diagram of the model is illustrated in Figure 4.1. In the flow diagram, the dashed lines represent the potential shedding of the virus to the environment by infected individuals with COVID-19, and possible infection of the susceptible individuals from the contaminated environment at a rate dependent on the force of infection.

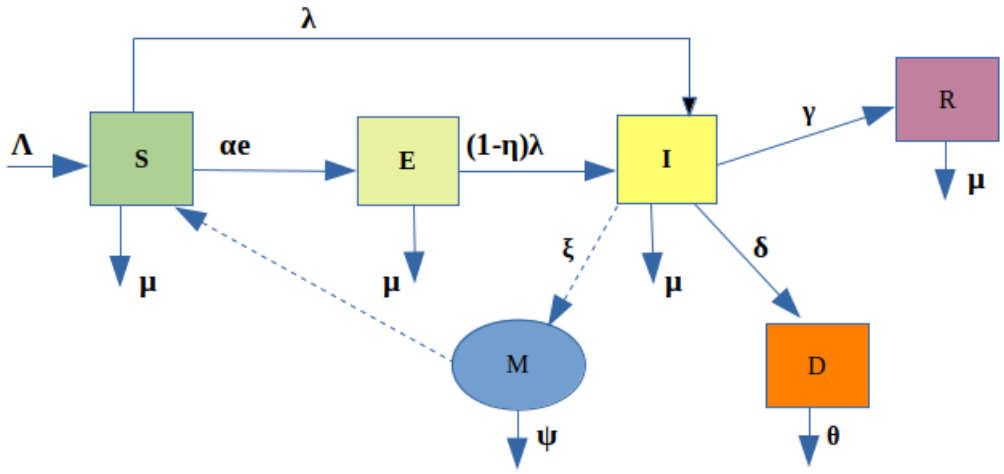

Figure 4.1: The flow diagram for the proposed model of COVID-19 pandemic

Based on our assumptions and the flow diagram, it results in systems of the following non-linear differential equations:

$$\begin{cases} \frac{dS}{dt} = \Lambda - (\lambda + \alpha e + \mu)S, \\ \frac{dE}{dt} = \alpha eS - (\mu + (1-\eta)\lambda)E, \\ \frac{dI}{dt} = \lambda S + (1-\eta)\lambda E - (\mu + \delta + \gamma)I, \\ \frac{dR}{dt} = \gamma I - \mu R, \\ \frac{dD}{dt} = \delta I - \theta D, \\ \frac{dM}{dt} = \xi I - \psi M \end{cases} \tag{4.1}$$

with non negative initial conditions $S(0) > 0$, $E(0) \geq 0$, $I(0) \geq 0$, $R(0) \geq 0$, $D(0) \geq 0$ and $M(0) \geq 0$.

In the model, the force of infection $\lambda = \lambda(I,M)$, and the behavior change function $e = e(\lambda)$ are state dependent parameters, and they depend on the states I, and M. All other parameters are constant numbers throughout our study, which do not depend on the states. We estimated the values of all the parameters using available data in section 4.4 by Matlab. The model in Equation (4.1) looks decoupled, but as the parameter (the force of infection) λ depends on I and M, λ couples the two subsystems. Through lambda, the state M influences the epidemic evolution.

4.2.1 Model Description

The susceptible population is increased by the recruitment of individuals at a rate Λ. All human individuals suffer from natural death at a constant rate of μ. Susceptible individuals can acquire COVID-19 infection directly from human to human interaction and indirectly from the environment to human interaction. The incidence is after direct contact with indi-

Table 4.2: Description of the model parameters

Parameter	Biological Description of the parameter
Λ	Rate of recruitment to the susceptible individuals
α	Rate of dissemination of information about the disease in the population
β_1	Rate of disease transmission directly from humans
β_2	Rate of disease transmission from the environment
λ	Force of infection (It is the probability of acquiring infection from an infected individual)
λ_0	Threshold value of the force of infection for a population to start reacting swiftly
K	the pathogen concentration in the environment that yields 50% of chance for a susceptible individual to catch the viral infection from the environment
e	Behavior change function
η	The average effectiveness of existing self-preventive measures
γ	Rate of recovery of the individuals from virus in the infected class
δ	Death rate due to the virus
μ	Natural death rate of the individuals
ψ	Decay rate of the virus from the environment
θ	The burial rate of people that died from COVID-19
ξ	Shedding rate of the virus from the infected class to the environment

viduals from the infected class (I) and contaminated environment M at the rates β_1 and β_2. The force of infection λ and the behavior change function e are given respectively by:

$$\lambda = \frac{\beta_1 I}{N} + \frac{\beta_2 M}{M+K} \quad \text{and} \quad e = \frac{\lambda^n}{\lambda_0^n + \lambda^n},$$

where β_1 is the rate of virus transmission directly from humans, β_2 is the rate of virus transmission from the environment, K is the pathogen concentration in the environment that yields a 50% chance for a susceptible individual to catch the viral infection from the surface, λ_0 is the value of the force of infection corresponding to the threshold infectivity in which individuals start reacting swiftly (the point at which the behavior change function changes its concavity), and n is a Hill coefficient that portrays the rate of reaction by the population (Kassa and Ouhinou, 2011).

At the beginning of an outbreak, individuals understand very little about the virus; there could be no reaction, and this can be related to the situation at the disease-free equilibrium such that $e(\lambda) = e(0) = 0$. However, as the risk of the disease increases, individuals start to think about the type of measures they take to avoid all means of contracting the disease. These protection measures, if perfect, account for an increase in the values of e to unity. The order n of the function $e(\lambda)$ is a Hill coefficient that portrays the rate of reaction by the population (Kassa and Ouhinou, 2011).

The rate of dissemination of information α describes the awareness of individuals from the disease. Individuals acquire information through multiple ways, such as TV news, re-

ports on a network, mouth-to-mouth communication, or even education. The information individuals gathered is an essential factor that impacts how individuals react to disease transmission and individuals make behavior changes to keep themselves from infection based on the information available to them during the pandemic (Zhao et al., 2015).

Individuals in the aware class becomes infected at a rate $(1-\eta)\lambda$ with the average effectiveness of existing self-preventive measures $\eta \leq 1$. Individuals with the symptoms of COVID-19 disease dies due to the virus-induced death at a rate δ. The infected individuals also become recover at a rate of γ. We assume that the recovered individuals R acquire a permanent immunity. A COVID-19 virus released from the infected individual through coughing or sneezing landed on materials or surfaces, and become infected at a rate ξ (Kassa et al., 2020; Berge et al., 2018). The virus decays from the infected surfaces with the decay rate of ψ.

4.3 Analysis of the Model.

In this section, we have seen the qualitative analysis of the model Equation (4.1) by examining the equilibrium points and its stability analysis.

4.3.1 Well-Posedness

Let us begin understanding the dynamics of a model by investigating the behavior of its steady states. We first show that the model is well posed in a biologically feasible domain, and then proceed with stability analysis of the equilibrium points of the model.

Theorem 4.3.1. *1. There exists a unique solution to the system of equations (4.1) in the region*
$\mathscr{D} = \{(S,E,I,R,D,M) \in \mathbb{R}^6_+\}$.

2. *If all of the initial conditions are positive, then all the solutions are positive for $t \geq 0$.*

3. *The solution trajectories of the model equations (4.1) evolve in a positive invariant region*

$$\Omega = \{(S,E,I,R,D) \in \mathbb{R}^5_+ : 0 \leq S+E+I+R+D \leq \frac{\Lambda}{\mu}, 0 \leq M \leq \frac{(\varepsilon+\xi)\Lambda}{\mu\psi}\}.$$

Proof. The Well-Posedness of the Model is proved as follow:

1. All the functions on the right hand side of equation (4.1) are C^1 on $\mathbb{R}^6$. Thus, by the Picard–Lindelöf theorem (Schroers, 2011), equations (4.1) has a unique solution.

2. The positivity of model state variables are proved based on proposition A.1 in (Thieme, 2018). Let the model equations (4.1) be written in the form $x' = F(x,t)$, where

$x = (S,E,I,R,D,M)$, and $F = (f_1,f_2,f_3,f_4,f_5,f_6) = \left(\frac{dS}{dt}, \frac{dE}{dt}, \frac{dI}{dt}, \frac{dR}{dt}, \frac{dD}{dt}, \frac{dM}{dt}\right)'$. The functions $f_j(x,t)$ on the right hand side of equations (4.1) have the property of $f_j(S,E,I,R,D,M,t) \geq 0$ whenever $x \in [0,\infty)^n$, $x_j = 0$, $t \geq 0$, and for all $j = 1,2,\ldots,5$. Here our x_j's are $x_1 = S$, $x_2 = E$, $x_3 = I$, $x_4 = R$, $x_5 = D$ and $x_6 = M$. By Theorem 4.3.1 (1), there exists a unique solution for the model equations (4.1). Thus, it follows from the Proposition that $x(t) \in [0,\infty)^n$ for all $t \geq t_0 \geq 0$ whenever $x(t_0) \geq 0$.

3. The change of total population $N(t) = S(t) + E(t) + I(t) + R(t) + D(t)$ at time t is governed by $N'(t) = S'(t) + E'(t) + I'(t) + R'(t) + D'(t)$. That is:

$$\frac{dN}{dt} = \Lambda - \mu(S+E+I+R) - \theta D \leq \Lambda - \mu N.$$

The solution for this linear first order ode is $N(t) \leq N(0)e^{-\mu t} + \frac{\Lambda}{\mu}(1-e^{-\mu t})$. Thus, if $0 \leq N(0) \leq \frac{\Lambda}{\mu}$ is the initial data, we obtain

$$0 \leq N(t) \leq \frac{\Lambda}{\mu}.$$

Moreover, for the environmental variable M, we have

$$\frac{dM}{dt} = \xi I - \psi M \leq \xi \frac{\Lambda}{\mu} - \psi M.$$

As $I(t)$ is less than $\frac{\Lambda}{\mu}$. Using the same procedure or by applying the Gronwall inequality, for $0 \leq M(0) \leq \frac{\xi\Lambda}{\mu\psi}$, we obtain:

$$0 \leq M(t) \leq \frac{\xi\Lambda}{\mu\psi}.$$

If x_0 is a point in $\mathscr{D}$, then the solution of the initial value problem (4.1), exists for all times $t \geq 0$ by Theorem 4.3.1 (1). By the result of Theorem 4.3.1 (2), the solution lies in $\mathscr{D}$, for all $t \geq 0$. Hence the region Ω is positive invariant, and we analyzed the model quantitative behaviors in Ω.

□

4.3.2 Local Stability of Disease-Free Equilibrium.

The equilibrium solutions of the model are obtained by setting the right-hand side of equation (4.1) equal to zero:

$$\begin{cases} \Lambda - (\lambda + \alpha e + \mu)S = 0, \\ \alpha eS - (\mu + (1-\eta)\lambda)E = 0, \\ \lambda S + (1-\eta)\lambda E - (\mu + \delta + \gamma)I = 0, \\ \gamma I - \mu R = 0, \\ \delta I - \theta D = 0, \\ \xi I - \psi M = 0. \end{cases} \tag{4.2}$$

The disease-free equilibrium point of our model is obtained by setting the disease state variable $I = 0$. If $I = 0$, then $R = 0$, $D = 0$ and $M = 0$. Then after the value of $\lambda = 0$ which leads to $E = 0$. It is then denoted and given by:

$$\varepsilon_0 = \left(\frac{\Lambda}{\mu}, 0, 0, 0, 0, 0\right).$$

Now let us calculate the basic reproduction number, which is denoted by R_0, and defined as the average number of secondary infections produced by a single infected individual in a completely susceptible population. Using the next generation matrix method (by linearizing the infected sub-system) (Driessche and Watmough, 2002), we calculate the basic reproduction number as follows. From the model equation (4.1), using the notation $X = (I, M)$, we have the vector functions:

$$\mathscr{F}(x) = \begin{bmatrix} \lambda S + (1-\eta)\lambda E \\ 0 \end{bmatrix} \quad \text{and} \quad \mathscr{V}(x) = \begin{bmatrix} (\mu + \delta + \gamma)I \\ \psi M - \xi I \end{bmatrix},$$

representing the appearance of new infections, and the transfer of individuals in to and out of the infected compartments, respectively. The Jacobian matrices of $\mathscr{F}(x)$ and $\mathscr{V}(x)$ are, respectively

$$F = D\mathscr{F}(\varepsilon_0) = \begin{bmatrix} \beta_1 & \frac{\beta_2 \Lambda}{\mu K} \\ 0 & 0 \end{bmatrix} \quad \text{and} \quad V = D\mathscr{V}(\varepsilon_0) = \begin{bmatrix} p_1 & 0 \\ -\xi & \psi \end{bmatrix},$$

where $p_1 = \mu + \delta + \gamma$ and the entries of F and V are obtained by $\left[\frac{\partial \mathscr{F}_i(\varepsilon_0)}{\partial x_j}\right]$ and $\left[\frac{\partial \mathscr{V}_i(\varepsilon_0)}{\partial x_j}\right]$ respectively. It is easy to calculate the inverse of V and given by

$$V^{-1} = \begin{bmatrix} \frac{1}{p_1} & 0 \\ \frac{\xi}{p_1 \psi} & \frac{1}{\psi} \end{bmatrix}.$$

The next-generation matrix FV^{-1} is

$$FV^{-1} = \begin{bmatrix} \frac{\beta_1}{p_1} + \frac{\beta_2 \Lambda \xi}{K\mu\psi p_1} & \frac{\beta_2 \Lambda}{\mu\psi K} \\ 0 & 0 \end{bmatrix}$$

and its eigenvalues are $\lambda_1 = \frac{\beta_1}{p_1} + \frac{\beta_2 \Lambda \xi}{K\mu\psi p_1}$ and $\lambda_2 = 0$. The spectral radius (the largest eigen value) of the next generation matrix is the basic reproduction number of the model. Hence we have the following result.

Theorem 4.3.2. *The basic reproduction number of the model equation (4.1) is given by*

$$R_0 = \frac{\beta_1}{p_1} + \frac{\beta_2 \Lambda \xi}{K\mu\psi p_1}.$$

Remark 4.3.1. *In general, if $R_0 > 1$, then on average, the number of new infections resulting from one infected individual is greater than one. Thus, COVID-19 infections will persist in the populations. If $R_0 < 1$, then on average, the number of new infections generated by one infected individual is less than one. This implies that the infections will eventually disappear from the populations. This threshold can as well be used to depict parameters that are most important during the infection.*

The local stability analysis of the equilibrium point is analyzed using linearization. For $n = 1$, the expression αe is simplified as $\alpha e = \alpha \frac{B_1}{B_2}$, where,

$$B_1 = \beta_1 I(K+M) + \beta_2 MN, \text{ and}$$
$$B_2 = \lambda_0 N(K+M) + \beta_1 I(K+M) + \beta_2 MN.$$

The Jacobean matrix of the model equation (4.1) is

$$J(S,E,I,R,D,M) = \begin{pmatrix} A_1 & A_2 & A_3 & -(\frac{\beta_1 SI}{N^2} + \alpha S\frac{C_4}{B_2^2}) & -(\frac{\beta_1 SI}{N^2} + \alpha S\frac{C_4}{B_2^2}) & A_4 \\ A_5 & A_6 & A_7 & \alpha S\frac{C_4}{B_2^2} + (1-\eta)\frac{\beta_1 EI}{N^2} & \alpha S\frac{C_4}{B_2^2} + (1-\eta)\frac{\beta_1 EI}{N^2} & A_8 \\ A_9 & A_{10} & A_{11} & \frac{\beta_1 SI}{N^2} - (1-\eta)\frac{\beta_1 EI}{N^2} & \frac{\beta_1 SI}{N^2} - (1-\eta)\frac{\beta_1 EI}{N^2} & A_{12} \\ 0 & 0 & \gamma & -\mu & 0 & 0 \\ 0 & 0 & \delta & 0 & -\theta & 0 \\ 0 & 0 & \xi & 0 & 0 & -\psi \end{pmatrix} \tag{4.3}$$

where,

$$
\begin{aligned}
A_1 &= -\left[\left(\frac{\beta_1 I(E+I+R+D)}{N^2}+\frac{\beta_2 M}{K+M}\right)+C_0+\alpha S\frac{C_1}{B_2^2}+\mu\right],\\
A_2 &= -\left[\frac{\beta_1 SI}{N^2}+\alpha S\frac{C_4}{B_2^2}\right],\\
A_3 &= -\left[\frac{\beta_1 S(S+E+R+D)}{N^2}+\alpha S\frac{C_2}{B_2^2}\right],\\
A_4 &= -\left[\frac{\beta_2 SK}{(K+M)^2}+\alpha S\frac{C_3}{B_2^2}\right],\\
A_5 &= \left[C_0+\alpha S\frac{C_1}{B_2^2}+(1-\eta)\left(\frac{\beta_1 EI}{N^2}\right)\right],\\
A_6 &= \alpha S\frac{C_4}{B_2^2}-(1-\eta)\left(\frac{(\beta_1 I(N-E)}{N^2}+\frac{\beta_2 M}{K+M}\right)-\mu,\\
A_7 &= \left[\alpha S\frac{C_2}{B_2^2}-(1-\eta)\frac{\beta_1 E(N-I)}{N^2}\right],\\
A_8 &= \left[\alpha S\frac{C_3}{B_2^2}-\frac{(1-\eta)\beta_2 EK}{(K+M)^2}\right],\\
A_9 &= \frac{\beta_1 I(E+I+R+D)}{N^2}+\frac{\beta_2 M}{K+M}-(1-\eta)\left(\frac{\beta_1 EI}{N^2}\right),\\
A_{10} &= \frac{-\beta_1 SI}{N^2}+(1-\eta)\left(\frac{\beta_1 I(N-E)}{N^2}+\frac{\beta_2 M}{K+M}\right)\\
A_{11} &= \left[\frac{\beta_1 S(S+E+R+D)}{N^2}+(1-\eta)\frac{\beta_1 E(N-I)}{N^2}-(\mu+\delta+\gamma)\right], \text{and}\\
A_{12} &= \left[\frac{\beta_2 SK}{(K+M)^2}+(1-\eta)\frac{\beta_2 EK}{(K+M)^2}\right].
\end{aligned}
$$

Here

$$
\begin{aligned}
C_0 &= \alpha\frac{B_1}{B_2}=\alpha e,\\
C_1 &= \beta_2 MB_2-(\lambda_0(K+M)+\beta_2 M)B_1,\\
C_2 &= (\beta_1(K+M)+\beta_2 M)B_2-((\lambda_0+\beta_1)(K+M)+\beta_2 M)B_1,\\
C_3 &= (\beta_1 I+\beta_2 N)B_2-(\beta_1 I+\beta_2 N+\lambda_0 N)B_1,\\
C_4 &= \beta_2 MB_2-(\lambda_0(K+M)+\beta_2 M)B_1.
\end{aligned}
$$

Theorem 4.3.3. *The disease-free equilibrium point ε_0 is locally asymptotically stable if $R_0 < 1$ and unstable if $R_0 > 1$.*

Proof. The locally asymptotical stability of ε_0 is analyzed using the sign of the eigenvalues of a Jacobian matrix at the disease-free equilibrium point ε_0. Substituting the equilibrium point ε_0 with $N_0 = \frac{\Lambda}{\mu}$ (at the disease-free equilibrium, the total population N is equal to the

total susceptible S population) in the matrix equation (4.3), we have:

$$J(\varepsilon_0) = \begin{pmatrix} -\mu & 0 & -\beta_1\left(1+\frac{\alpha}{\lambda_0}\right) & 0 & 0 & -\frac{\beta_2}{K}\left(\frac{\Lambda}{\mu}+\frac{\alpha}{\lambda_0}\right) \\ 0 & -\mu & \frac{\alpha\beta_1}{\lambda_0} & 0 & 0 & \frac{\alpha\beta_2}{K\lambda_0} \\ 0 & 0 & \beta_1 - p_1 & 0 & 0 & \frac{\beta_2\Lambda}{K\mu} \\ 0 & 0 & \gamma & -\mu & 0 & 0 \\ 0 & 0 & \delta & 0 & -\theta & 0 \\ 0 & 0 & \xi & 0 & 0 & -\psi \end{pmatrix}$$

By expanding the characteristic equation $|\lambda I - J(\varepsilon_0)| = 0$ with the first, second, fourth and fifth columns, we obtain four eigenvalues $\lambda_{1,2,3} = -\mu$, and $\lambda_4 = -\theta$. We calculate the remaining two eigenvalues from the reduced matrix

$$J_2 = \begin{pmatrix} \beta_1 - p_1 & \frac{\beta_2\Lambda}{K\mu} \\ \xi & -\psi \end{pmatrix}$$

Using the sign of trace and determinant of J_2, we can determine the sign of its eigenvalues. The trace of J_2 is $trace = \beta_1 - p_1 - \psi$, and its determinant is $det = \psi(p_1 - \beta_1) - \frac{\xi\beta_2\Lambda}{k\mu}$. $trace < 0$, if $\beta_1 < p_1 + \psi$, and $det > 0$, if $\psi p_1 > \psi\beta_1 + \frac{\xi\beta_2\Lambda}{k\mu}$. Simplification of the determinant inequality gives $det(J_2) > 0$, if $\frac{\beta_1}{p_1} + \frac{\beta_2\xi\Lambda}{\mu k\psi p_1} = R_0 < 1$. The trace less than zero condition $\beta_1 < p_1 + \psi$, that is $\frac{\beta_1}{p_1+\psi} < 1$ is satisfied for $R_0 < 1$ as $\frac{\beta_1}{p_1+\psi} < \frac{\beta_1}{p_1} < \frac{\beta_1}{p_1} + \frac{\beta_2\xi\Lambda}{\mu k\psi p_1}$. Hence, the disease-free equilibrium point ε_0 is stable if $R_0 < 1$, and unstable for $R_0 > 1$. □

4.3.3 Global Stability of Disease-Free Equilibrium.

Let us rewrite our model system (4.1) as

$$\begin{cases} \frac{dX}{dt} = F(X,Z) \\ \frac{dZ}{dt} = G(X,Z), \quad G(X,0) = 0. \end{cases} \tag{4.4}$$

where $X = (S,E,R,D)$ and $Z = (I,M)$, with the components of $X \in \mathbb{R}^4_+$ denoting the number of uninfected individuals and $Z \in \mathbb{R}^2_+$ denoting the number of infected ones. The disease-free equilibrium is denoted now as

$$U_0 = (X_0, 0), \quad \text{where,} \quad X_0 = (\frac{\Lambda}{\mu}, 0, 0, 0).$$

The conditions (H_1) and (H_2) below must be met to guarantee global asymptotic stability (Castillo-Chavez et al., 2002):
(H_1) For $\frac{dX}{dt} = F(X,0)$, U_0 is globally asymptotically stable;
(H_2) $G(X,Z) = AZ - \hat{G}(X,Z)$, $\hat{G}(X,Z) \geq 0$ for $(X,Z) \in \Omega$, where $A = D_Z G(U_0,0)$ is a

Metzler matrix (the off diagonal elements of A are non-negative) and Ω is the region where the model makes biological sense.

Theorem 4.3.4. *The disease-free equilibrium point $U_0 = (X_0, 0)$ is a globally asymptotically stable equilibrium point of (4.1) if $R_0 < 1$ and the assumptions (H_1) and (H_2) are satisfied.*

Proof. We have

$$\frac{dX}{dt} = F(X,Z) = \begin{bmatrix} \Lambda - (\lambda + \alpha e + \mu)S \\ \alpha eS - (\mu + (1-\eta)\lambda)E, \\ \gamma I - \mu R \\ \delta I - \theta D \end{bmatrix} \quad F(X,0) = \begin{bmatrix} \Lambda - \mu S \\ -\mu E \\ 0 \\ 0 \end{bmatrix}$$

$$\frac{dZ}{dt} = G(X,Z) = \begin{bmatrix} \lambda S + (1-\eta)\lambda E - (\mu + \delta + \gamma)I \\ \xi I - \psi M \end{bmatrix}.$$

Therefore,

$$A = D_Z G(U_0, 0) = \begin{bmatrix} \beta_1 - p_1 & \frac{\beta_2 \Lambda}{K\mu} \\ \xi & -\psi \end{bmatrix} \text{ which is a Metzler Matrix.}$$

Here $\hat{G}(X,Z) = AZ - G(X,Z)$, and so,

$$\hat{G}(X,Z) = \begin{bmatrix} \hat{G}_1(X,Z) \\ \hat{G}_2(X,Z) \end{bmatrix} = \begin{bmatrix} \frac{\alpha}{\lambda_0}\left(\beta_1 I + \frac{\beta_2 \Lambda M}{\mu K}\right) + \alpha eS + (1-\eta)\lambda E \\ \beta_1(E + \nu I) + \frac{\beta_2 \Lambda}{K\mu} M - \lambda(S + (1-\eta)E) \end{bmatrix}.$$

Since $N \leq \frac{\Lambda}{\mu}$ and $(1-\eta) \leq 1$,

$$\hat{G_2} = \beta_1 I + \frac{\beta_2 \Lambda}{K\mu} M - \lambda(S + (1-\eta)E) \geq \beta_1(E + \nu I) + N\frac{\beta_2}{K} M - \lambda(S + E + I + R + D).$$

Taking N as a common factor, implying

$$\hat{G_2} \geq N\left(\frac{\beta_1 I}{N} + \frac{\beta_2}{K} M - \lambda\right) \geq 0.$$

It follows that $\hat{G}_1(X,Z) \geq 0$, and $\hat{G}_2(X,Z) \geq 0$. Thus, $\hat{G} \geq 0$. Conditions (H_1) and (H_2) are satisfied, and we conclude that U_0 is globally asymptotically stable for $R_0 < 1$. □

4.4 Parameter Estimation and Numerical Simulations.

In this section, we discuss and estimate the parameter choices and the numerical solutions of the model equations (4.1). We outline the initial conditions and fit the existing WHO data with the model for that choice of parameters.

4.4.1 Parameter Estimation

The systems of model equations (4.1) can be expressed as a dynamical system of the form:

$$\frac{dX}{dt} = F(t, X, \Phi), \qquad X(0) = X_0,$$

where t is the independent variable (time), X is the state vector of the system, $\frac{dX}{dt} = [\frac{dx_1}{dt}, ..., \frac{dx_{N'}}{dt}]^T$, $X = [x_1, \ldots, x_{N'}]$, $F = [f_1, ..., f_{N'}]$ and N' is the number of compartments in the population. $\Phi = [\phi_1, \ldots, \phi_p]$ are p unknown parameters of the system and X_0 are the initial values.

In order to estimate the unknown parameters Φ, the state variable $X(t)$ is observed at l time instants $t_1, \ldots, t_l$, so that we have

$$Y(t_i) = X(t_i) + E_i, \qquad i = 1, \ldots, l,$$

where $Y(t_i)$ is the observed values of the state variables at time instant t_i and $\{E_i\}_{i=1}^{l}$ are the difference between the observed value y_i and the corresponding fitted value x_i i.e., $E_i = y_i - x_i$. The objective is to determine appropriate parameter values so that the sum of squared errors between the outputs of the estimated model $(X(t))$ and the measured data $(Y(t))$ should be minimized.

We wish to find the vector of least-square estimators, Φ, that minimizes

$$\sum_{i=1}^{l} E_i^2 = \sum_{i=1}^{l} (y_i - x_i)^2. \tag{4.5}$$

To find the values of parameters Φ that minimizes Equation (4.5), we use a type of Bayesian technique combined with least square estimation to estimate the unknown parameters.

In this parameter estimation procedure, the acceptance and rejection procedure in the Metropolis-Hastings (MH) algorithm is replaced by comparing the minimum of the sum squared errors between the proposed parameter and the previously assigned parameter. $\Phi = [\phi_1, ..., \phi_p]$ is a vector of parameters, where, p is the number of parameters to be estimated. In our case, the number of parameters is $p = 12$.

To do so, first we have to initialize the parameters in their parameter space and propose the next parameter value by sampling from the proposal density. The proposal density we assign $\phi_i^{prop} = \phi_i \ \pm \ U[\phi_i - c_1, \phi_i + c_1]$, where c_1 is tuning value which is a small number and help us to move the parameter ϕ_i up and down through the parameter estimation process. A rough outline of the algorithm is given in Algorithm (1). Convergence analysis of the parameter estimation is assessed by line plots of separate parameters.

Algorithm 1 MH algorithm with Least square
Input: L (number of iteration), ϕ_i^0 (initial value for parameters) , Y (Observed data)

Step 1. for $k = 0, 1, \ldots, L$.

Step 2. Solve ode's for equation (4.1) at ϕ_i^k and compute the sum of squared errors for equation (4.5), where i is the number of parameters to be estimated.

Step 3. Select new parameter $\phi_i^{prop} \sim q(\phi_i^{prop}|\phi_i^k)$.

Step 4. Solve Ode's at ϕ_i^{prop} and Compute equation (4.5)

Step 5. if the sum of squared errors in Step 4 is less than in Step 2

$\phi_i^{k+1} = \phi_i^{prop}$.

else,

$\phi_i^{k+1} = \phi_i^k$.

Step 6. end.

4.4.2 Numerical Results and Discussion

The parameters must be estimated and assigned a value to make the model operable. In this chapter, we use total active cases, totally recovered and total death data extracted from WHO situation reports $1-192$, and worldometer (Worldometers), with the daily data from January 21, 2020 to August 16, 2020. We use this data in parameter estimation for countries such as China, Italy, Brazil, South Africa, and Ethiopia. We denote the observed data $Y = [I, R, D]$ with having different length of time T for those countries. The goal is to find the value of the parameters which minimize the squared errors between the model predictions and the observed data.

We use different initial states of the dynamics for each of the countries accordingly the same with their total population and its compartments. We take initial values for Infected(I_0), Recovered(R_0) and Death(D_0) cases reasonably the same as the observed data Y_0. By an initial guess of the parameters ϕ^0, we use $B = 10,000$ number of iterations for estimation in the MH algorithm. In each country, two of the parameter values (μ and Λ) are calculated based on reported data. According to the World Bank data, the Ethiopian average life expectancy at birth for the year 2020 is 67.07, and its total population is 114963578. Therefore, the natural death rate of individuals per day is estimated as the reciprocal of the life expectancy at birth in time days, which is given by $\mu = \frac{1}{67.07 \times 365.25}$. We approximated the recruitment rate from $\frac{\Lambda}{\mu}$ give the total population to obtain $\Lambda = 4696$ individuals per day. We also use a constant pathogens concentration in the environment of about $K = 2091775$ in each country. Others are the estimated values from the given data.

Based on the available data and the prediction of the proposed model, we computed the error terms for the three state compartments. We then updated the parameter based on the minimization of sum squared differences between measurements and the model predictions.

Table 4.3: Estimated Parameter Values at the End of 10,000 Iterations

Parameter	Estimated Value				
	China	Italy	Ethiopia	Brazil	South Africa
α	0.9906	0.9471	0.6521	0.8485	0.0911
μ	0.000036	0.000033	0.000041	0.000036	0.000042
η	0.9947	0.6531	0.2116	0.4750	0.9998
δ	0.0909	0.0662	0.0014	0.0030	0.0014
γ	0.0629	0.0251	0.0331	0.0560	0.0567
ξ	0.0003	0.0400	0.0183	0.0362	0.0268
ψ	0.5649	0.5222	0.0051	0.7274	0.2850
β_1	0.0993	0.0779	0.0619	0.0418	0.0533
β_2	0.1162	0.0514	0.0010	0.0184	0.0227
λ_0	0.0001	0.0010	0.0001	0.0005	0.0437
θ	0.4523	0.4671	0.4571	0.5171	0.4932
K	2091775	2091775	2091775	2091775	2091775
Λ	49908	1959	4696	7670	2532

From the estimated parameter values in Table 4.3, the induced death rate due to COVID-19 δ is relatively high in Italy. The contact rates of the virus from the environment is relatively high in China, and the virus decay rate from the infected objects is relatively small in Brazil. From the estimated parameters, one can find the number of days required for the death and recovery periods.

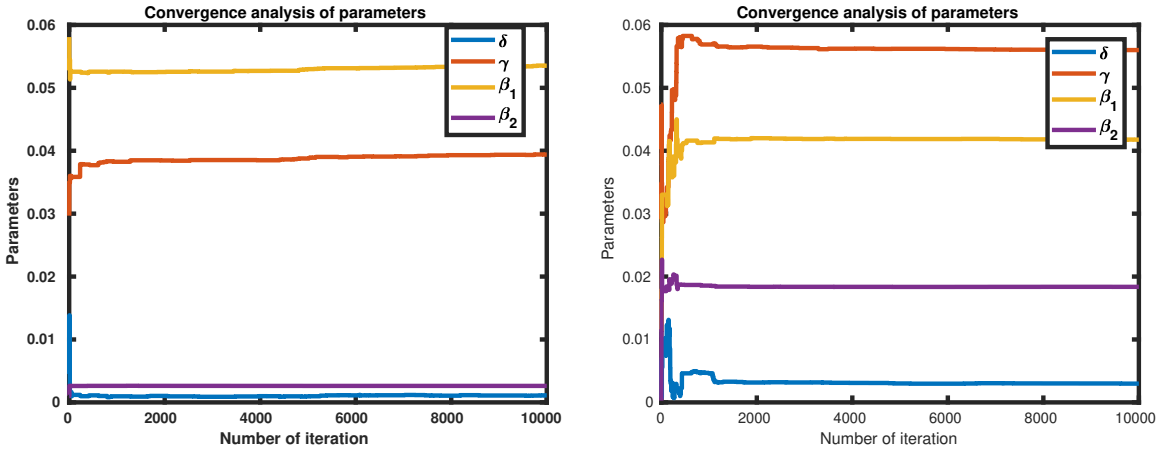

(a) Ethiopia (b) Brazil

Figure 4.2: Convergence analysis of a sample of parameters for the COVID-19 induced death rate δ, recovery rate γ, and the contact rates β_1, β_2 for the case of Ethiopia and Brazil.

The convergence analysis of some estimated parameters for the Ethiopian case is given in Figure 4.2 and our parameter estimation algorithm seems to converge at 2,000 iterations.

We use the values at the final iteration as the estimated parameter value for the proposed model. The estimated parameters for the countries China, Italy, Ethiopia, South Africa, and Brazil are given in Table 4.3.

Figures 4.3 shows the fitted model with the observed data for South Africa. The estimated parameters for the infected compartment is well fitted and approximated compared with the observed data. It is also shown that the recovered and death compartment has relatively small under predictions. The under prediction of the compartments occur due to the consideration of constant parameter values. These gap will be achieved if one consider time dependent parameter values, and study the different waves of the pandemic in countries.

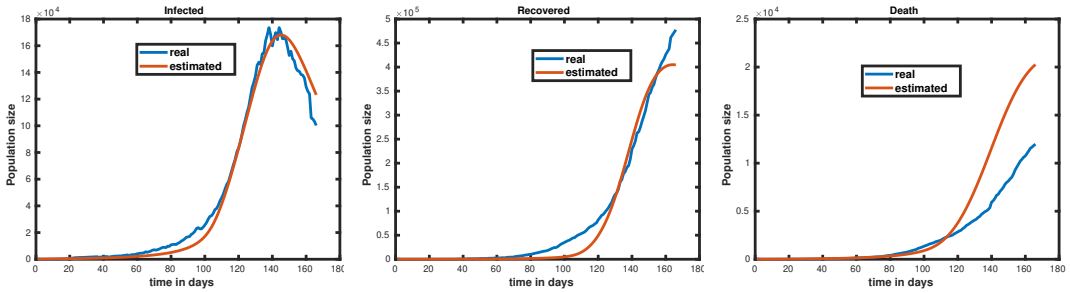

(a) Infected (b) Recovered (c) Death

Figure 4.3: Numerical results of the fitted and observed values of Infected, Recovered and Death cases for South Africa.

The Figures in 4.4 shows the fitted model with the observed data for Brazil. We observe that the estimated parameters for the infected and recovered compartments are well fitted and approximated compared with the observed data. The death compartment has relatively small over predictions.

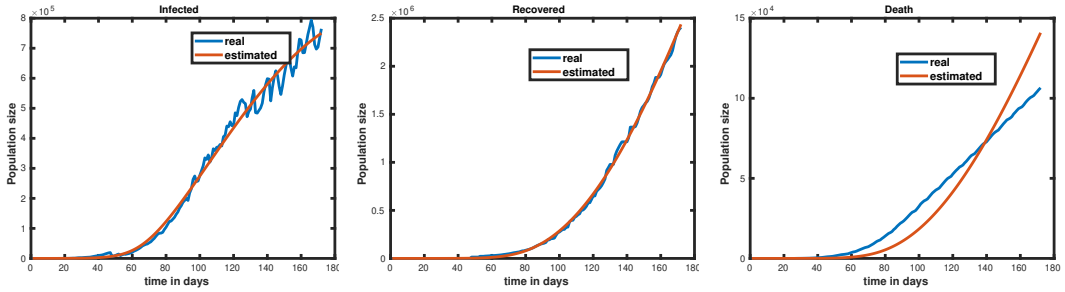

(a) Infected (b) Recovered (c) Death

Figure 4.4: Numerical results of the fitted and observed values of Infected, Recovered and Death cases for Brazil.

The Figures 4.5 shows the fitted model with the observed values for Ethiopian data. We see that the estimated parameters for the infected and death compartments are well fitted and approximated compared with the observed data. When we estimate parameters with the

existing Ethiopian COVID-19 data, the recovered compartment have relatively small under predictions.

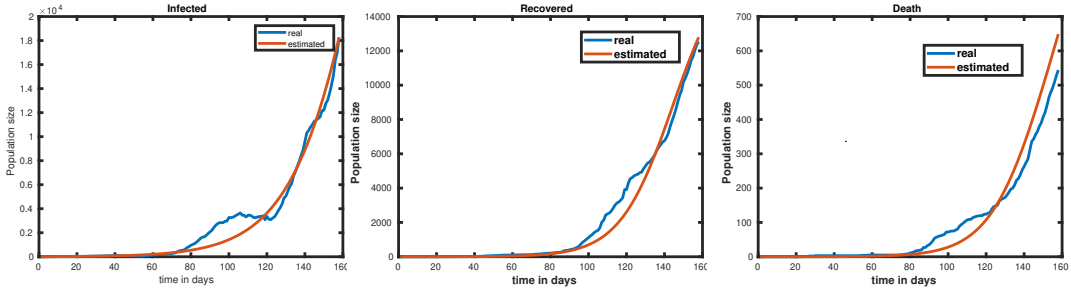

(a) Infected (b) Recovered (c) Death

Figure 4.5: The numerical results of the fitted and observed values of Infected, Recovered and Death cases for Ethiopia.

4.4.3 Sensitivity of the Basic Reproduction Number.

Sensitivity analysis is used to determine how sensitive a model is to changes in the value of the parameters and to changes in the structure of the model (Breierova, 1996; Saltelli et al., 2008). In this paper, we focus on parameter sensitivity. Sensitivity analysis is a useful tool in model building as well as in model evaluation by showing how the model behavior responds to changes in parameter values (Martcheva, 2015). The indices allow us to measure the relative change in the reproduction number with the change in a parameter values, and indicate the importance of different factors involved in disease transmission which are essential to develop control strategies.

Definition 4.4.1. *The Sensitivity and elasticity indices of the basic reproduction ratio,* R_0 *, with respect to model parameter* p *are respectively given by* $S_p = \frac{\partial R_0}{\partial p}$ *and* $e_p = \frac{\partial R_0}{\partial p}\frac{p}{R_0}$*. That is, the elasticity indices is given by* $e_p = S_p \frac{p}{R_0}$ *(Martcheva, 2015).*

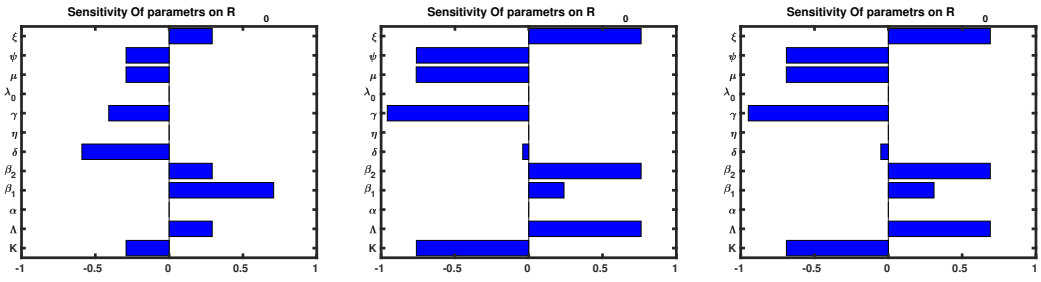

(a) China (b) Ethiopia (c) Brazil

Figure 4.6: The visual representation of the elasticity indices of R_0 with respect to the estimated parameters of countries China, Ethiopia and Brazil cases.

The graph in Figure 4.6 shows that in all the three countries, the infection rates β_1, β_2, the recruitment rate Λ, and shedding rate of the virus from the infected class to the envi-

ronment ξ has the highest elasticity indices with COVID-19 being positively correlated to R_0. An increase in these parameters increases the spread of the COVID-19 pandemic. The recovery rate γ, the natural and virus-induced death rates μ, δ, the pathogen concentration in the environment K, and the virus shedding rate ψ have a negative correlation of R_0 implying the virus decreases with an increase of these parameters.

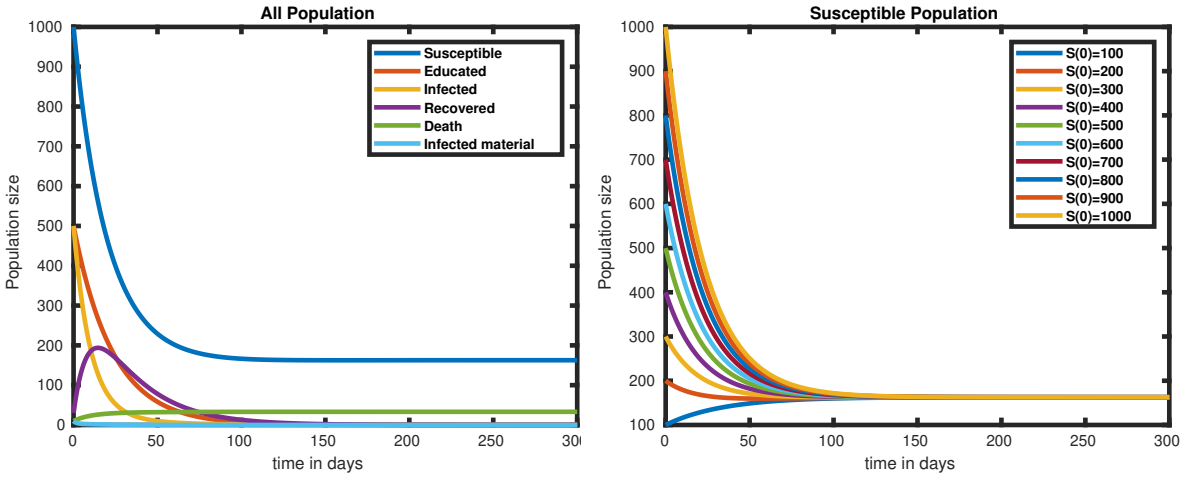

(a) All state variables

(b) Susceptible with different initials

Figure 4.7: The trajectories of state variables for $R_0 = 0.2552$, which is less than one.

In Figure 4.7a, we observe that for the basic reproduction number $R_0 < 1$, all solutions curve goes to the disease-free equilibrium point. These indicate that the disease-free equilibrium point is locally and globally asymptotically stable for the values of $R_0 < 1$. In Figure 4.7b with $R_0 < 1$ and different initial conditions for the susceptible population, all trajectory goes to the equilibrium point $\frac{\Lambda}{\mu}$, which indicates its stability.

In Figure 4.8, we observe that for the basic reproduction number $R_0 > 1$, all solutions curves goes away from the disease-free equilibrium point. These indicate that the disease-free equilibrium point is unstable for the values of $R_0 > 1$, and the solutions will go to the endemic equilibrium point.

4.4.4 Predictions

One of the most crucial applications of the dynamical system is to predict the future spread of the disease in the population. As the number of infected individuals increases, the new predictions help the government to prepare medical facilities and health care workers for the patients. Here we predicted the number of active infections, recoveries and deaths for the countries Ethiopia, Brazil and South Africa for the next 45 days. In Figure 4.9, the fitted areas are similar to Figures 4.3-4.5 while the prediction areas show the possible values of cases (active, recovered and death) predicted until September 30, 2020.

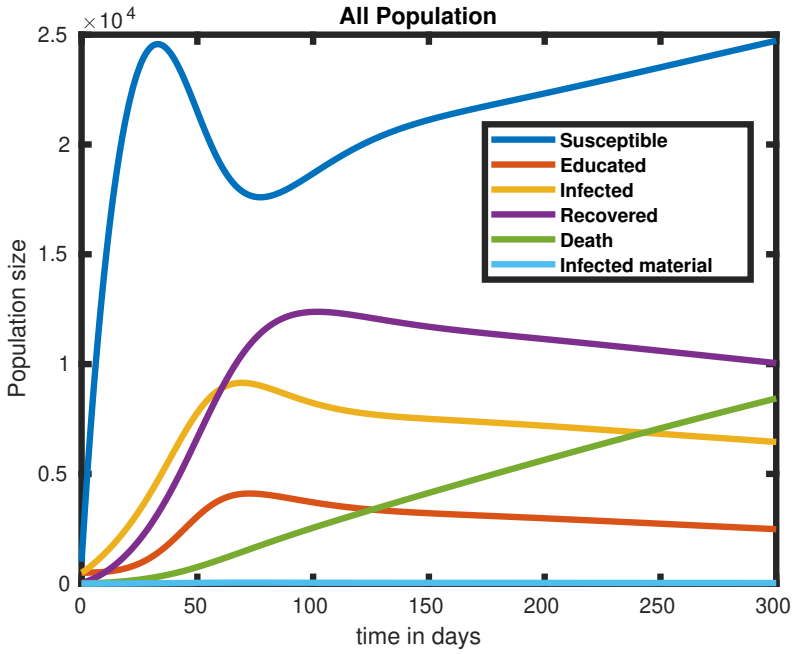

Figure 4.8: Trajectories of state variables for $R_0 = 8.3636$, which is greater than one.

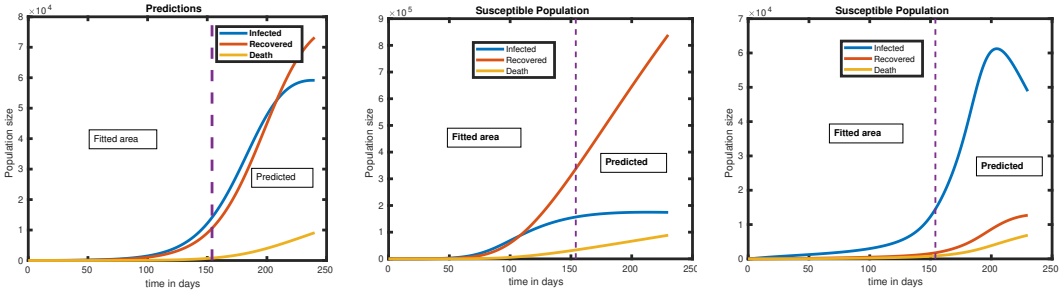

(a) Ethiopia (b) Brazil (c) South Africa

Figure 4.9: Predictions of active cases, recovered cases and death Ethiopia, Brazil and South Africa up to September 30, 2020.

According to our prediction, the total number of active infected populations of Ethiopia (Figure 4.9a) on September 30, 2020, was being around 55,000, the number of recovered individuals surpass 60,000, and the total deaths would reach above 1000. The number of infected populations would also stabilize and the number of recovered individuals would overshadow those of the infected ones thereafter on September 25, 2020.

When we see the predictions of Brazil (Figure 4.9b), the number of active infections and deaths is stable, and the number of recovered classes increases. The number of deaths reach 100,000 by the last of September 2020. In Figure 4.9c, the total number of active infections had decreased (after reaching the peak of the curve around 98,000 active infections) on August 15,2020; those of recovered and death class would also stabilize on that day for South Africa.

CHAPTER 5

MATHEMATICAL MODELING AND ANALYSIS OF TB AND COVID-19 COINFECTION WITH OPTIMAL CONTROL

5.1 Model Formulation

In this section, we propose a deterministic mathematical model to analyze the dynamics of TB and COVID-19 coinfection. We divided the total population into eight mutually exclusive epidemiological states depending on individuals health status: S denotes the susceptible class; L_T represents TB-latent human populations who are not infectious while the active TB-infected compartment is denoted as I_T. In the same way, the compartment of COVID-19 infected individuals with no symptoms but infectious is denoted by E_C, and COVID-19 infected individuals with symptoms is represented by I_C. The compartment for TB-latent co-infected with symptomatic COVID-19 is L_{TC} while symptomatic COVID-19 infected individuals co-infected with active TB is represented by I_{TC}. The recovered class from both diseases is denoted by R. With these in mind, the total population at time t, denoted by $N(t)$, is given by

$$N(t) = S(t) + L_T(t) + I_T(t) + E_C(t) + I_C(t) + L_{TC}(t) + I_{TC}(t) + R(t).$$

We consider the following basic assumptions to formulate the model.

1. A mathematical investigation has been made of the prevalence of a disease in a population from which certain individuals are being removed as the result of the disease, whilst fresh individuals are being introduced as the result of birth or immigration.

2. An average member of the population makes contact sufficient to transmit infection with others per unit time (mass-action incidence).

3. The transmission dynamics of COVID-19 and tuberculosis is an extension of the SEIR model.

4. We consider the contribution of asymptomatic infectious individuals in the transmission dynamics of both COVID-19 and tuberculosis diseases.

5. We assumed that the disease induced death occurs only due to TB, COVID-19 and their coinfection which omits the death that come from other diseases.

6. After recovering from the diseases, we assume that individuals are developing a permanent immunity.

The model assumptions and descriptions for the flow of coinfection are diagrammatically illustrated in Figure5.1.

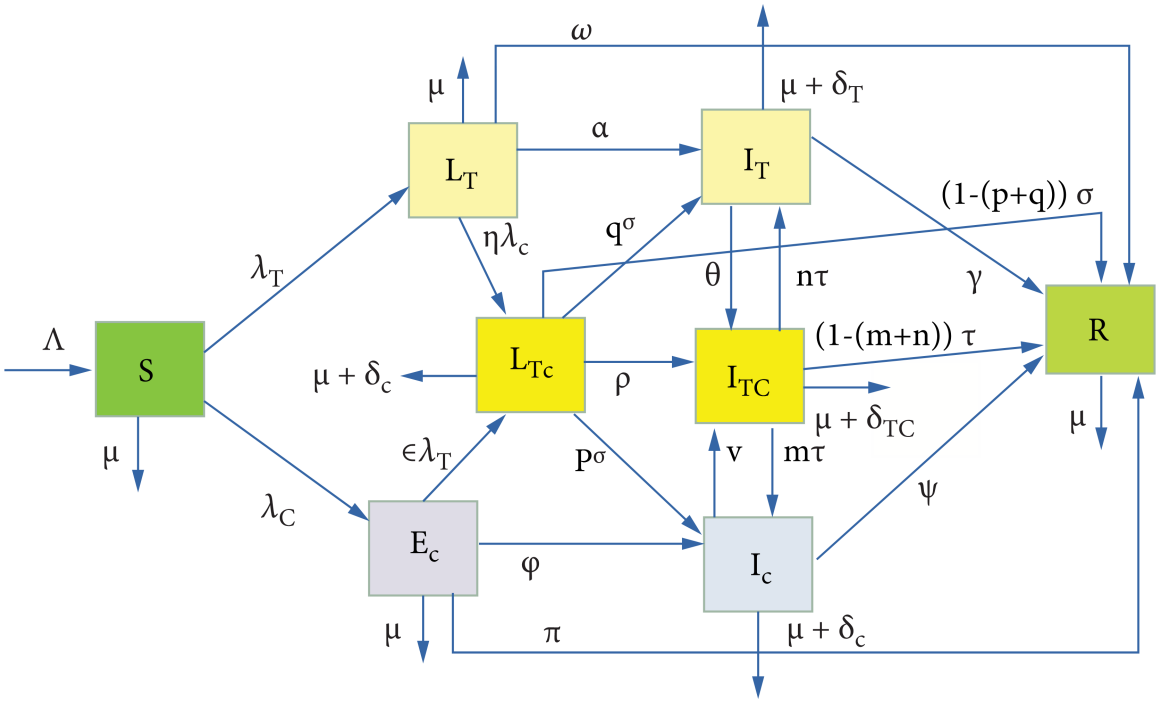

Figure 5.1: Flow Diagram of the Model

Thus, the above assumptions and descriptions can be summarized into the following systems of first-order nonlinear ordinary differential equations:

$$
\begin{cases}
\frac{dS}{dt} = \Lambda - (\lambda_T + \lambda_C + \mu)S, \\
\frac{dL_T}{dt} = \lambda_T S - (\mu + \alpha + \eta\lambda_C + \omega)L_T, \\
\frac{dI_T}{dt} = \alpha L_T + q\sigma L_{TC} + n\tau I_{TC} - (\mu + \theta + \delta_T + \gamma)I_T, \\
\frac{dE_C}{dt} = \lambda_C S - (\mu + \epsilon\lambda_T + \varphi + \pi)E_C, \\
\frac{dI_C}{dt} = \varphi E_C + p\sigma L_{TC} + m\tau I_{TC} - (\mu + \delta_C + \nu + \psi)I_C, \\
\frac{dL_{TC}}{dt} = \eta\lambda_C L_T + \epsilon\lambda_T E_C - (\mu + \delta_C + \rho + \sigma)L_{TC}, \\
\frac{dI_{TC}}{dt} = \rho L_{TC} + \theta I_T + \nu I_C - (\mu + \delta_{TC} + \tau)I_{TC}, \\
\frac{dR}{dt} = \omega L_T + \pi E_C + \gamma I_T + \psi I_C + (1 - (p+q))\sigma L_{TC} + (1 - (m+n))\tau I_{TC} - \mu R,
\end{cases}
\tag{5.1}
$$

where

$$\lambda_T(t) = \frac{\beta_1}{N(t)}\left(I_T(t)+I_{TC}(t)\right), \tag{5.2}$$

$$\lambda_C(t) = \frac{\beta_2}{N(t)}\left(E_C(t)+I_C(t)+L_{TC}(t)+I_{TC}(t)\right), \tag{5.3}$$

and non-negative initial conditions $S(0) > 0$, $E_T(0) \geq 0$, $I_T(0) \geq 0$, $E_C(0) \geq 0$, $I_C(0) \geq 0$, $L_{TC}(0) \geq 0$, $I_{TC}(0) \geq 0$, and $R(0) \geq 0$. All parameters of the model are assumed to be positive, and redefined in Table 5.1 for simplicity of reference.

5.1.1 Description of the Model

The susceptible individuals increases by a constant recruitment rate Λ, and individuals in all compartments die with a natural death rate μ. Susceptible individuals acquire TB through contact with active TB-infectious individuals at a force of infection λ_T given as in equation (5.2). In this expression β_1 denotes the effective contact rate for TB infection. The latent TB infected individuals are assumed to be asymptomatic that does not transmit the disease (Silva et al., 2015). Besides, susceptible individuals obtain COVID-19 infection through effective contact with COVID-19 infected individuals at a force of infection λ_C defined in equation (5.3). Moreover, latent TB individuals L_T progress to an active TB infectious with a constant rate α, and leaves the compartment by becoming co-infected with COVID-19 at a force of infection $\eta\lambda_C$ or recovered at a rate ω. The population in the compartment I_T become recovered at a recovery rate γ or acquire coinfection of TB and COVID-19 at a rate θ while TB-induced death rate is denoted as δ_T.

Further, individuals in the co-infected compartment L_{TC} progress to the I_{TC} class at a rate ρ while the remaining leave the class with a transfer rate σ or dies due to COVID-19 induced death rate δ_C. In the same way, individuals in compartment I_{TC} leave at a constant rate τ while the coinfection induced death rate is represented as δ_{TC} or become recovered simultaneous from both disease at a constant rate $(1-(m+n))\tau$.

Moreover, individuals in compartment E_C develop COVID-19 symptom and progress to class I_C at a rate φ while $\varepsilon\lambda_T$ jointed compartment L_{TC} or becomes recover at a constant rate π. Also, individuals in class I_C becomes recover from the disease at a rate ψ. The remaining individuals either transfer to the coinfection compartment at a rate ν or dies due to the COVID-19 induced death at a rate δ_C.

Table 5.1: Description of the model parameters

Parameter	Biological description of the parameter
Λ	Recruitment rate for the susceptible individuals
β_1	TB transmission rate
β_2	The effective contact rate for COVID-19 transmission
α	Transferring rate TB exposed individuals to become infected
λ_T	Force of infection for TB disease
λ_C	Force of infection for COVID-19 infections
ν	TB infection rate from the COVID-19 infected classes
θ	COVID-19 infection rate from the TB infected ones
π	Recovery rate of the exposed COVID-19 individuals
σ	Rate at which individuals leave the L_{TC} class
p	Recovery rate of L_{TC} individuals from the latent TB infections
q	Recovery rate of the L_{TC} individuals from the COVID-19 infections
τ	Rate at which individuals leave the I_{TC} class
m	Recovery rate of I_{TC} individuals from the active TB disease
n	The COVID-19 recovery rate of I_{TC} individuals
η	Rate of TB exposed individuals becoming exposed with COVID-19
γ	Recovery rate of the TB infected (I_T) individuals
δ_T	TB induced death rate
δ_C	Death rate due to the induced COVID-19
δ_{TC}	Death rate due to both TB and COVID-19
μ	The natural death rate of all individuals
ρ	Transfer rate of TB latent individuals co-infected with COVID-19 to become infected with both disease
φ	Transfer rate of the exposed COVID-19 individuals to become infected
ψ	Recovery rate of infected COVID-19 individual
ε	Rate of COVID-19 exposed individuals to become co-infected with latent TB
ω	Recovery rate of TB latent infected individuals

5.1.2 Positivity and Boundedness of the Solutions

The system of equations (5.1) governs the co-dynamics of both disease and can be used to guide the policy makers in the control of these infectious disease provided that the proposed model is well posed. To assure these, we examine the existence, uniqueness, positivity and boundedness of solutions using standard theorems.

Theorem 5.1.1. *The solutions of the system of equations (5.1) are positive and invariant in the region*

$$\Omega = \{(S, L_T, I_T, E_C, I_C, L_{TC}, I_{TC}, R) \in \mathbb{R}^8_+ : 0 \leq N(t) \leq \frac{\Lambda}{\mu}\}.$$

Proof. All the functions on the right hand side of equation (5.1) are $C^1(\mathbb{R}^8_+)$. Thus, by the Picard–Lindelöf theorem (Schroers, 2011), the model equations (5.1) has a unique solution.

From the equation of susceptible individuals $\frac{dS}{dt} = \Lambda - (\lambda_T + \lambda_C + \mu)S$, one can obtain that $\frac{dS}{dt} + (\lambda_T + \lambda_C + \mu)S = \Lambda$. This is a separable first order ordinary differential equation for

the variable S. Integrating the equation and after some simplification, we obtain the solution in terms of λ_T and λ_C as follows:

$$S(t) = (S(0) + \Lambda t))\, e^{-(\lambda_T + \lambda_C + \mu)t}.$$

Using a non negative initial condition $S(0) > 0$ and for $t \geq 0$, the solution for $S(t)$ is always positive. Again, from the second equation

$$\frac{dL_T}{dt} = \lambda_T S - (\mu + \alpha + \eta\lambda_C + \omega)L_T.$$

Here, $\frac{dL_T}{dt} \geq -(\mu + \alpha + \eta\lambda_C + \omega)L_T$ for $S \geq 0$. Solving this equation one can obtain that $L_T(t) \geq L_T(0)e^{-(\mu+\alpha+\eta\lambda_C+\omega)}$ which is always positive for a non-negative initial condition $L_T(0) \geq 0$. The positivity of the remaining state variables can be proved in the same procedure.

The dynamics of total population $N(t)$ with respect to time t is governed by:

$$\frac{dN}{dt} = \Lambda - \delta_T I_T - \delta_c(I_c + L_{TC}) - \delta_{TC} I_{TC} - \mu N.$$

In the absence of disease induced death, that is, $\delta_T = \delta_c = \delta_{TC} = 0$, the dynamics becomes $\frac{dN}{dt} \leq \Lambda - \mu N$. The solution for this equation becomes $N(t) \leq N(0)e^{-\mu t} + \frac{\Lambda}{\mu}(1 - e^{-\mu t})$. Thus, for $t \to \infty, N(0) \leq \frac{\Lambda}{\mu}$, and

$$0 \leq N(t) \leq \frac{\Lambda}{\mu}.$$

Hence, all the solutions of the model exists, are unique and bounded in a feasible region Ω, which concludes the proof. □

5.2 Model Analysis

To understand the dynamics of the proposed model, we investigate the model analysis both analytically and numerically. The analysis have been done by investigating the behavior of the sub-models for TB and COVID-19 as well as the coinfection model.

5.2.1 COVID-19 Sub-model

Without considering the infections of people with tuberculosis, the COVID-19 sub-model is given by:

$$\begin{cases} \frac{dS}{dt} = \Lambda - \frac{\beta_2}{N}(E_C + I_C)S - \mu S = f_1, \\ \frac{dE_C}{dt} = \frac{\beta_2}{N}(E_C + I_C)S - (\mu + \varphi + \pi)E_C = f_2, \\ \frac{dI_C}{dt} = \varphi E_C - (\mu + \delta_C + \psi)I_C = f_3, \\ \frac{dR}{dt} = \pi E_C + \psi I_C - \mu R = f_4. \end{cases} \tag{5.4}$$

Local Stability of Equilibrium Points

The equilibrium point of the COVID-19 sub-model is a solution to the system of equations:

$$\begin{aligned} &\Lambda - \frac{\beta_2}{N}(E_C + I_C)S - \mu S = 0, \\ &\frac{\beta_2}{N}(E_C + I_C)S - (\mu + \varphi + \pi)E_C = 0, \\ &\varphi E_C - (\mu + \delta_C + \psi)I_C = 0, \\ &\pi E_C + \psi I_C - \mu R = 0. \end{aligned} \tag{5.5}$$

The disease-free equilibrium point is obtained by putting $E_C = 0$ and $I_C = 0$ in equation (5.5). Hence, the disease-free equilibrium point, denoted by E_0^C becomes $E_0^C = (\frac{\Lambda}{\mu}, 0, 0, 0)$.

The basic reproduction number of the sub-model, defined as the average number of secondary infections produced by a single COVID-19 infected individual in a completely susceptible population. It is computed using the next generation matrix method (Driessche and Watmough, 2002). Let $\mathscr{F}_i(t,x)$ be the input rate of newly infected individuals in the i^{th} compartment and $\mathscr{V}_i^+(t,x)$ and $\mathscr{V}_i^-(t,x)$ respectively be the input rates by other means and rate of transfer of individuals out of a compartment i, where the x_i's are our state variables and $\mathscr{V}_i(t,x) = \mathscr{V}_i^-(t,x) - \mathscr{V}_i^+(t,x)$.

Hence, from equations (5.4) it follows that

$$\mathscr{F}_i = \begin{pmatrix} \frac{\beta_2}{N}(E_C + I_C)S \\ 0 \end{pmatrix}, \mathscr{V}_i^+ = \begin{pmatrix} 0 \\ \varphi E_C \end{pmatrix} \text{ and } \mathscr{V}_i^- = \begin{pmatrix} (\mu + \varphi + \pi)E_C \\ (\mu + \delta_C + \psi)I_C \end{pmatrix} \tag{5.6}$$

The Jacobian matrices of $\mathscr{F}(x)$ and $\mathscr{V}(x)$ respectively, are

$$F = D\mathscr{F}(E_0^C) = \begin{bmatrix} \beta_2 & \beta_2 \\ 0 & 0 \end{bmatrix} \quad \text{and} \quad V = D\mathscr{V}(E_0^C) = \begin{bmatrix} \mu + \varphi + \pi & 0 \\ -\varphi & \mu + \delta_c + \psi \end{bmatrix}.$$

Hence, the next-generation matrix FV^{-1} becomes

$$FV^{-1} = \begin{bmatrix} \frac{\beta_2}{\mu+\varphi+\pi}\left(1+\frac{\varphi}{\mu+\delta_c+\psi}\right) & \frac{\beta_2}{\mu+\delta_c+\psi} \\ 0 & 0 \end{bmatrix}.$$

The eigenvalues of the next generation matrix are found to be $\lambda_1 = \frac{\beta_2}{\mu+\varphi+\pi}\left(1+\frac{\varphi}{\mu+\delta_c+\psi}\right)$, and $\lambda_2 = 0$. The largest spectral radius of the next generation matrix denotes the basic reproduction number for the sub-model. Thus, we have the following result.

Theorem 5.2.1. *The basic reproduction number of the COVID-19 sub-model is*

$$R_0^C = \frac{\beta_2}{\mu+\varphi+\pi}\left(\frac{\mu+\delta_c+\psi+\varphi}{\mu+\delta_c+\psi}\right). \tag{5.7}$$

We use the Jacobean matrix to determine the local stability of the equilibrium points. For the sub model (5.4), the Jacobean matrix becomes

$$J(S,E_C,I_C,R) = \begin{pmatrix} \frac{-\beta_2(E_C+I_C)(E_C+I_C+R)}{N^2} - \mu & \frac{-\beta_2(S+R)S}{N^2} & \frac{-\beta_2(S+R)S}{N^2} & 0 \\ \frac{\beta_2(E_C+I_C)(E_C+I_C+R)}{N^2} & \frac{\beta_2(S+R)S}{N^2} - (\mu+\varphi+\pi) & \frac{\beta_2(S+R)S}{N^2} & 0 \\ 0 & \varphi & -(\mu+\delta_C+\psi) & 0 \\ 0 & \pi & \psi & -\mu \end{pmatrix} \tag{5.8}$$

The Jacobean matrix of the sub-model at the disease-free equilibrium point E_0^c is given as

$$J(E_0^C) = \begin{pmatrix} -\mu & -\beta_2 & -\beta_2 & 0 \\ 0 & \beta_2-(\mu+\varphi+\pi) & \beta_2 & 0 \\ 0 & \varphi & -(\mu+\delta_C+\psi) & 0 \\ 0 & \pi & \psi & -\mu \end{pmatrix}. \tag{5.9}$$

Here, the eigenvalues for $J(E_0^C)$ are $\lambda_{1,2} = -\mu$, and the remaining eigenvalues can be easily obtained from the sub matrix

$$J_2 = \begin{pmatrix} \beta_2-(\mu+\varphi+\pi) & \beta_2 \\ \varphi & -(\mu+\delta_C+\psi) \end{pmatrix}.$$

In order to determine the local stability of the disease-free equilibrium point, it is sufficient to show that the trace of J_2 is less than zero and its determinant is greater than zero.

The trace of $trJ_2 = \beta_2 - (2\mu+\varphi+\pi+\psi+\delta_C)$ which is less than zero if $\beta_2 < (2\mu+\varphi+\pi+\psi+\delta_c)$. If $\frac{\beta_2(\mu+\delta_C+\psi+\varphi)}{(\mu+\varphi+\pi)(\mu+\delta_C+\psi)} = R_0^C < 1$, then $tr(J_2) < 0$. Moreover, the determinant of

$$detJ_2 = -(\beta_2-(\mu+\varphi+\pi))(\mu+\delta_C+\psi) - \varphi\beta_2 = -\beta_2(\mu+\delta_C+\psi+\varphi) + (\mu+\varphi+\pi)(\mu+\delta_C+\psi).$$

This value is greater than zero if $\frac{\beta_2(\mu+\delta_C+\psi+\varphi)}{(\mu+\varphi+\pi)(\mu+\delta_C+\psi)} < 1$, that is, $detJ_2 > 0$ if $R_0^C < 1$ and $detJ_2 < 0$ if $R_0^C > 1$. Hence, the disease-free equilibrium point of the COVID-19 sub-model is stable if $R_0^C < 1$ and unstable if $R_0^C > 1$.

The endemic equilibrium point of the COVID-19 sub-model is the solution of the system of equation in (5.10).

$$\begin{aligned} \Lambda - (\lambda_C + \mu)S &= 0, \\ \lambda_C S - (\mu + \varphi + \pi)E_C &= 0, \\ \varphi E_C - (\mu + \delta_C + \psi)I_C &= 0, \\ \pi E_C + \psi I_C - \mu R &= 0. \end{aligned} \tag{5.10}$$

Now solving this system of equations in terms $\lambda_C^* = \frac{\beta_2}{N^*}(E_C^* + I_C^*)$ one can obtain the following expressions for the endemic equilibrium point $\Sigma_C = (S^*, E_C^*, I_C^*, R)$ where

$$S^* = \frac{\Lambda}{\lambda_C^* + \mu}, E_C^* = \frac{\lambda_C^* \Lambda}{c_1(\lambda_C^* + \mu)}, I_C^* = \frac{\lambda_C^* \Lambda \varphi}{c_1 c_2(\lambda_C^* + \mu)} \text{ and } R^* = \frac{\lambda_C^* \Lambda(c_2\pi + \varphi\psi)}{\mu c_1 c_2(\lambda_C^* + \mu)}. \tag{5.11}$$

Here, $c_1 = \mu + \varphi + \pi$, $c_2 = \mu + \delta_C + \psi$, and $N^* = \frac{\Lambda - \delta_C I_C^*}{\mu}$. Using (5.11) in the expression for λ_C^* it gives $\lambda_C^* = \frac{\beta_2 \mu(c_2+\varphi) - c_1 c_2 \mu}{c_1 c_2 - \delta_C \mu}$. After simplification, we have in compact form

$$\lambda_C^* = \frac{\mu c_1 c_2 \left(\frac{\beta_2(c_2+\varphi)}{c1c2} - 1\right)}{\mu\pi c_2 + \varphi(\mu + \psi)} = \frac{\mu c_1 c_2 \left(R_0^C - 1\right)}{\mu\pi c_2 + \varphi(\mu + \psi)}.$$

This implies that, the force of infection λ_C^* is positive at endemic equilibrium point only if $R_0^C > 1$. Thus we have just proved the following theorem.

Theorem 5.2.2. *If $R_0^c > 1$, then the sub-model system (5.4) has a unique endemic equilibrium point.*

Global Stability of the Endemic Equilibrium Point

The global stability analysis of the endemic equilibrium point Σ_C is analyzed using Lyapunov function. For this, we define the following:

$$L(S, E_C, I_C, R) = \frac{1}{2}\left((S - S^*) + (E_C - E_C^*) + (I_C - I_C^*) + (R - R^*)\right)^2.$$

The function L is greater than zero, and it is equal to zero at the endemic equilibrium point Σ_C. Differentiating the function with respect to time, we obtain

$$\begin{aligned}\frac{dL}{dt} &= ((S-S^*)+(E_C-E_C^*)+(I_C-I_C^*)+(R-R^*))\left(\frac{dS}{dt}+\frac{dE_C}{dt}+\frac{dI_C}{dt}+\frac{dR}{dt}\right)\\ &= (N-\frac{\Lambda-\delta_C I_C^*}{\mu})(\Lambda-\delta_C I_C-\mu N)\\ &\leq (N-\frac{\Lambda}{\mu})(\Lambda-\mu N)\\ &\leq -\frac{(\Lambda-\mu N)^2}{\mu}\leq 0.\end{aligned}$$

This holds true for $R_0^C > 1$ which corresponds the existence of Σ_C. Thus, $\frac{dL}{dt} < 0$ implies the function is a strictly Lyapunov function which indicates that the endemic equilibrium point Σ_C is globally asymptotically stable. Epidemically, this result implies that COVID-19 continues to exist in the human population for a long duration.

Sensitivity Analysis of the Sub-model

In this section, we perform the sensitivity analysis of the model parameters for the COVID-19 sum-model given in (5.4). The sensitivity of a parameters is computed by the normalized forward sensitivity index:

$$S_p = \frac{\partial R_0^C}{\partial p}\frac{p}{R_0^C}.$$

In our context, the sensitivity analysis of each parameters for equation(5.4) becomes

$$\begin{aligned}S_{\beta_2} &= \frac{\partial R_0^C}{\partial \beta_2}\frac{\beta_2}{R_0^C} = 1,\\ S_\mu &= \frac{\partial R_0^C}{\partial \mu}\frac{\mu}{R_0^C} = -\frac{\mu\,(\delta_C(\delta_C+2\mu+3\psi+\varphi)+\mu(\mu+4\psi+2\varphi)+\psi(2\psi+2\varphi+\pi)+\varphi(\varphi+\pi))}{(\delta_C+\mu+\psi)(\mu+\pi+\varphi)(\delta_C+\mu+2\psi+\varphi)},\\ S_{\delta_C} &= \frac{\partial R_0^C}{\partial \delta_C}\frac{\delta_C}{R_0^C} = -\frac{\delta_C\varphi}{(\delta_C+\mu+\psi)(\delta_C+\mu+\psi+\varphi)},\\ S_\psi &= \frac{\partial R_0^C}{\partial \psi}\frac{\psi}{R_0^C} = -\frac{\psi\varphi}{(\delta_C+\mu+\psi)(\delta_C+\mu+\psi+\varphi)},\\ S_\varphi &= \frac{\partial R_0^C}{\partial \varphi}\frac{\varphi}{R_0^C} = -\frac{\varphi(\delta_C+\psi-\pi)}{(\mu+\pi+\varphi)(\delta_C+\mu+\psi+\varphi)},\\ S_\pi &= \frac{\partial R_0^C}{\partial \pi}\frac{\pi}{R_0^C} = -\frac{\pi}{(\mu+\pi+\varphi)}.\end{aligned}$$

Here, we can observe that the contact rate β_2 positively influence the spread of COVID-19. Further, if $\delta_C + \psi - \pi < 0$ the transfer rate φ from exposed compartment to infected class, has a positive impact on the spread of the virus. That is, increasing the value of these parameters increases the pandemic. The remaining parameters, μ, ψ, δ_C and π, have negative impact, which means increasing the value of these parameters decreases the number of people infected with COVID-19. However, it is unethical to increase human mortality rate to control disease epidemic and hence do not considered.

Bifurcation Analysis for COVID-19 Sub-model

Next, we study the solution behavior of equations (5.4) by taking β_2 as the bifurcation parameter. Calculating the value of β_2 from $R_0^C = 1$, i.e., $\frac{\beta_2}{\mu+\varphi+\pi}\left(\frac{\mu+\delta_C+\psi+\varphi}{\mu+\delta_C+\psi}\right) = 1$, we have $\beta_2^* = \frac{(\mu+\varphi+\pi)(\mu+\delta_C+\psi)}{\mu+\delta_C+\psi+\varphi}$. Following the result given in (Castillo-Chavez and Song, 2004, Theorem 4.1), we can calculate the eigenvalues of the Jacobin matrix at the disease-free equilibrium point by substituting β_2^*. Thus, substituting $\beta_2 = \beta_2^*$ in equations (5.9) it gives zero eigenvalue. This means, the Jacobean matrix $J(E_0^c)$ in equation (5.9) at $\beta_2 = \beta_2^*$ has a left eigenvector (associated with the zero eigenvalue) which is calculated from $v^T J(E_0^c) = 0$. Here, $v = [v_1, v_2, v_3, v_4]$, where,

$$v_1 = 0, \;\; v_2 = \frac{(\delta_C + \mu + \varphi + \psi)}{(\mu + \pi + \varphi)}, \;\; v_3 = 1, \text{ and } \;\; v_4 = 0.$$

Similarly, the right eigenvector associated with the zero eigenvalue can be calculated from $J(E_0^c)w = 0$ with $w = [w_1, w_2, w_3, w_4]$ where,

$$w_1 = \frac{\mu(\delta_C + \pi + \mu) + (\pi + \varphi)(\delta_C + \mu + \psi)}{\pi(\delta_C + \mu + \psi) + \psi\varphi}, \;\; w_2 = \frac{\mu(\delta_C + \mu + \psi)}{\pi(\delta_C + \mu + \psi) + \psi\varphi},$$
$$w_3 = \frac{\mu\varphi}{\pi(\delta_C + \mu + \psi) + \psi\varphi}, \qquad \text{and} \qquad w_4 = 1.$$

Now assume that f_k represents the right-hand side of the k^{th} equation in COVID-19 su-model(5.4) and let x_k denote the corresponding state variable for $k = 1, \ldots, 4$. Define

$$a = \sum_{k,i,j=1}^{n} v_k w_i w_j \frac{\partial^2 f_k}{\partial x_i \partial x_j}(0,0) \quad \text{and} \;\; b = \sum_{k,i=1}^{n} v_k w_i \frac{\partial^2 f_k}{\partial x_i \partial \phi}(0,0).$$

The local dynamics of equation (5.4) near the bifurcation point $\beta_2 = \beta^*$ is then determined by the signs of two associated constants a and b with $\phi = \beta_2 - \beta^*$. Note that, in $f_k(0,0)$, the first zero corresponds to the DFE, E_0^C, for the sub-model (5.4). In other words, $f_k(0,\phi) = 0$, for $k = 1, \ldots, 4$, if and only if the right-hand sides of equations (5.4) are equal to zero at E_0^C. Moreover, from $\phi = \beta_2 - \beta^*$ we have $\phi = 0$ when $\beta_2 = \beta^*$, which is the second zero component in $f_k(0,0)$.

For the sub-model (5.4), the associated non-zero partial derivatives at the disease-free equilibrium E_0^C are given by

$$\frac{\partial^2 f_1}{\partial E_C^2} = \frac{-2\beta_2^*\mu}{\Lambda}, \quad \frac{\partial^2 f_1}{\partial E_C \partial I_C} = \frac{-2\beta_2^*\mu}{\Lambda}, \quad \frac{\partial^2 f_1}{\partial E_C \partial R} = \frac{\beta_2^*\mu}{\Lambda},$$

$$\frac{\partial^2 f_1}{\partial I_C^2} = \frac{-2\beta_2^*\mu}{\Lambda}, \quad \frac{\partial^2 f_1}{\partial I_C \partial E_C} = \frac{-2\beta_2^*\mu}{\Lambda}, \quad \frac{\partial^2 f_1}{\partial I_C \partial R} = \frac{\beta_2^*\mu}{\Lambda},$$

$$\frac{\partial^2 f_2}{\partial E_C^2} = \frac{2\beta_2^*\mu}{\Lambda}, \quad \frac{\partial^2 f_2}{\partial E_C \partial I_C} = \frac{2\beta_2^*\mu}{\Lambda}, \quad \frac{\partial^2 f_2}{\partial E_C \partial R} = \frac{-\beta_2^*\mu}{\Lambda},$$

$$\frac{\partial^2 f_2}{\partial I_C^2} = \frac{2\beta_2^*\mu}{\Lambda}, \quad \frac{\partial^2 f_2}{\partial I_C \partial E_C} = \frac{2\beta_2^*\mu}{\Lambda}, \quad \frac{\partial^2 f_2}{\partial I_C \partial R} = \frac{-\beta_2^*\mu}{\Lambda}.$$

Then, using the above expressions for a, it follows that

$$a = \frac{\mu^2(\mu+\delta_C+\psi)(\delta_C+\mu+\varphi+\psi)}{\Lambda(\pi(\delta_C+\mu+\psi)+\psi\varphi)}\left(\frac{2\mu(\delta_C+\mu+\psi+\varphi)}{\pi(\delta_C+\mu+\psi)+\psi\varphi}-1\right).$$

For the sign of b, it can be shown that the associated non-vanishing partial derivatives are

$$\frac{\partial^2 f_1}{\partial E_C \partial \beta_2} = -1, \quad \frac{\partial^2 f_1}{\partial I_3 \partial \beta_2} = -1 \quad \frac{\partial^2 f_2}{\partial E_C \partial \beta_2} = 1, \quad \frac{\partial^2 f_2}{\partial I_3 \partial \beta_2} = 1$$

Clearly, it also follows from the above expressions that

$$b = \frac{\mu(\delta_C+\mu+\psi+\varphi)^2}{(\mu+\pi+\varphi)(\pi(\delta_C+\mu+\psi)+\psi\varphi)}.$$

From the computations of a and b, we observe that b is always positive and the sign of the bifurcation coefficient a depends on the expression (κ). Thus, using Theorem 4.1 of (Castillo-Chavez and Song, 2004), the following result is proved.

Theorem 5.2.3. *If the value of* $\kappa = \frac{2\mu(\delta_C+\mu+\psi+\varphi)}{\pi(\delta_C+\mu+\psi)+\psi\varphi}$ *is less than unity, then there exists a forward bifurcation for the COVID-19 sub-model* (5.4).

The trans-critical bifurcation diagram (with the value of $\kappa = 0.0463$ by plugging in the parameter values as given in Table 5.3) is given in Figure 5.2. As $\kappa = 0.0463$ which is less than unity, it results that the bifurcation is forward at $R_0^C = 1$.

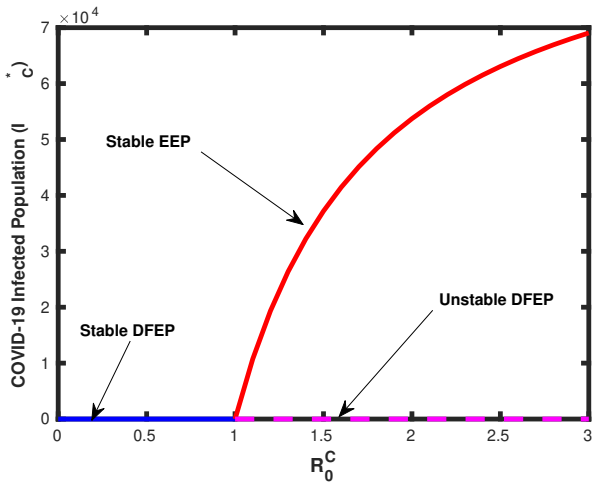

Figure 5.2: Trans-critical bifurcation of the COVID-19 sub-model.

5.2.2 TB Sub-model

In the absence of COVID-19 disease, equation (5.1) automatically reduced to TB-sub-model expressed as

$$\begin{aligned}
\frac{dS}{dt} &= \Lambda - \frac{\beta_1}{N} I_T S - \mu S, \\
\frac{dL_T}{dt} &= \frac{\beta_1}{N} I_T S - (\mu + \alpha + \omega) L_T, \\
\frac{dI_T}{dt} &= \alpha L_T - (\mu + \delta_T + \gamma) I_T, \\
\frac{dR}{dt} &= \omega L_T + \gamma I_T - \mu R.
\end{aligned} \tag{5.12}$$

In a similar argument, the disease-free equilibrium point of equation (5.12) becomes $E_0^T = \left(\frac{\Lambda}{\mu}, 0, 0, 0\right)$ and the corresponding basic reproduction number is given by

$$R_0^T = \frac{\beta_1 \alpha}{(\mu + \alpha + \omega)(\mu + \delta_T + \gamma)}. \tag{5.13}$$

Theorem 5.2.4. *The disease-free equilibrium point of the TB sub-model* (5.12) *is locally asymptotically stable if* $R_0^T < 1$.

Proof. The Jacobean matrix at the disease free equilibrium point for the TB sub-model is given by

$$J(E_0^T) = \begin{bmatrix} -\mu & 0 & -\beta_1 & 0 \\ 0 & -(\mu + \alpha + \omega) & \beta_1 & 0 \\ 0 & \alpha & -(\mu + \delta_T + \gamma) & 0 \\ 0 & \omega & \gamma & -\mu \end{bmatrix}.$$

Clearly, the two eigenvalues are equal to $-\mu$, while the remaining can be obtained from the

reduced matrix

$$J_3 = \begin{bmatrix} -(\mu+\alpha+\omega) & \beta_1 \\ \alpha & -(\mu+\delta_T+\gamma) \end{bmatrix}.$$

Here, the trace of the matrix $tr(J_3) = -(2\mu+\alpha+\omega+\delta_T+\gamma) < 0$, and its determinant $det(J_3) = (\mu+\alpha+\omega)(\mu+\delta_T+\gamma) - \alpha\beta_1$. Thus, the determinant is greater than zero if $R_0^T < 1$. Therefore, the disease-free equilibrium point of the TB sub-model is locally asymptotically stable if $R_0^T < 1$. This complete the proof. □

The endemic equilibrium point of the TB-sub-model is obtained by solving the system of equations:

$$\begin{aligned} &\Lambda - \lambda_T S - \mu S = 0, \\ &\lambda_T S - (\mu+\alpha+\omega)L_T = 0, \\ &\alpha L_T - (\mu+\delta_T+\gamma)I_T = 0, \\ &\omega L_T + \gamma I_T - \mu R = 0, \end{aligned}$$

where $\lambda_T = \frac{\beta_1 I_T}{N}$. Solving this equation we have,

$$S^* = \frac{\Lambda}{\lambda_T^* + \mu}, \quad L_T^* = \frac{\lambda_T^* \Lambda}{k_1(\lambda_T^* + \mu)}, \quad I_T^* = \frac{\alpha\lambda_T^* \Lambda}{k_1 k_2(\lambda_T^* + \mu)}, \text{and} R^* = \frac{\lambda_T^* \Lambda(\omega k_2 + \alpha\gamma)}{k_1 k_2 \mu(\lambda_T^* + \mu)}.$$

The simplified expression for λ_T in terms of S^*, L_T^*, I_T^* and R^* becomes

$$\lambda_T^* = \frac{\alpha\beta_1\mu - k_1 k_2 \mu}{k_1 k_2 - \alpha\delta_T} = \frac{\alpha\beta_1\mu\left(1 - \frac{1}{R_0^T}\right)}{k_1 k_2 - \alpha\delta_T}.$$

Note that the endemic equilibrium point exists if and only if $R_0^T > 1$, since $k_1 k_2 - \alpha\delta_T > 0$.

Theorem 5.2.5. *The endemic equilibrium point of the TB sub-model (5.12) is globally asymptotically stable if $R_0^T > 1$.*

Proof. To proof this theorem, we define the following function:

$$V(S, L_T, I_T, R) = \frac{1}{2}\left((S - S^*) + (L_T - L_T^*) + (I_T - I_T^*) + (R - R^*)\right)^2.$$

Next we show that this function V is a Lyapunov function. Differentiating the function V with respect to time t, we obtain

$$\begin{aligned} \frac{dV}{dt} &= ((S - S^*) + (L_T - L_T^*) + (I_T - I_T^*) + (R - R^*))\left(\frac{dS}{dt} + \frac{dL_T}{dt} + \frac{dI_T}{dt} + \frac{dR}{dt}\right) \\ &= (N - \frac{\Lambda - \delta_T I_T^*}{\mu})(\Lambda - \delta_T I_T - \mu N) \leq (N - \frac{\Lambda}{\mu})(\Lambda - \mu N) \\ &\leq -\frac{(\Lambda - \mu N)^2}{\mu} \leq 0. \end{aligned}$$

For $R_0^T > 1$ the endemic equilibrium point exists. Thus, $\frac{dV}{dt} < 0$ implies that the function V is strictly Lyapunov function which deduce that the endemic equilibrium point is globally asymptotically stable. □

5.2.3 Analysis of the Coinfection Model

The equilibrium point of the coinfection model (5.1) is obtained by solving the system of equations (5.14):

$$\begin{aligned}
&\Lambda - (\lambda_T + \lambda_C + \mu)S = 0,\\
&\lambda_T S - (\mu + \alpha + \eta\lambda_C + \omega)L_T = 0,\\
&\alpha L_T + q\sigma L_{TC} + n\tau I_{TC} - (\mu + \theta + \delta_T + \gamma)I_T = 0,\\
&\lambda_C S - (\mu + \varepsilon\lambda_T + \varphi + \pi)E_C = 0,\\
&\varphi E_C + p\sigma L_{TC} + m\tau I_{TC} - (\mu + \delta_C + \nu + \psi)I_C = 0,\\
&\eta\lambda_C L_T + \varepsilon\lambda_T E_C - (\mu + \delta_C + \rho + \sigma)L_{TC} = 0,\\
&\rho L_{TC} + \theta I_T + \nu I_C - (\mu + \delta_{TC} + \tau)I_{TC} = 0,\\
&\omega L_T + \pi E_C + \gamma I_T + \psi I_C + (1 - (p+q))\sigma L_{TC} + (1 - (m+n))\tau I_{TC} - \mu R = 0,
\end{aligned} \tag{5.14}$$

where λ_T and λ_C are as given in equations (5.2) and (5.3) respectively. The disease-free equilibrium point (E_0) of the system becomes

$$E_0 = \left(\frac{\Lambda}{\mu}, 0, 0, 0, 0, 0, 0, 0\right).$$

In the following, we calculate the basic reproduction number (R_0) of the coinfection model. For this, we use the notation $X = (L_T, I_T, E_C, I_C, L_{TC}, I_{TC})$ to denote the vector functions:

$$\mathscr{F}(X) = \begin{bmatrix} \lambda_T S \\ 0 \\ \lambda_C S \\ 0 \\ 0 \\ 0 \end{bmatrix} \text{ and } \mathscr{V}(X) = \begin{bmatrix} (\mu + \alpha + \eta\lambda_C + \omega)L_T \\ (\mu + \theta + \delta_T + \gamma)I_T - \alpha L_T - q\sigma L_{TC} - n\tau I_{TC} \\ (\mu + \varepsilon\lambda_T + \varphi + \pi)E_C \\ (\mu + \nu + \delta_C + \psi)I_C - \varphi E_C - p\sigma L_{TC} - m\tau I_{TC} \\ (\mu + \delta_C + \rho + \sigma)L_{TC} - \eta\lambda_C L_T - \varepsilon\lambda_T E_C \\ (\mu + \delta_{TC} + \tau)I_{TC} - \rho L_{TC} - \theta I_T - \nu I_C \end{bmatrix},$$

representing the appearance of new infections, and the transfer of individuals into and out of the infected compartments, respectively. The Jacobian matrices of $\mathscr{F}(X)$ and $\mathscr{V}(X)$ at the

disease free equilibrium point E_0 are,

$$F = D\mathscr{F}(E_0) = \begin{bmatrix} 0 & \beta_1 & 0 & 0 & 0 & \beta_1 \\ 0 & 0 & 0 & 0 & 0 & 0 \\ 0 & 0 & \beta_2 & \beta_2 & \beta_2 & \beta_2 \\ 0 & 0 & 0 & 0 & 0 & 0 \\ 0 & 0 & 0 & 0 & 0 & 0 \\ 0 & 0 & 0 & 0 & 0 & 0 \end{bmatrix}, \text{ and}$$

$$V = D\mathscr{V}(E_0) = \begin{bmatrix} c_1 & 0 & 0 & 0 & 0 & 0 \\ -\alpha & c_2 & 0 & 0 & -q\sigma & -n\tau \\ 0 & 0 & c_3 & 0 & 0 & 0 \\ 0 & 0 & -\varphi & c_4 & -p\sigma & -m\tau \\ 0 & 0 & 0 & 0 & c_5 & 0 \\ 0 & -\theta & 0 & -\nu & -\rho & c_6 \end{bmatrix},$$

where $c_1 = \mu + \alpha + \omega$, $c_2 = \mu + \theta + \delta_T + \gamma$, $c_3 = \mu + \varphi + \pi$, $c_4 = \mu + \nu + \delta_C + \psi$, $c_5 = \mu + \delta_C + \rho + \sigma$, $c_6 = \mu + \tau + \delta_{TC}$. The next-generation matrix FV^{-1} is then given by

$$FV^{-1} = \begin{bmatrix} \frac{\alpha A_1}{c_1 B} & \frac{A_1}{B} & \frac{\varphi A_3}{c_3 B} & \frac{A_3}{B} & \frac{A_5}{c_5 B} & \frac{-\beta_1 c_4 (c_2 + n\tau)}{B} \\ 0 & 0 & 0 & 0 & 0 & 0 \\ \frac{\alpha A_2}{c_1 B} & \frac{A_2}{B} & \frac{A_4}{c_3 B} & \frac{-\beta_2 (c_2 (c_6 + \nu) - n\theta\tau}{B} & \frac{A_6}{c_5 B} & \frac{-\beta_2 c_2 (c_4 + m\tau))}{B} \\ 0 & 0 & 0 & 0 & 0 & 0 \\ 0 & 0 & 0 & 0 & 0 & 0 \\ 0 & 0 & 0 & 0 & 0 & 0 \end{bmatrix},$$

where

$$A_1 = -\beta_1 (c_4 c_6 + c_4\theta - m\nu\tau), \;\; A_2 = -\beta_2 \theta (c_4 + m\tau), A_3 = -\beta_1 \nu (c_2 + n\tau),$$
$$A_4 = -\beta_2 c_2 (c_4 c_6 + c_6\varphi + \nu\varphi - m\nu\tau) - n\theta\tau (c_4 + \varphi),$$
$$A_5 = -\beta_1 \left(c_4\rho (c_2 + \nu\tau) + c_4 q\sigma (c_6 + \theta) + c_2 p\nu\sigma + \nu\rho\tau (np - mq) \right),$$
$$A_6 = -\beta_2 \left(c_2 c_4 (c_6 + \rho) + c_2 m\tau (\rho - \nu) + c_2 p\sigma (c_6 + \nu) + q\sigma\theta (c_4 + m\tau) - n\theta\tau (c_4 + p\sigma) \right), \text{ and}$$
$$B = c_2 m\nu\tau + c_4 (n\theta\tau - c_2 c_6).$$

we obtained that four of the eigenvalues of the matrix FV^{-1} are equal to zero. The remaining eigenvalues are obtained from the reduced matrix $\begin{bmatrix} \frac{\alpha A_1}{c_1 B} & \frac{\varphi A_3}{c_3 B} \\ \frac{\alpha A_2}{c_1 B} & \frac{A_4}{c_3 B} \end{bmatrix}$. Thus, computing the

eigenvalues of FV^{-1} one can easily obtain that

$$\lambda_1 = \frac{c_1A_4 + \alpha c_3A_1 - \sqrt{D}}{2c_1c_3B}, \text{ and}$$
$$\lambda_2 = \frac{c_1A_4 + \alpha c_3A_1 + \sqrt{D}}{2c_1c_3B},$$

where, $D = \sqrt{\alpha^2c_3^2A_1^2 - 2\alpha c_1c_3A_1A_2 + 4\varphi\alpha c_1c_3A_2^2 + c_1^2A_4^2}$. We can observe that $\lambda_2 \geq \lambda_1$. Hence, the basic reproduction number R_0 of the coinfection model (5.1) is given by

$$R_0 = \frac{c_1A_4 + \alpha c_3A_1 + \sqrt{D}}{2c_1c_3B}.$$

Local Stability Analysis of the Disease-free Equilibrium Point E_0

The local stability analysis of the disease-free equilibrium point for the coinfection model is analyzed using the method of linearization. The Jacobean matrix of the model equation (5.1) at disease-free equilibrium point E_0 represented as

$$J(E_0) = \begin{pmatrix} -\mu & 0 & -\beta_1 & -\beta_2 & -\beta_2 & -\beta_2 & -\beta_1-\beta_2 & 0 \\ 0 & -c_1 & \beta_1 & 0 & 0 & 0 & \beta_1 & 0 \\ 0 & \alpha & -c_2 & 0 & 0 & q\sigma & n\tau & 0 \\ 0 & 0 & 0 & \beta_2-c_3 & \beta_2 & \beta_2 & \beta_2 & 0 \\ 0 & 0 & 0 & \varphi & -c_4 & p\sigma & m\tau & 0 \\ 0 & 0 & 0 & 0 & 0 & -c_5 & 0 & 0 \\ 0 & 0 & \theta & 0 & \nu & \rho & -c_6 & 0 \\ 0 & \omega & \gamma & \pi & \psi & (1-(p+q))\sigma & (1-(m+n))\tau & -\mu \end{pmatrix} \tag{5.15}$$

The local asymptotic stability of E_0 is analyzed based on the sign of the eigenvalues. Expanding the characteristic equation $|\lambda I_8 - J(E_0)| = 0$ with the first and eighth columns, and the sixth row, we obtain three eigenvalues $\lambda_{1,2} = -\mu$, and $\lambda_3 = -c_5$. Further, we obtain the remaining five eigenvalues from the characteristic equation of the reduced matrix

$$(J_5 - \lambda I_5) = \begin{pmatrix} -c_1-\lambda & \beta_1 & 0 & 0 & \beta_1 \\ \alpha & -c_2-\lambda & 0 & 0 & n\tau \\ 0 & 0 & \beta_2-c_3-\lambda & \beta_2 & \beta_2 \\ 0 & 0 & \varphi & -c_4-\lambda & m\tau \\ 0 & \theta & 0 & \nu & -c_6-\lambda \end{pmatrix}.$$

Here, the characteristic polynomial is computed using elementary row operations method (Willis, 2005). Thus, the row reduced form of the matrix becomes

$$\begin{pmatrix} \alpha & -c_2-\lambda & 0 & 0 & n\tau \\ 0 & \theta & 0 & \nu & -c_6-\lambda \\ 0 & 0 & \varphi & -c_4-\lambda & m\tau \\ 0 & 0 & 0 & \beta_2+\frac{(\beta_2-c_3-\lambda)(c_4+\lambda)}{\varphi} & \beta_2+\frac{(\beta_2-c_3-\lambda)(c_4+\lambda)}{\varphi} \\ 0 & 0 & 0 & 0 & \beta_1(1+\frac{c_6+\lambda}{\theta})+\frac{c_2+\lambda}{\alpha}\left(n\tau-\frac{(c_2+\lambda)(c_6+\lambda)}{\theta}\right) \end{pmatrix}.$$

Hence, the characteristic polynomial of our matrix is the product of the diagonal entries times $(-1)^k$, where k is the number of row swaps. We perform three row swaps, so that the characteristic polynomial is

$$\mathscr{X}_5(\lambda) = -\alpha\theta\varphi\left(\beta_2+\frac{(\beta_2-c_3-\lambda)(c_4+\lambda)}{\varphi}\right)\left[\beta_1(1+\frac{c_6+\lambda}{\theta})+\frac{c_2+\lambda}{\alpha}\left(n\tau-\frac{(c_2+\lambda)(c_6+\lambda)}{\theta}\right)\right].$$

Simplifying it gives,

$$\mathscr{X}_5(\lambda) = -\left(\beta_2\varphi+c_4(\beta_2-c_3)+(\beta_2-c_3-c_4)\lambda-\lambda^2\right)$$

$$\left[\alpha\beta_1(\theta+c_6)+c_1(n\tau\theta-c_2c_6)+(\alpha\beta_1+n\tau\theta-c_2c_6-c_1(c_2+c_6))\lambda+(c_2+c_6-c_1)\lambda^2-\lambda^3\right].$$

That is, the eigenvalues are the solutions of the characteristic equation

$$\mathscr{X}_5(\lambda) = \lambda^5+D_1\lambda^4+D_2\lambda^3+D_3\lambda^2+D_4\lambda+D_5 = 0, \tag{5.16}$$

where,

$$\begin{aligned}
D_1 &= (\beta_2+c_2+c_6-(c_3+c_4+c_1)),\\
D_2 &= \beta_2\varphi+c_4(\beta_2-c_3)-(\beta_2-c_3-c_4)(c_2+c_6-c_1)+(\alpha\beta_1+n\tau\theta-c_2c_6-c_1(c_2+c_6)),\\
D_3 &= \alpha\beta_1(\theta+c_6)+c_1(n\tau\theta-c_2c_6)-(\beta_2\varphi+c_4(\beta_2-c_3))(c_2+c_6-c_1)-\\
&\quad(\beta_2-c_3-c_4)(\alpha\beta_1+n\tau\theta-c_2c_6-c_1(c_2+c_6)),\\
D_4 &= -(\beta_2\varphi+c_4(\beta_2-c_3))(\alpha\beta_1+n\tau\theta-c_2c_6-c_1(c_2+c_6))-\\
&\quad(\beta_2-c_3-c_4)(\alpha\beta_1(\theta+c_6)+c_1(n\tau\theta-c_2c_6)), \text{ and}\\
D_5 &= (\beta_2\varphi+c_4(\beta_2-c_3))\left(\alpha\beta_1(\theta+c_6)+c_1(n\tau\theta-c_2c_6)\right).
\end{aligned}$$

Thus, using the Routh-Hurwitz stability criterion, the roots of the equation (5.16) have negative real parts if the following condition holds.

$$\begin{cases} D_i > 0, \text{ for all } i = 1,...,5,\ D_1D_2D_3 > D_3^2+D_1^2D_4, \text{ and} \\ (D_1D_4-D_5)(D_1D_2D_3-D_3^2-D_1^2D_4) > D_5(D_1D_2-D_3)^2+D_1D_5^2 \end{cases} \tag{5.17}$$

Hence, we have proved the following result.

Theorem 5.2.6. *The disease-free equilibrium point of the coinfection model (5.1) is locally asymptotically stable if the condition given in equation (5.17) holds.*

Global Stability of Disease-free Equilibrium (E_0)

Let us rewrite the coinfection model (5.1) as

$$\begin{cases} \frac{dX}{dt} = F(X,Z) \\ \frac{dZ}{dt} = G(X,Z), \quad G(X,0) = 0. \end{cases} \tag{5.18}$$

where $X = (S,R)$ and $Z = (L_T, I_T, E_C, I_C, L_{TC}, I_{TC})$. Here, the components of $X \in \mathbb{R}^2_+$ denotes the number of uninfected individuals while $Z \in \mathbb{R}^6_+$ represents the number of infected ones. The disease-free equilibrium is denoted now as

$$U_0 = (X_0, 0), \text{ where, } X_0 = (\frac{\Lambda}{\mu}, 0).$$

The conditions (H_1) and (H_2) of the method in (Castillo-Chavez et al., 2002) must be met to guarantee global asymptotically stability of the disease free equilibrium point.

From coinfection model (5.1), we have

$$\frac{dX}{dt} = F(X,Z) = \begin{bmatrix} \Lambda - (\lambda_T + \lambda_C + \mu)S \\ \omega L_T + \pi E_C + \gamma I_T + \psi I_C + (1-(p+q))\sigma L_{TC} + (1-(m+n))\tau I_{TC} - \mu R \end{bmatrix},$$

Hence,

$$F(X,0) = \begin{bmatrix} \Lambda - \mu S \\ 0 \end{bmatrix},$$

and

$$\frac{dZ}{dt} = G(X,Z) = \begin{bmatrix} \lambda_T S - (\mu + \alpha + \eta\lambda_C + \omega)L_T \\ \alpha L_T + q\sigma L_{TC} + n\tau I_{TC} - (\mu + \theta + \delta_T + \gamma)I_T \\ \lambda_C S - (\mu + \varepsilon\lambda_T + \varphi + \pi)E_C \\ \varphi E_C + p\sigma L_{TC} + m\tau I_{TC} - (\mu + \delta_C + \nu + \psi)I_C \\ \eta\lambda_C L_T + \varepsilon\lambda_T E_C - (\mu + \delta_C + \rho + \sigma)L_{TC} \\ \rho L_{TC} + \theta I_T + \nu I_C - (\mu + \delta_{TC} + \tau)I_{TC} \end{bmatrix}.$$

Therefore,

$$A = D_Z G(U_0, 0) = \begin{bmatrix} -c_1 & \beta_1 & 0 & 0 & 0 & \beta_1 \\ \alpha & -c_2 & 0 & 0 & q\sigma & n\tau \\ 0 & 0 & \beta_2 - c_3 & \beta_2 & \beta_2 & \beta_2 \\ 0 & 0 & \varphi & -c_4 & p\sigma & m\tau \\ 0 & 0 & 0 & 0 & -c_5 & 0 \\ 0 & \theta & 0 & \nu & \rho & -c_6 \end{bmatrix} \text{ which is a Metzler Matrix.}$$

Here, $\hat{G}(X,Z) = AZ - G(X,Z)$, and hence,

$$\hat{G}(X,Z) = \begin{bmatrix} \hat{G}_1(X,Z) \\ \hat{G}_2(X,Z) \\ \hat{G}_3(X,Z) \\ \hat{G}_4(X,Z) \\ \hat{G}_5(X,Z) \\ \hat{G}_6(X,Z) \end{bmatrix} = \begin{bmatrix} \eta\lambda_C L_T + \beta_1(I_T + I_{TC}) - \lambda_T S \\ 0 \\ \beta_2(E_C + I_C + L_{TC} + I_{TC}) + \varepsilon\lambda_T E_C - \lambda_C S \\ 0 \\ -\eta\lambda_C L_T - \varepsilon\lambda_T E_C \\ 0 \end{bmatrix}.$$

Thus, $\hat{G}_5(X,Z) = -\eta\lambda_C L_T - \varepsilon\lambda_T E_C < 0$. This shows that condition (H2) is not satisfied. As a result, U_0 and then the disease-free equilibrium point E_0 can not be globally asymptotically stable. This indicate that a backward bifurcation may occur at $R_0 = 1$, which means a stable endemic equilibrium co-exists with a stable disease-free equilibrium when the basic reproduction number is less than unity.

In the following, we comparatively study the impact of each disease via their reproduction number. For this, first we analyze the contribution of tuberculosis on the spread of COVID-19 in the community.

5.2.4 Impacts of TB on COVID-19

The basic reproduction number for the COVID-19 only sub-model is given by:

$$R_0^C = \frac{\beta_2(\mu + \delta_C + \psi + \varphi)}{(\mu + \varphi + \pi)(\mu + \delta_C + \psi)}. \tag{5.19}$$

Likewise, the basic reproduction number for TB only sub-model is given as

$$R_0^T = \frac{\beta_1\alpha}{(\mu + \alpha + \omega)(\mu + \delta_T + \gamma)}. \tag{5.20}$$

To analyze the impact of the TB disease in facilitating COVID-19 pandemic, we began by expressing the basic reproduction numbers R_0^C in terms of R_0^T (Okosun and Makinde,

2014). Expressing the parameter μ in the equation (5.20) in terms of R_0^T, we have

$$R_0^T = \frac{\beta_1 \alpha}{(\mu + k_1)(\mu + k_2)}, \quad \text{where } k_1 = \alpha + \omega,\ k_2 = \delta_T + \gamma.$$

Solving for μ and simplifying it we obtain

$$\mu = \frac{\sqrt{R_0^T \left((k_1 - k_2)^2 R_0^T + 4\alpha\beta_1 \right)} - (k_1 + k_2) R_0^T}{2R_0^T}.$$

Substituting this value of μ in R_0^C (in the equation (5.19)), we obtain R_0^C in terms of R_0^T as

$$R_0^C = \frac{\beta_2 R_0^T \left(h_1 + \frac{\sqrt{h_2}}{2} \right)}{\left(\frac{\sqrt{h_2}}{2} + (\varphi + \psi) R_0^T - \frac{(k_1+k_2)R_0^T}{2} \right) \left(\frac{\sqrt{h_2}}{2} + (\delta_C + \psi) R_0^T - \frac{(k_1+k_2)R_0^T}{2} \right)}$$

where, $h_1 = R_0^T \left((\delta_C + \varphi + \psi) - \frac{k_1+k_2}{2} \right)$, and $h_2 = R_0^T \left((k_1 - k_2)^2 R_0^T + 4\alpha\beta_1 \right)$.
The partial derivative of R_0^C with respect to R_0^T is then given by

$$\frac{\partial R_0^C}{\partial R_0^T} = \frac{\beta_2 R_0^T \left(h_1\sqrt{h_2} + h_3 + h_4 \right) \left(\sqrt{h_2}(k_1 + k_2) - (k_1 - k_2)^2 R_0^T - 2\alpha\beta_1 \right)}{2\sqrt{h_2} \left(\frac{\sqrt{h_2}}{2} + (\varphi + \psi) R_0^T - \frac{(k_1+k_2)R_0^T}{2} \right)^2 \left(\frac{\sqrt{h_2}}{2} + (\delta_C + \psi) R_0^T - \frac{(k_1+k_2)R_0^T}{2} \right)^2}$$

with $h_3 = \left(\varphi^2 + (\pi + \delta_C + \psi)\varphi + (\delta_C + \psi)^2 \right) \left(R_0^T \right)^2$, and

$$h_4 = R_0^T \left(\frac{\left(k_1^2 + k_2^2 \right) R_0^T + 2\alpha\beta_1}{2} - (k_1 + k_2)(\delta_C + \varphi + \psi) R_0^T \right)$$

Here, we observe $\frac{\partial R_0^C}{\partial R_0^T}$ is positive which implies that the expansion of TB infection exacerbates the pandemic of COVID-19 in the community. This means, the increases of TB infection in the community positively influence the spread of COVID-19.

Remark 5.2.1. *If $\frac{\partial R_0^C}{\partial R_0^T} = 0$, the expansion of TB in the community have no significant impact on the spread of COVID-19. In the contrary, when $\frac{\partial R_0^C}{\partial R_0^T} < 0$, the increase in TB epidemic negatively influences the spread of COVID-19.*

5.2.5 Impacts of COVID-19 on TB

In this subsection, we study the role of COVID-19 pandemic on the expansion of TB epidemic. For this, we write the expression of R_0^T in terms of R_0^C and identify the sign of the partial derivative of R_0^T with respect to R_0^C. For R_0^C given in equation (5.19), we have

$$R_0^C = \frac{\beta_2(\mu + a_1 + \varphi)}{(\mu + \varphi + \pi)(\mu + a_1)}, \quad \text{where } a_1 = \delta_C + \psi.$$

Simplifying and writing the equation as a function of μ, we obtain:

$$\mu = \frac{\sqrt{h_5} - (\pi + \varphi + a_1) R_0^C + \beta_2}{2R_0^C}$$

where, $h_5 = (\pi + \varphi - a_1)^2 (R_0^C)^2 + 2\beta_2 (\varphi + a_1 - \pi) R_0^C + {\beta_2}^2$.
Substituting the expression μ in $R_0^T = \frac{\beta_1 \alpha}{(\mu + k_1)(\mu + k_2)}$, we have the following expression for R_0^T in terms of R_0^C.

$$R_0^T = \frac{4\alpha\beta_1 (R_0^C)^2}{\left(\sqrt{h_5} - (\pi + \varphi + a_1) R_0^C + \beta_2 + 2R_0^C k_1\right)\left(\sqrt{h_5} - (\pi + \varphi + a_1) R_0^C + \beta_2 + 2R_0^C k_2\right)}.$$

The simplified form for the partial derivative of R_0^T with respect to R_0^C is then given by:

$$\frac{\partial R_0^T}{\partial R_0^C} = \frac{8\alpha R_0^C \beta_1 \beta_2 \left(\sqrt{h_5} + R_0^C (\varphi + a_1 - \pi) + \beta_2\right)\left(\sqrt{h_5} + (k_1 + k_2 - (\pi + \varphi + a_1)) R_0^C + \beta_2\right)}{\sqrt{h_5}\left(\sqrt{h_5} - (\pi + \varphi + a_1 - 2k_1) R_0^C + \beta_2\right)^2 \left(\sqrt{h_5} - (\pi + \varphi + a_1 - 2k_2) R_0^C + \beta_2\right)^2}.$$

Observe that the denominator of the expression $\frac{\partial R_0^T}{\partial R_0^C}$ is always positive, and the numerator is positive if $\varphi + a_1 > \pi$ and $k_1 + k_2 > (\pi + \varphi + a_1)$. Hence, an increase in the number of COVID-19 infected individuals has a positive impact for the spread of TB disease.

5.3 Numerical Simulation

In the previous sections, we have discussed the analytical behaviors of the model equation (5.1) and the sub-models. In the following, we perform numerical solutions of sub-models as well as the coinfection model. The solutions of the system equations are integrated using the ode45 solver in MATLAB. To do so first we estimate and appropriately assume the parameter values of the model.

5.3.1 Parameter Estimation

In this subsection, we estimate the parameter values of the model from the real Ethiopian data of cumulative infected cases of TB and COVID-19. The data for COVID-19 is collected monthly from the initial report month of March, 2020 to March, 2022, which is available on the source (J.H.University, 2022). Beside, the TB data is collected yearly from 2010 to 2020 available online at the source (Stop-TB-Partnership, 2020). To fit the model and estimate the parameters to the data, we used a least square and Bayesian combined method, described as

in the algorithm 1, and nonlinear curve fitting method with the help of 'fminsearch', builtin MATLAB function. Some of the parameter values are estimated from literature: according to the data by Worldometer, the Ethiopian average life expectancy at birth for the year 2020 is 67.07 (Macrotrends; Deressa and Duressa, 2021) and we use a sub-total population of 5160563. Therefore, the natural death rate of individuals per month is estimated as the reciprocal of the life expectancy at birth in time months, which is given by $\mu = \frac{1}{67.08\times 12} = 0.0012$. We approximated the recruitment rate from $\frac{\Lambda}{\mu}$ give the initial population to obtain $\Lambda = 6193$ individuals per month. Due to the scarcity of the coinfection data, some co-infected related parameters are assumed and the others are estimated with the real data. In the estimation process, we use the initial conditions of the state variables as given in Table 5.2.

Table 5.2: The initial values for the coinfection model state variables.

State variable	S	L_T	I_T	E_C	I_C	E_{TC}	I_{TC}	R
Initial Values	4605410	300000	235000	96	26	25	6	20000

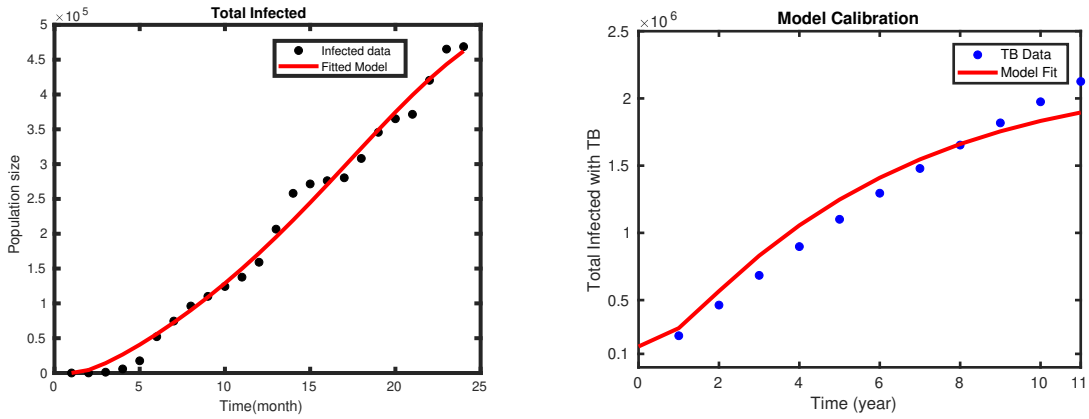

(a) COVID-19 Fitted

(b) TB Fitted

Figure 5.3: Model fitting using reported data of COVID-19 and TB

Figure 5.3 shows the fitting of the infected COVID-19, and infected TB population of the proposed model. Figure 5.3a depicts the fitting of the infected COVID-19 model output to the observed data of COVID-19 infected population. Furthermore, the fitting of observed data for the TB infected population with the model simulation is seen in 5.3b. In both cases, continuous lines depict the output of the model simulation, while the dotted lines act for the actual observed data of the two diseases taken from Ethiopia. We saw that the model simulation and the actual data are fitted very well. The estimated parameter values are given Table 5.3. The assumed values of the parameters are taken same with the coinfection of malaria and COVID-19 in (Tchoumi et al., 2021) for our simulation purpose.

Table 5.3: Parameter values of the coinfection model

Parameter	Value	Source	parameter	Value	Source
Λ	6193	calculated	μ	0.0012	calculated
β_1	3.75	fitted	β_2	0.4372	fitted
φ	1.60	fitted	θ	0.1229	assumed
δ_C	0.009	fitted	δ_t	0.0018	fitted
ψ	0.1393	fitted	α	0.0039	fitted
η	1.01	assumed	σ	1.3523	assumed
ε	1.06	assumed	ν	0.0299	assumed
τ	0.0422	assumed	δ_{tc}	0.002	assumed
ρ	1.1148	assumed	π	0.20	fitted
ω	0.0244	fitted	γ	0.0031	fitted

5.3.2 Numerical Simulation of COVID-19 Sub-model

The analytical findings of the sub-model (5.4) is illustrated in section 5.2.1. Next, we present the numerical solutions using initial conditions for state variables $S(0) = 5140441$, $E_C(0) = 96$, $I_C(0) = 26$, $R(0) = 2$ and the parameter values described in Table 5.3.

Figure 5.4 presents the solution of the COVID-19 sub-model using the parameter values described in the caption. The basic reproduction number is obtained as $R_0^C = 0.499$, which implies the disease free equilibrium point is stable and no endemic equilibrium point exists. Using different initial conditions for each compartment, all solution curves converge to the disease-free equilibrium point as seen in Figure 5.5. In Figure 5.5a-5.5c, the susceptible populations approaches to the value of $\frac{\Lambda}{\mu}$, while the other compartments go to zero, which supports our analytical findings in the previous sections.

Figure 5.6 illustrates the time serious plot of the COVID-19 sub-model, for which its basic reproduction number is greater than unity. In the analytical findings, we have shown that the disease-free equilibrium point is unstable and the endemic equilibrium point is stable. Using different initial conditions for each compartment, all solution curves converge to the endemic equilibrium point as seen for the susceptible, infected, and recovered plots of Figure 5.7. As time goes, in Figures 5.7a, 5.7c, and 5.7b, the solutions close to the endemic equilibrium point given in equation (5.11) which agrees with the analytical properties.

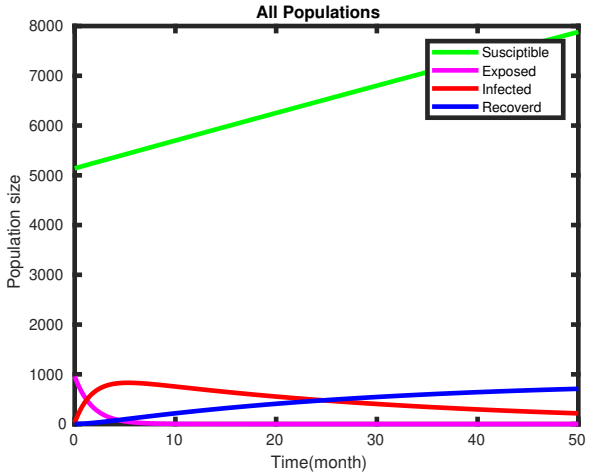

Figure 5.4: Solutions of COVID-19 sub-model with parameter values $\mu = 0.012$, $\beta_2 = 0.03324$ and other parameters given in Table 5.3 with its basic reproduction number is $R_0^C = 0.499 < 1$

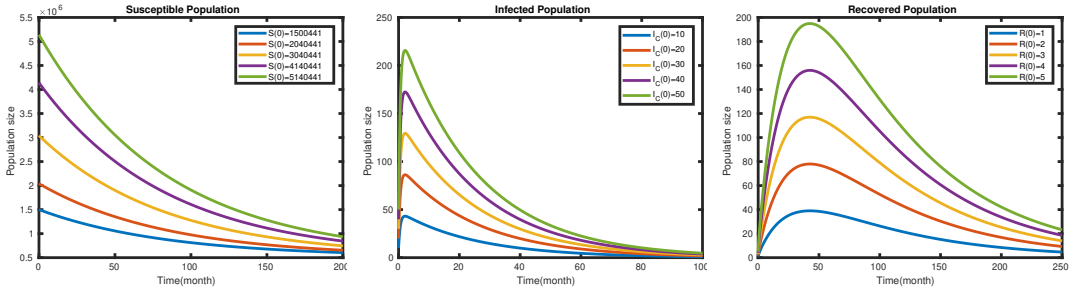

(a) Susceptible (b) Infected (c) Recovered

Figure 5.5: The solution curves of the susceptible, infected and recovered populations for different initial values of the COVID-19 sub-model with $R_0^C = 0.499 < 1$.

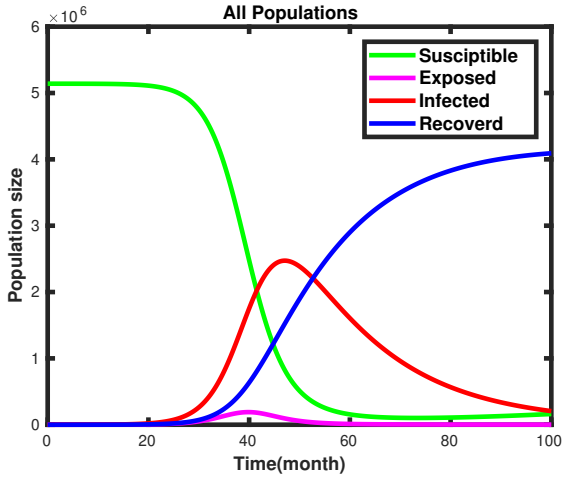

Figure 5.6: Solutions of COVID-19 sub-model with parameter values given in Table 5.3 and its basic reproduction number is $R_0^C = 5.3859 > 1$

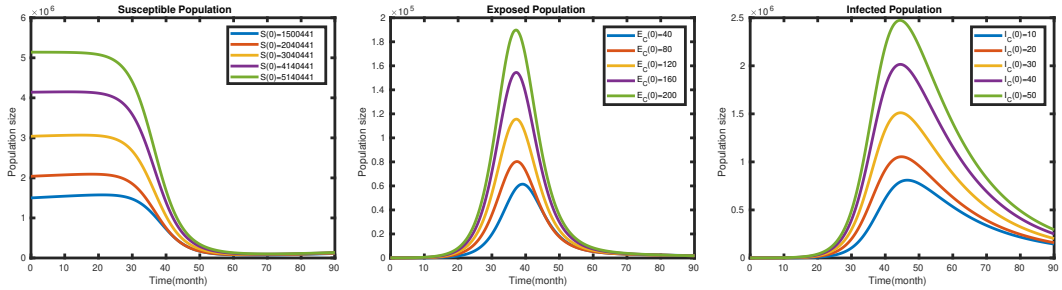

(a) Susceptible (b) Exposed (c) Infected

Figure 5.7: The stable solution curves of the susceptible, infected and recovered populations for different initial values of the COVID-19 sub-model use parameter values of the figure (5.6) in which its basic reproduction number is greater than unity ($R_0^C = 5.3859$).

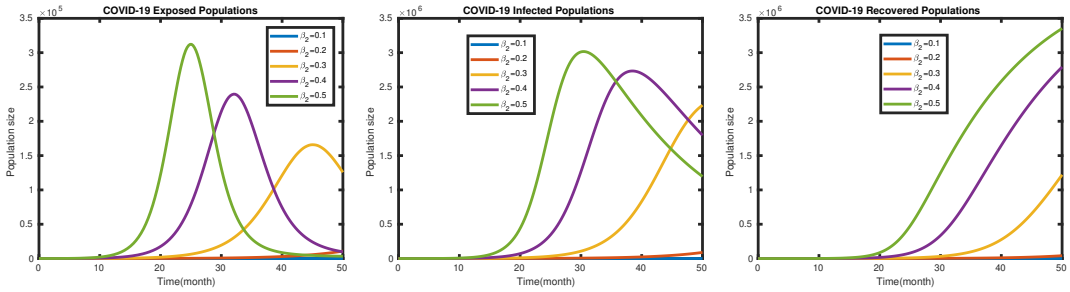

(a) Exposed (b) Infected (c) Recovered

Figure 5.8: The effect of the transmission rate (β_2) for COVID-19 sub-model.

Figures 5.8 and 5.9 show the effects of the COVID-19 transmission rate and the recovery rate of the COVID-19 infected individuals. The parameter values used in the simulation of the figures are as of Table 5.3 with varying β_2 in Figure 5.8, and varying ψ in Figure 5.9. When the transmission rates are increasing, the populations (exposed, infected, and recovered) also increase accordingly. If there are low contact rates, then the exposed and infected individuals are low and as a result, the number of recovered individuals is also low.

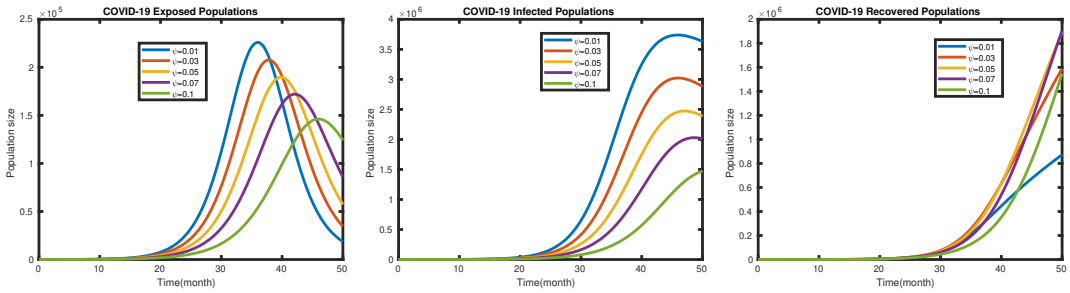

(a) Exposed (b) Infected (c) Recovered

Figure 5.9: The effect of the recovery rate of infected individuals (ψ) for COVID-19 sub-model.

5.3.3 Numerical Solutions of TB Sub-model

The numerical solutions of the TB sub-model with the basic reproduction number of $R_0^T = 2.263$, are given in Figure 5.10. The solutions are executed using the given data as initial conditions of the state variables $S(0) = 4605563$, $L_T(0) = 300000$, $I_T(0) = 235000$, $R(0) = 20000$. We observe that all solution curves approaches to their endemic equilibrium point. This supports the analytical results that corresponds to $R_0^T > 1$, where the endemic equilibrium point of TB sub-model is globally asymptotically stable. Figures 5.11 shows the impact of the contact rate (β_1) of TB endemic. As it increases, the number of individuals in the compartments, Latent TB, active TB, and recovered ones are also increasing. If there is a low contact rate, then the transmission of TB disease decrease.

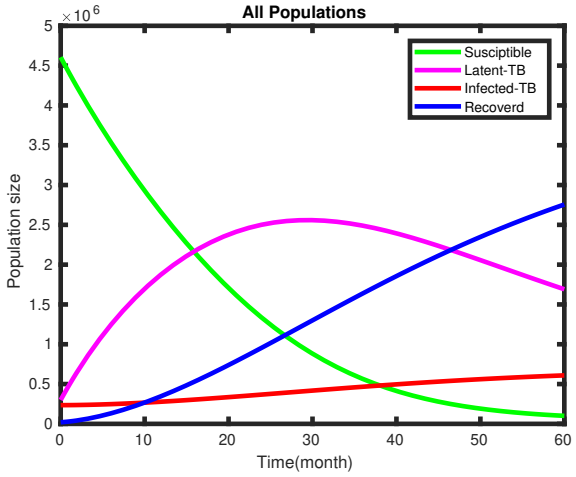

Figure 5.10: Solutions of TB sub-model with its parameter values given in Table 5.3 and its basic reproduction number is $R_0^T = 2.263 > 1$.

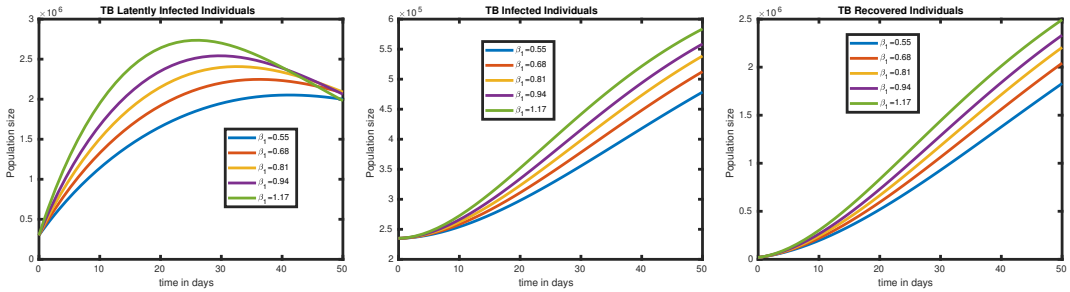

(a) Latent TB (b) Infected TB (c) Recovered

Figure 5.11: The impact of the contact rate of individuals (β_1) for TB sub-model, with other parameter values described in figure (5.10).

5.3.4 Numerical Solutions of the Coinfection Model

In this subsection, we present the numerical solutions of the coinfection model (5.1). In doing so, we use initial values of the state variables for the coinfection model given in Table

5.2 and all parameter values are illustrated in the Table 5.3.

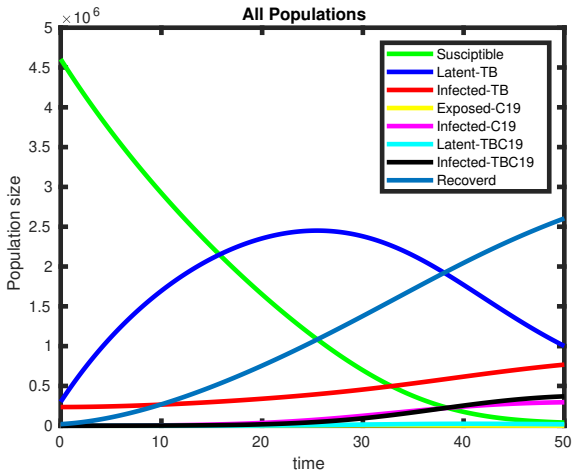

Figure 5.12: Solutions of coinfection model (5.1), with parameter values as given in Table 5.3.

The time series graphs for the numerical solutions of the coinfection model (5.1) are plotted in Figure 5.12 with parameter values given in Table 5.3.

Figure 5.13 displays the impact of transferring rates to co-infected with TB and COVID-19 from each actively infected individual of the two diseases. In Figure 5.14, we have shown that the impact of contact rates of the disease with infected compartments of system (5.1). Thus, we conclude that the states I_T, I_C, L_{TC}, and I_{TC} increase as the transmission coefficients increases.

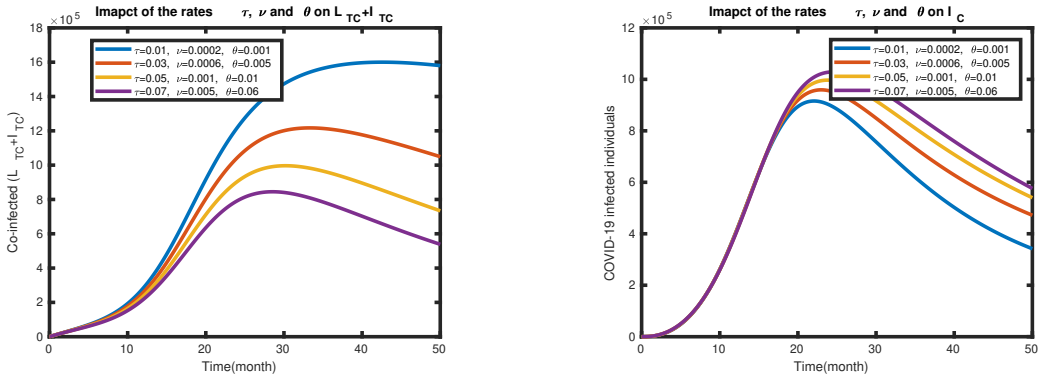

(a) Co-infected

(b) Infected COVID-19

Figure 5.13: Impacts of τ,ν and θ on the co infected classes ($L_{TC}+I_{TC}$) and on the COVID-19 infected class (I_C).

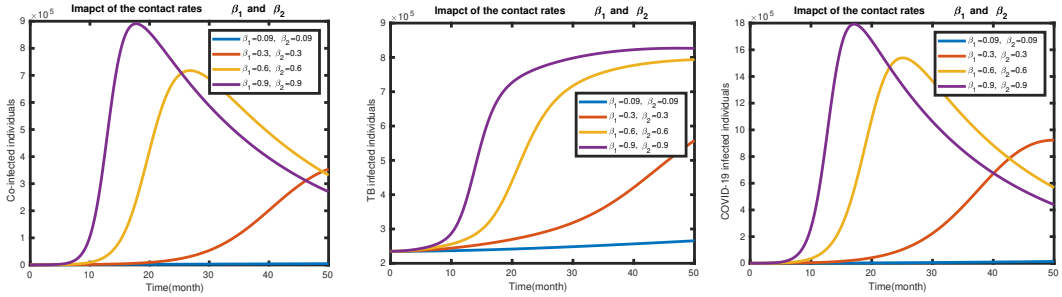

(a) Co-infected (b) Infected TB (c) Infected COVID-19

Figure 5.14: Impacts of the contact rates β_1 and β_2 on the transmission dynamics of infected TB (I_T), infected COVID-19(I_C) and the co-infected ones (I_{TC}).

The impact of the rates (σ and τ) at which individuals leave the co-infected classes L_{TC} and I_{TC} are illustrated in Figure 5.15. It was shown that an increase in the leaving rate of the compartment decreases the number of co-infected individuals. The rates σ and τ are the transfer rates of the two classes of individuals to other compartments through treatments or natural recoveries. In Figure 5.15a, as the transfer rate decreases from 1.5 to 0.5, the number of latent TB individuals co-infected with symptomatic COVID-19 increases, and then decreases to stabilizes at some level. Similarly, if the rate τ is half, then the number of TB and COVID-19 co-infected people initially increases to a stable value of some levels as time goes. But we can observe from Figure 5.15b, as the transfer rate decreases from 0.5 to 0.003, the number of individuals who get co-infected with the two diseases increases, and stabilizes to some level.

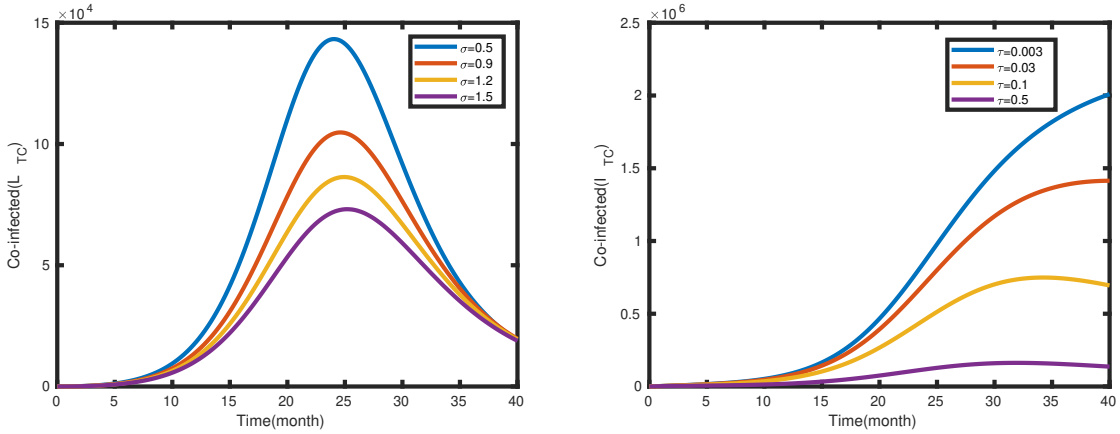

(a) Co-infected (L_{TC}) (b) Co-infected (I_{TC})

Figure 5.15: The dynamics of L_{TC} and I_{TC} individuals with the values of σ and τ as given in the legend.

In Sections 5.1-5.3 we proposed and analyzed a mathematical model for the co-dynamics of COVID-19 and TB both qualitatively and numerically. The sections presented a model to study and understand certain characteristics of coinfection without giving ways to interfere and prevent the disease induced burden.

5.4 Extension of the Model into Optimal Control Problem

We extend the model proposed in (5.1) via incorporating four control functions $u_1(t)$, $u_2(t)$, $u_3(t)$ and $u_4(t)$ to reduce coinfection induced burdens. The control functions are defined as follows:

(a) $u_1(t)$ denotes prevention measures against TB. The prevention measure includes: keeping the immune system healthy, avoiding exposure to someone with active TB, vaccination of children, improving ventilation in indoor spaces, isolation of TB infected individuals, screening those at high risk, and early detection,

(b) $u_2(t)$ represents the prevention techniques against COVID-19 which comprise: wearing a mask, keeping physical distance, contact tracing, keeping personal hygiene (handwashing), and vaccination that helps to reduce contact rate,

(c) $u_3(t)$ stands for the treatment of infected individuals with TB through intensive medical care,

(d) $u_4(t)$ represents medical care measures for COVID-19 infected individuals.

Precisely, the governing control induced mathematical model is given by a system of nonlinear ordinary differential equations:

$$\begin{aligned}
\frac{dS}{dt} &= \Lambda - ((1-u_1)\lambda_T + (1-u_2)\lambda_C + \mu)\,S,\\
\frac{dL_T}{dt} &= (1-u_1)\lambda_T S - (\mu + \alpha + \eta(1-u_2)\lambda_C + \omega)L_T,\\
\frac{dI_T}{dt} &= \alpha L_T + q\sigma L_{TC} + n\tau I_{TC} - (\mu + \theta + \delta_T + \gamma + u_3)I_T,\\
\frac{dE_C}{dt} &= (1-u_2)\lambda_C S - (\mu + \varepsilon(1-u_1)\lambda_T + \varphi + \pi)E_C,\\
\frac{dI_C}{dt} &= \varphi E_C + p\sigma L_{TC} + m\tau I_{TC} - (\mu + \delta_C + \nu + \psi + u_4)I_C,\\
\frac{dL_{TC}}{dt} &= \eta(1-u_2)\lambda_C L_T + \varepsilon(1-u_1)\lambda_T E_C - (\mu + \delta_C + \rho + \sigma + u_4)L_{TC},\\
\frac{dI_{TC}}{dt} &= \rho L_{TC} + \theta I_T + \nu I_C - (\mu + \delta_{TC} + \tau + u_3 + u_4)I_{TC},\\
\frac{dR}{dt} &= \omega L_T + \pi E_C + (\gamma + u_3)I_T + (\psi + u_4)I_C + ((1-(p+q))\sigma + u_4)L_{TC}\\
&\quad + ((1-(m+n))\tau + u_3 + u_4)I_{TC} - \mu R.
\end{aligned} \tag{5.21}$$

where,

$$\lambda_T(t) = \frac{\beta_1}{N(t)}\left(I_T(t) + I_{TC}(t)\right), \tag{5.22}$$

$$\lambda_C(t) = \frac{\beta_2}{N(t)}\left(E_C(t) + I_C(t) + L_{TC}(t) + I_{TC}(t)\right). \tag{5.23}$$

The goal is to find the optimal values of the control functions $u = (u_1, u_2, u_3, u_4)$ so that the associated states are the solution of governing system (5.21) satisfying the corresponding initial conditions and at the same time minimize the objective functional. Here, we need to minimize infected populations with TB, COVID-19, TB and COVID-19 coinfection and cost incurred due to intervention. With this aim, we define the integral objective functional for the minimization problem as

$$J(u) = \min_{u} \int_0^{t_f} \left[w_1 I_T(t) + w_2 I_C(t) + w_3 L_{TC}(t) + w_4 I_{TC}(t) + \frac{1}{2} \sum_{i=1}^{4} b_i u_i^2 \right] dt \tag{5.24}$$

subject to the constraint given in (5.21) with the same initial data. Integrals are natural expressions of many systems where the accumulation of a quantity is maximized or minimized. The parameters b_i, $i = 1,2,3,4$ measure relative cost of the interventions associated with the controls u_i, $i = 1,2,3,4$, while the coefficients w_i, $i = 1,2,3,4$ represent the weight constants corresponds to infected individuals that can be chosen to balance cost factors. The four control functions $u_1(t)$, $u_2(t)$, $u_3(t)$ and $u_4(t)$ are assumed as bounded and Lebesgue integrable functions. Besides, in the cost functional, the term $w_1 I_T(t)$ describes the cost related to infected TB, $w_2 I_C(t)$ express the cost associated with COVID-19 infected population, while $w_3 L_{TC}(t)$ represent the cost allied to latent TB infected individuals co-infected with COVID-19, and $w_4 I_{TC}(t)$ denotes the cost incurred due to coinfection of TB and COVID-19. Furthermore, the fixed constant t_f denotes the final intervention time. The integrand is defined in quadratic form since we assumed that costs are non-linear in its nature. Thus, we are going to find an optimal control $u^* = (u_1^*, u_2^*, u_3^*, u_4^*)$ such that:

$$J(u^*) = \min J(u) | u = (u_1, u_2, u_3, u_4) \in \Gamma \tag{5.25}$$

and the associated state trajectories solve the system (5.21). Here, Γ denotes an admissible control set defined by:

$$\Gamma = \{(u_1, u_2, u_3, u_4) | u_i \text{ are measurable with } 0 \leq u_i(t) \leq 1 \ , t \in [0, t_f], i = 1,2,3,4\}$$

The lower bounds for u_i, $i = 1,2,3,4$ corresponds to no control interventions are taken while the upper bounds assumed to be the maximum effort exerted to minimize the epidemic and related costs.

5.4.1 Existence of Optimal Controls

Here, observe that all the solutions to state system (5.21) are bounded in $\mathbb{R}_+^8$ and the objective functional is convex with respect to the control functions. Hence, the existence and uniqueness of optimal controls to the control induced model is a direct result of Theorem 4.1 given in (Fleming and Rishel, 2012). Thus, we have the following result.

Theorem 5.4.1. *For $t \in [0, t_f]$, there exist optimal controls $u^* = (u_1^*, u_2^*, u_3^*, u_4^*)$ with a corresponding state solution $(S^*, L_T^*, I_T^*, E_c^*, I_C^*, L_{TC}^*, I_{TC}^*, R^*)$ to control induced initial value problem (5.21) that minimizes the objective functional $J(u)$ of (5.24) over the set of admissible control Γ.*

Proof. The proof of Theorem 5.4.1 is based on the result of (Fleming and Rishel, 2012). The necessary conditions for existence are stated and verified as follows

1. The set of all solutions to the control system (5.21) and its associated initial conditions and the corresponding control functions in Γ is non-empty.

2. The control system is written as a linear function of the control variables with coefficients dependent on time and state variables.

3. The integrand ,

$$\mathscr{L}(t,x,u) = w_1 I_T(t) + w_2 I_C(t) + w_3 L_{TC}(t) + w_4 I_{TC}(t) + \frac{1}{2}\sum_{i=1}^{4} b_i u_i^2$$

   in the objective functional of equation (5.24) is convex in u, where x denotes the state variable and u represents the control variable.

The right hand sides of the control induced system (5.21) are C^1, and bounded. As a result, the solutions to the state equations are bounded. The Picard–Lindelöf theorem (Schroers, 2011) implies that, the system is Lipschitz with respect to the state variables. Thus, condition (1) holds.

The right hand side equation of the control system $F(t,x,u)$ in equation (5.21) is given by:

$$\begin{pmatrix} \Lambda - (\lambda_T + \lambda_C + \mu)S \\ \lambda_T S - (\mu + \alpha + \eta\lambda_C + \omega)L_T \\ f_3 \\ \lambda_C S - (\mu + \varepsilon\lambda_T + \varphi + \pi)E_C \\ f_5 \\ f_6 \\ f_7 \\ f_8 \end{pmatrix} + \begin{pmatrix} \lambda_T S & \lambda_C S & 0 & 0 \\ -\lambda_T S & \eta\lambda_C L_T & 0 & 0 \\ 0 & 0 & -I_T & 0 \\ \varepsilon\lambda_T E_C & -\lambda_C S & 0 & 0 \\ 0 & 0 & 0 & -I_T \\ -\varepsilon\lambda_T E_C & -\eta\lambda_C L_T & 0 & -L_{TC} \\ 0 & 0 & -ITC & -I_{TC} \\ 0 & 0 & I_T + I_{TC} & I_C + L_{TC} + I_{TC} \end{pmatrix} \begin{pmatrix} u_1 \\ u_2 \\ u_3 \\ u_4 \end{pmatrix}$$

where,

$$
\begin{aligned}
f_3 =& \alpha L_T + q\sigma L_{TC} + n\tau I_{TC} - (\mu + \theta + \delta_T + \gamma) I_T, \\
f_5 =& \varphi E_C + p\sigma L_{TC} + m\tau I_{TC} - (\mu + \delta_C + \nu + \psi) I_C, \\
f_6 =& \eta \lambda_C L_T + \varepsilon \lambda_T E_C - (\mu + \delta_C + \rho + \sigma) L_{TC}, \\
f_7 =& \rho L_{TC} + \theta I_T + \nu I_C - (\mu + \delta_{TC} + \tau +) I_{TC}, \text{ and} \\
f_8 =& \omega L_T + \pi E_C + (\gamma) I_T + (\psi) I_C + ((1 - (p+q))\sigma) L_{TC} + ((1 - (m+n))\tau) I_{TC} - \mu R.
\end{aligned}
$$

Clearly, the right hand side expressions are linearly dependent on the controls u_1, u_2, u_3 and u_4. Thus, condition (2) also holds.

To proof the condition (3), we want to prove for any $\theta \in (0,1)$ such that,

$$(1-\theta)\mathscr{L}(t,x,u) + \theta\mathscr{L}(t,x,v) \geq \mathscr{L}(t,x,(1-\theta)u + \theta v).$$

Here,

$$(1-\theta)\mathscr{L}(t,x,u) + \theta\mathscr{L}(t,x,v) = w_1 I_T(t) + w_2 I_C(t) + w_3 L_{TC}(t) + w_4 I_{TC}(t) + \frac{1-\theta}{2}\sum_{i=1}^{4} b_i u_i^2 + \frac{\theta}{2}\sum_{i=1}^{4} b_i v_i^2,$$

and

$$\mathscr{L}(t,x,(1-\theta)u + \theta v) = w_1 I_T(t) + w_2 I_C(t) + w_3 L_{TC}(t) + w_4 I_{TC}(t) + \frac{1}{2}\sum_{i=1}^{4} b_i((1-\theta)u_i + \theta v_i)^2.$$

Further,

$$
\begin{aligned}
&(1-\theta)\mathscr{L}(t,x,u) + \theta\mathscr{L}(t,x,v) - \mathscr{L}(t,x,(1-\theta)u + \theta v) \\
&= \frac{(1-\theta)}{2}\sum_{i=1}^{4} b_i u_i^2 + \frac{\theta}{2}\sum_{i=1}^{4} b_i v_i^2 - \frac{1}{2}\sum_{i=1}^{4} b_i((1-\theta)u_i + \theta v_i)^2 \\
&= \frac{1}{2}\sum_{i=1}^{4} b_i\left[(1-\theta)u_i^2 + \theta v_i^2 - ((1-\theta)u_i + \theta v_i)^2\right] \\
&= \frac{1}{2}\sum_{i=1}^{4} b_i\left(\sqrt{\theta(1-\theta)}u_i - \sqrt{\theta(1-\theta)}v_i\right)^2 \\
&= \frac{1}{2}\theta(1-\theta)\sum_{i=1}^{4} b_i(u_i - v_i)^2 \geq 0.
\end{aligned}
$$

Hence, the integrand is convex with respect to the control u on the admissible set Γ. This complete the proof. □

5.4.2 Characterization of Optimal Control Solutions

In this section, we characterize the optimal controls $u^* = (u_1^*, u_2^*, u_3^*, u_4^*)$ which gives the optimal values for the control measures and the corresponding state variables $(S^*, L_T^*, I_T^*, E_C^*, I_C^*, L_{TC}^*, I_{TC}^*, R^*)$. The necessary conditions for the optimal controls are obtained using the Pontryagin's Minimum Principle (Pontryagin, 2018). This principle converts the model system (5.21) into a problem of minimizing point wise a Hamiltonian function

$$\begin{aligned}\mathscr{H} =& w_1 I_T(t) + w_2 I_C(t) + w_3 L_{TC}(t) + w_4 I_{TC}(t) + \frac{1}{2}\sum_{i=1}^{4} b_i u_i^2 \\ &+\lambda_1\left(\Lambda - ((1-u_1)\lambda_T + (1-u_2)\lambda_C + \mu)S\right) + \lambda_2\left((1-u_1)\lambda_T S - (\mu+\alpha+\eta(1-u_2)\lambda_C + \omega)L_T\right) \\ &+\lambda_3\left(\alpha L_T + q\sigma L_{TC} + n\tau I_{TC} - (\mu+\theta+\delta_T+\gamma+u_3)I_T\right) + \lambda_4\left((1-u_2)\lambda_C S - (\mu+\varepsilon(1-u_1)\lambda_T\right) \\ &+\lambda_4(\varphi+\pi)E_C) + \lambda_5\left(\varphi E_C + p\sigma L_{TC} + m\tau I_{TC} - (\mu+\delta_C+\nu+\psi+u_4)I_C\right) + \lambda_6\eta(1-u_2)\lambda_C L_T \\ &+\lambda_6\left(\varepsilon(1-u_1)\lambda_T E_C - (\mu+\delta_C+\rho+\sigma+u_4)L_{TC}\right) + \lambda_7\left(\rho L_{TC} - (\mu+\delta_{TC}+\tau+u_3+u_4)I_{TC}\right) \\ &+\lambda_7(\theta I_T + \nu I_C) + \lambda_8\left(\omega L_T + \pi E_C + (\gamma+u_3)I_T + (\psi+u_4)I_C + ((1-(p+q))\sigma+u_4)L_{TC}\right) \\ &+\lambda_8\left(((1-(m+n))\tau+u_3+u_4)I_{TC} - \mu R\right).\end{aligned} \tag{5.26}$$

with respect to the control functions u_1, u_2, u_3 and u_4 as detailed below.

Theorem 5.4.2. *Let $x = (S, L_T, I_T, E_C, I_C, L_{TC}, I_{TC}, R)$ and $u = (u_1, u_2, u_3, u_4)$. If $(x^*(t), u^*(t))$ is an optimal control pair, then there exists a continuously differentiable vector $\lambda(t) = (\lambda_1(t), \lambda_2(t), \lambda_3(t), \lambda_4(t), \lambda_5(t), \lambda_6(t), \lambda_7(t), \lambda_8(t))$ satisfying the following:*

$$
\begin{cases}
\lambda_1'(t) = & \Big((\lambda_1-\lambda_2)(1-u_1)\beta_1\frac{(I_T+I_{TC})(N-S)}{N^2}+(\lambda_1-\lambda_4)(1-u_2)\beta_2\frac{(E_C+I_C+L_{TC}+I_{TC})(N-S)}{N^2}\Big)\\
& +\Big((\lambda_6-\lambda_2)\eta(1-u_2)\beta_2 L_T\frac{(E_C+I_C+L_{TC}+I_{TC})}{N^2}+(\lambda_6-\lambda_4)\varepsilon(1-u_1)\beta_1 E_C\frac{(I_T+I_{TC})}{N^2}-\lambda_1\mu\Big),\\
\lambda_2'(t) = & \Big(((\lambda_2-\lambda_1)S+\varepsilon E_C(\lambda_6-\lambda_4))(1-u_1)\beta_1\frac{(I_T+I_{TC})}{N^2}+\lambda_2(\mu+\alpha+\omega)+\lambda_3\alpha+\lambda_8\omega\Big)\\
& +\Big(((\lambda_4-\lambda_1)S+\eta L_T(\lambda_6-\lambda_2))(1-u_2)\beta_2\frac{(E_C+I_C+L_{TC}+I_{TC})}{N^2}+(\lambda_6-\lambda_2)\eta(1-u_2)\lambda_c\Big),\\
\lambda_3'(t) = & \Big(-w_1+[(\lambda_1-\lambda_2)S+\varepsilon E_C(\lambda_4-\lambda_6)](1-u_1)\beta_1\frac{(N-(I_T+I_{TC}))}{N^2}+\lambda_3(\mu+\theta+\delta_T+\gamma+u_3)\Big)\\
& +\Big(((\lambda_4-\lambda_1)S+\eta L_T(\lambda_6-\lambda_2))(1-u_2)\beta_2\frac{(E_C+I_C+L_{TC}+I_{TC})}{N^2}-\lambda_7\theta-\lambda_8(\gamma+u_3)\Big),\\
\lambda_4'(t) = & \Big(((\lambda_2-\lambda_1)S+\varepsilon E_C(\lambda_6-\lambda_4))(1-u_1)\beta_1\frac{(I_T+I_{TC})}{N^2}+\lambda_4(\mu+\varphi+\pi)+(\lambda_4-\lambda_6)\varepsilon(1-u_1)\lambda_T\Big)\\
& +\Big(((\lambda_1-\lambda_4)S+\eta L_T(\lambda_2-\lambda_6))(1-u_2)\beta_2\frac{(S+L_T+I_T+R)}{N^2}-\lambda_5\varphi-\lambda_8\pi\Big),\\
\lambda_5'(t) = & \Big(-w_2+((\lambda_2-\lambda_1)S+\varepsilon E_C(\lambda_6-\lambda_4))(1-u_1)\beta_1\frac{(I_T+I_{TC})}{N^2}+\lambda_5(\mu+\delta_C+\nu+\psi+u_4)\Big)\\
& +\Big(((\lambda_1-\lambda_4)S+\eta L_T(\lambda_2-\lambda_6))(1-u_2)\beta_2\frac{(S+L_T+I_T+R)}{N^2}-\lambda_7\nu-\lambda_8(\psi+u_4)\Big),\\
\lambda_6'(t) = & \Big(-w_3+[(\lambda_2-\lambda_1)S+\varepsilon E_C(\lambda_6-\lambda_4)](1-u_1)\beta_1\frac{(I_T+I_{TC})}{N^2}+\lambda_6(\mu+\delta_C+\rho+\sigma+u_4)\Big)\\
& +\Big((\lambda_1-\lambda_4)S(1-u_2)\beta_2\frac{(S+L_T+I_T+R)}{N^2}+\eta L_T(\lambda_2-\lambda_6)(1-u_2)\beta_2\frac{(E_C+I_C+L_{TC}+I_{TC})}{N^2}\Big)\\
& -[(\lambda_3 q+\lambda_5 p)\sigma+\lambda_7\rho+\lambda_8((1-(p+q))\sigma+u_4)],\\
\lambda_7'(t) = & \Big(-w_4+(\lambda_2-\lambda_1)(1-u_1)\beta_1 S\frac{(I_T+I_{TC})}{N^2}+\lambda_7(\mu+\delta_{TC}+\rho+\tau+u_3+u_4)-(\lambda_3 n+\lambda_5 m)\tau\Big)\\
& +\Big(((\lambda_1-\lambda_4)S+(\lambda_2-\lambda_6)\eta L_T)(1-u_2)\beta_2\frac{(S+L_T+I_T+R)}{N^2}-\lambda_8((1-(m+n))\tau+u_3+u_4)\Big)\\
& +\Big(\varepsilon(\lambda_4-\lambda_6)(1-u_1)\beta_1 E_C\frac{(S+L_T+E_C+I_C+L_{TC}+R)}{N^2}\Big),\\
\lambda_8'(t) = & \Big(((\lambda_2-\lambda_1)S+\varepsilon E_C(\lambda_6-\lambda_4))(1-u_1)\beta_1\frac{(I_T+I_{TC})}{N^2}+\lambda_8\mu\Big)\\
& +\Big(((\lambda_4-\lambda_1)S+\eta L_T(\lambda_6-\lambda_2))(1-u_2)\beta_2\frac{(E_C+I_C+L_{TC}+I_{TC})}{N^2}\Big)
\end{cases}
\tag{5.27}
$$

with transversality conditions

$$
\lambda_i(t_f)=0, \textit{for all } i=1,2,\ldots 8 \tag{5.28}
$$

and optimal controls:

$$
\begin{aligned}
u_1^* &= \min\left\{1,\max\left(0,\frac{(\lambda_2-\lambda_1)\lambda_T S+(\lambda_6-\lambda_4)\varepsilon\lambda_T E_C}{b_1}\right)\right\},\\
u_2^* &= \min\left\{1,\max\left(0,\frac{(\lambda_4-\lambda_1)\lambda_C S+(\lambda_6-\lambda_2)\eta\lambda_C L_T}{b_2}\right)\right\}\\
u_3^* &= \min\left\{1,\max\left(0,\frac{(\lambda_3-\lambda_8)I_T+(\lambda_7-\lambda_8)I_{TC}}{b_3}\right)\right\},\\
u_4^* &= \min\left\{1,\max\left(0,\frac{(\lambda_5-\lambda_8)I_C+(\lambda_6-\lambda_8)L_{TC}+(\lambda_7-\lambda_8)I_{TC}}{b_4}\right)\right\}.
\end{aligned}
\tag{5.29}
$$

Proof. The Hamiltonian function ($\mathscr{H}$) for the optimal control system (5.21) is given in equation (5.26). Now, the proof is a direct consequence of the Pontryagin's Minimum Principle, which asserts that the solution to optimal control problem satisfies the adjoint equations and

transversality conditions such that:

$$\lambda_1'(t) = -\frac{\partial \mathscr{H}}{\partial S}, \quad \lambda_2'(t) = -\frac{\partial \mathscr{H}}{\partial L_T}, \quad \lambda_3'(t) = -\frac{\partial \mathscr{H}}{\partial I_T}, \quad \lambda_4'(t) = -\frac{\partial \mathscr{H}}{\partial E_C}$$
$$\lambda_5'(t) = -\frac{\partial \mathscr{H}}{\partial I_C}, \quad \lambda_6'(t) = -\frac{\partial \mathscr{H}}{\partial L_{TC}}, \quad \lambda_7'(t) = -\frac{\partial \mathscr{H}}{\partial I_{TC}}, \quad \lambda_8'(t) = -\frac{\partial \mathscr{H}}{\partial R}$$

Calculating and simplifying the derivatives, we obtain:

$$\begin{aligned}
\lambda_1'(t) &= -\frac{\partial \mathscr{H}}{\partial S} = -\left((\lambda_2-\lambda_1)(1-u_1)\beta_1\frac{(I_T+I_{TC})(N-S)}{N^2} + (\lambda_4-\lambda_1)(1-u_2)\beta_2\frac{(E_C+I_C+L_{TC}+I_{TC})(N-S)}{N^2}\right) \\
&\quad -\left((\lambda_2-\lambda_6)\eta(1-u_2)\beta_2 L_T\frac{(E_C+I_C+L_{TC}+I_{TC})}{N^2} + (\lambda_4-\lambda_6)\varepsilon(1-u_1)\beta_1 E_C\frac{(I_T+I_{TC})}{N^2} - \lambda_1\mu\right), \\
\lambda_2'(t) &= -\frac{\partial \mathscr{H}}{\partial L_T} = -\left(((\lambda_1-\lambda_2)S+\varepsilon E_C(\lambda_4-\lambda_6))(1-u_1)\beta_1\frac{(I_T+I_{TC})}{N^2} - \lambda_2(\mu+\alpha+\omega)+\lambda_3\alpha+\lambda_8\omega\right) \\
&\quad -\left(((\lambda_1-\lambda_4)S+\eta L_T(\lambda_2-\lambda_6))(1-u_2)\beta_2\frac{(E_C+I_C+L_{TC}+I_{TC})}{N^2} + (\lambda_2-\lambda_6)\eta(1-u_2)\lambda_c\right), \\
\lambda_3'(t) &= -\frac{\partial \mathscr{H}}{\partial I_T} = -\left(w_1+((\lambda_2-\lambda_1)S+\varepsilon E_C(\lambda_6-\lambda_4))(1-u_1)\beta_1\frac{(N-(I_T+I_{TC}))}{N^2} - \lambda_3(\mu+\theta+\delta_T+\gamma+u_3)\right) \\
&\quad -\left(((\lambda_1-\lambda_4)S+\eta L_T(\lambda_2-\lambda_6))(1-u_2)\beta_2\frac{(E_C+I_C+L_{TC}+I_{TC})}{N^2} + \lambda_7\theta+\lambda_8(\gamma+u_3)\right), \\
\lambda_4'(t) &= -\frac{\partial \mathscr{H}}{\partial E_C} = -\left(((\lambda_1-\lambda_2)S+\varepsilon E_C(\lambda_4-\lambda_6))(1-u_1)\beta_1\frac{(I_T+I_{TC})}{N^2} - \lambda_4(\mu+\varphi+\pi)+(\lambda_6-\lambda_4)\varepsilon(1-u_1)\lambda_T\right) \\
&\quad -\left(((\lambda_4-\lambda_1)S+\eta L_T(\lambda_6-\lambda_2))(1-u_2)\beta_2\frac{(S+L_T+I_T+R)}{N^2} + \lambda_5\varphi+\lambda_8\pi\right), \\
\lambda_5'(t) &= -\frac{\partial \mathscr{H}}{\partial I_C} = -\left(w_2+[(\lambda_1-\lambda_2)S+\varepsilon E_C(\lambda_4-\lambda_6)](1-u_1)\beta_1\frac{(I_T+I_{TC})}{N^2} - \lambda_5(\mu+\delta_C+\nu+\psi+u_4)\right) \\
&\quad -\left(((\lambda_4-\lambda_1)S+\eta L_T(\lambda_6-\lambda_2))(1-u_2)\beta_2\frac{(S+L_T+I_T+R)}{N^2} + \lambda_7\nu+\lambda_8(\psi+u_4)\right), \\
\lambda_6'(t) &= -\frac{\partial \mathscr{H}}{\partial L_{TC}} = -\left(w_3+[(\lambda_1-\lambda_2)S+\varepsilon E_C(\lambda_4-\lambda_6)](1-u_1)\beta_1\frac{(I_T+I_{TC})}{N^2} - \lambda_6(\mu+\delta_C+\rho+\sigma+u_4)\right) \\
&\quad -\left((\lambda_4-\lambda_1)S(1-u_2)\beta_2\frac{(S+L_T+I_T+R)}{N^2} + \eta L_T(\lambda_6-\lambda_2)(1-u_2)\beta_2\frac{(E_C+I_C+L_{TC}+I_{TC})}{N^2}\right) \\
&\quad -((\lambda_3 q+\lambda_5 p)\sigma+\lambda_7\rho+\lambda_8((1-(p+q))\sigma+u_4)), \\
\lambda_7'(t) &= -\frac{\partial \mathscr{H}}{\partial I_{TC}} = -\left(w_4+(\lambda_1-\lambda_2)(1-u_1)\beta_1 S\frac{(I_T+I_{TC})}{N^2} - \lambda_7(\mu+\delta_{TC}+\rho+\tau+u_3+u_4)\right) \\
&\quad -\left(((\lambda_4-\lambda_1)S+(\lambda_6-\lambda_2)\eta L_T)(1-u_2)\beta_2\frac{(S+L_T+I_T+R)}{N^2} + (\lambda_3 n+\lambda_5 m)\tau+\lambda_8((1-(m+n))\tau+u_3+u_4)\right) \\
&\quad -\left(\varepsilon(\lambda_6-\lambda_4)(1-u_1)\beta_1 E_C\frac{(S+L_T+E_C+I_C+L_{TC}+R)}{N^2}\right), \\
\lambda_8'(t) &= -\frac{\partial \mathscr{H}}{\partial R} = -\left(((\lambda_1-\lambda_2)S+\varepsilon E_C(\lambda_4-\lambda_6))(1-u_1)\beta_1\frac{(I_T+I_{TC})}{N^2} - \lambda_8\mu\right) \\
&\quad -\left(((\lambda_1-\lambda_4)S+\eta L_T(\lambda_2-\lambda_6))(1-u_2)\beta_2\frac{(E_C+I_C+L_{TC}+I_{TC})}{N^2}\right).
\end{aligned}$$

Since all state variables are free at the final time, the transversality conditions are as given in Equation (5.28). The Hamiltonian is minimized with respect to the controls at the optimal control $u^* = (u_1^*, u_2^*, u_3^*, u_4^*)$. Therefore, $\mathscr{H}$ is differentiated with respect to u_1, u_2, u_3 and u_4

on Γ, to obtain

$$
\begin{aligned}
0 = \frac{\partial \mathscr{H}}{\partial u_1} &= b_1 u_1 + (\lambda_1 - \lambda_2)\lambda_T S + (\lambda_4 - \lambda_6)\varepsilon\lambda_T E_C \\
0 = \frac{\partial \mathscr{H}}{\partial u_2} &= b_2 u_2 + (\lambda_1 - \lambda_4)\lambda_C S + (\lambda_2 - \lambda_6)\eta\lambda_C L_T \\
0 = \frac{\partial \mathscr{H}}{\partial u_3} &= b_3 u_3 + (\lambda_8 - \lambda_3) I_T + (\lambda_8 - \lambda_7) I_{TC} \\
0 = \frac{\partial \mathscr{H}}{\partial u_4} &= b_4 u_4 + (\lambda_8 - \lambda_5) I_C + (\lambda_8 - \lambda_6) L_{TC} + (\lambda_8 - \lambda_7) I_{TC}.
\end{aligned}
$$

Thus, solving for u_1, u_2, u_3 and u_4 on the feasible sets gives

$$
u_1^* = \frac{(\lambda_2 - \lambda_1)\lambda_T S + (\lambda_6 - \lambda_4)\varepsilon\lambda_T E_C}{b_1}, \quad u_2^* = \frac{(\lambda_4 - \lambda_1)\lambda_C S + (\lambda_6 - \lambda_2)\eta\lambda_C L_T}{b_2},
$$

$$
u_3^* = \frac{(\lambda_3 - \lambda_8) I_T + (\lambda_7 - \lambda_8) I_{TC}}{b_3}, \quad u_4^* = \frac{(\lambda_5 - \lambda_8) I_C + (\lambda_6 - \lambda_8) L_{TC} + (\lambda_7 - \lambda_8) I_{TC}}{b_4}.
$$

By standard control arguments involving the bounds on the controls, $0 \leq u_i(t) \leq 1$ for all $i = 1, 2, 3, 4$, we conclude that:

$$
\begin{aligned}
u_1^* &= \min\left\{1, \max\left\{0, \frac{(\lambda_2 - \lambda_1)\lambda_T S + (\lambda_6 - \lambda_4)\varepsilon\lambda_T E_C}{b_1}\right\}\right\}, \\
u_2^* &= \min\left\{1, \max\left\{0, \frac{(\lambda_4 - \lambda_1)\lambda_C S + (\lambda_6 - \lambda_2)\eta\lambda_C L_T}{b_2}\right\}\right\}, \\
u_3^* &= \min\left\{1, \max\left\{0, \frac{(\lambda_3 - \lambda_8) I_T + (\lambda_7 - \lambda_8) I_{TC}}{b_3}\right\}\right\}, \\
u_4^* &= \min\left\{1, \max\left\{0, \frac{(\lambda_5 - \lambda_8) I_C + (\lambda_6 - \lambda_8) L_{TC} + (\lambda_7 - \lambda_8) I_{TC}}{b_4}\right\}\right\}.
\end{aligned}
$$

□

In summary, the optimality system consists of the control system (5.21) and the adjoint system (5.27) with its transversality conditions (5.28), coupled with the control characteri-

zations (5.29). That is the optimality systems are:

$$
\begin{cases}
\frac{dS}{dt} & = \Lambda - ((1-u_1)\lambda_T + (1-u_2)\lambda_C + \mu)\,S, \\
\frac{dL_T}{dt} & = (1-u_1)\lambda_T S - (\mu+\alpha+\eta(1-u_2)\lambda_C+\omega)L_T, \\
\frac{dI_T}{dt} & = \alpha L_T + q\sigma L_{TC} + n\tau I_{TC} - (\mu+\theta+\delta_T+\gamma+u_3)I_T, \\
\frac{dE_C}{dt} & = (1-u_2)\lambda_C S - (\mu+\varepsilon(1-u_1)\lambda_T+\varphi+\pi)E_C, \\
\frac{dI_C}{dt} & = \varphi E_C + p\sigma L_{TC} + m\tau I_{TC} - (\mu+\delta_C+\nu+\psi+u_4)I_C, \\
\frac{dL_{TC}}{dt} & = \eta(1-u_2)\lambda_C L_T + \varepsilon(1-u_1)\lambda_T E_C - (\mu+\delta_C+\rho+\sigma+u_4)L_{TC}, \\
\frac{dI_{TC}}{dt} & = \rho L_{TC} + \theta I_T + \nu I_C - (\mu+\delta_{TC}+\tau+u_3+u_4)I_{TC}, \\
\frac{dR}{dt} & = \omega L_T + \pi E_C + (\gamma+u_3)I_T + (\psi+u_4)I_C + ((1-(p+q))\sigma+u_4)L_{TC} \\
 & \quad +((1-(m+n))\tau+u_3+u_4)I_{TC} - \mu R, \\
\lambda_1'(t) = & \left((\lambda_1-\lambda_2)(1-u_1)\beta_1\frac{(I_T+I_{TC})(N-S)}{N^2} + (\lambda_1-\lambda_4)(1-u_2)\beta_2\frac{(E_C+I_C+L_{TC}+I_{TC})(N-S)}{N^2}\right) \\
 & + \left((\lambda_6-\lambda_2)\eta(1-u_2)\beta_2 L_T\frac{(E_C+I_C+L_{TC}+I_{TC})}{N^2} + (\lambda_6-\lambda_4)\varepsilon(1-u_1)\beta_1 E_C\frac{(I_T+I_{TC})}{N^2} - \lambda_1\mu\right), \\
\lambda_2'(t) = & \left(((\lambda_2-\lambda_1)S+\varepsilon E_C(\lambda_6-\lambda_4))(1-u_1)\beta_1\frac{(I_T+I_{TC})}{N^2} + \lambda_2(\mu+\alpha+\omega) + \lambda_3\alpha + \lambda_8\omega\right) \\
 & + \left(((\lambda_4-\lambda_1)S+\eta L_T(\lambda_6-\lambda_2))(1-u_2)\beta_2\frac{(E_C+I_C+L_{TC}+I_{TC})}{N^2} + (\lambda_6-\lambda_2)\eta(1-u_2)\lambda_c\right), \\
\lambda_3'(t) = & \left(-w_1 + [(\lambda_1-\lambda_2)S+\varepsilon E_C(\lambda_4-\lambda_6)](1-u_1)\beta_1\frac{(N-(I_T+I_{TC}))}{N^2} + \lambda_3(\mu+\theta+\delta_T+\gamma+u_3)\right) \\
 & + \left(((\lambda_4-\lambda_1)S+\eta L_T(\lambda_6-\lambda_2))(1-u_2)\beta_2\frac{(E_C+I_C+L_{TC}+I_{TC})}{N^2} - \lambda_7\theta - \lambda_8(\gamma+u_3)\right), \\
\lambda_4'(t) = & \left(((\lambda_2-\lambda_1)S+\varepsilon E_C(\lambda_6-\lambda_4))(1-u_1)\beta_1\frac{(I_T+I_{TC})}{N^2} + \lambda_4(\mu+\varphi+\pi) + (\lambda_4-\lambda_6)\varepsilon(1-u_1)\lambda_T\right) \\
 & + \left(((\lambda_1-\lambda_4)S+\eta L_T(\lambda_2-\lambda_6))(1-u_2)\beta_2\frac{(S+L_T+I_T+R)}{N^2} - \lambda_5\varphi - \lambda_8\pi\right), \\
\lambda_5'(t) = & \left(-w_2 + ((\lambda_2-\lambda_1)S+\varepsilon E_C(\lambda_6-\lambda_4))(1-u_1)\beta_1\frac{(I_T+I_{TC})}{N^2} + \lambda_5(\mu+\delta_C+\nu+\psi+u_4)\right) \\
 & + \left(((\lambda_1-\lambda_4)S+\eta L_T(\lambda_2-\lambda_6))(1-u_2)\beta_2\frac{(S+L_T+I_T+R)}{N^2} - \lambda_7\nu - \lambda_8(\psi+u_4)\right), \\
\lambda_6'(t) = & \left(-w_3 + [(\lambda_2-\lambda_1)S+\varepsilon E_C(\lambda_6-\lambda_4)](1-u_1)\beta_1\frac{(I_T+I_{TC})}{N^2} + \lambda_6(\mu+\delta_C+\rho+\sigma+u_4)\right) \\
 & + \left((\lambda_1-\lambda_4)S(1-u_2)\beta_2\frac{(S+L_T+I_T+R)}{N^2} + \eta L_T(\lambda_2-\lambda_6)(1-u_2)\beta_2\frac{(E_C+I_C+L_{TC}+I_{TC})}{N^2}\right) \\
 & - [(\lambda_3 q+\lambda_5 p)\sigma + \lambda_7\rho + \lambda_8((1-(p+q))\sigma+u_4)], \\
\lambda_7'(t) = & \left(-w_4 + (\lambda_2-\lambda_1)(1-u_1)\beta_1 S\frac{(I_T+I_{TC})}{N^2} + \lambda_7(\mu+\delta_{TC}+\rho+\tau+u_3+u_4) - (\lambda_3 n+\lambda_5 m)\tau\right) \\
 & + \left(((\lambda_1-\lambda_4)S+(\lambda_2-\lambda_6)\eta L_T)(1-u_2)\beta_2\frac{(S+L_T+I_T+R)}{N^2} - \lambda_8((1-(m+n))\tau+u_3+u_4)\right) \\
 & + \left(\varepsilon(\lambda_4-\lambda_6)(1-u_1)\beta_1 E_C\frac{(S+L_T+E_C+I_C+L_{TC}+R)}{N^2}\right), \\
\lambda_8'(t) = & \left(((\lambda_2-\lambda_1)S+\varepsilon E_C(\lambda_6-\lambda_4))(1-u_1)\beta_1\frac{(I_T+I_{TC})}{N^2} + \lambda_8\mu\right) \\
 & + \left(((\lambda_4-\lambda_1)S+\eta L_T(\lambda_6-\lambda_2))(1-u_2)\beta_2\frac{(E_C+I_C+L_{TC}+I_{TC})}{N^2}\right).
\end{cases}
$$

with transversality and optimality conditions,

$$\lambda_1(t_f)=0, \lambda_2(t_f)=0, \lambda_3(t_f)=0, \lambda_4(t_f)=0, \lambda_5(t_f)=0, \lambda_6(t_f)=0, \lambda_7(t_f)=0, \text{ and } \lambda_8(t_f)=0;$$

$$u_1 = \min\left\{1, \max\left\{0, \frac{(\lambda_2-\lambda_1)\lambda_T S + (\lambda_6-\lambda_4)\varepsilon\lambda_T E_C}{b_1}\right\}\right\},$$
$$u_2 = \min\left\{1, \max\left\{0, \frac{(\lambda_4-\lambda_1)\lambda_C S + (\lambda_6-\lambda_2)\eta\lambda_C L_T}{b_2}\right\}\right\},$$
$$u_3 = \min\left\{1, \max\left\{0, \frac{(\lambda_3-\lambda_8)I_T + (\lambda_7-\lambda_8)I_{TC}}{b_3}\right\}\right\},$$
$$u_4 = \min\left\{1, \max\left\{0, \frac{(\lambda_5-\lambda_8)I_C + (\lambda_6-\lambda_8)L_{TC} + (\lambda_7-\lambda_8)I_{TC}}{b_4}\right\}\right\}.$$

5.4.3 Numerical Simulation of Control-induced Model

In the above sections, we have discussed the qualitative behaviors of the model equation (5.21)–(5.24). In this section, we are going to see the numerical simulations of the model to support our analytical findings. For our numerical simulations, we used the initial values of the model state variables as given in Table 5.2, and the values of model parameters given in Table 5.3 as estimated in Section 5.3. The weight coefficients of the infected individuals are assumed to be $w_1 = 10$, $w_2 = 35$, $w_3 = 15$ and $w_4 = 60$; and the costs implemented for the control extremals are assumed as $b_1 = 100$, $b_2 = 300$, $b_3 = 500$, and $b_4 = 700$ for our numerical simulations of the optimality systems.

The numerical solutions of the control-induced model is computed using the forward-backward sweep method. The method implements as follows. First, we initialize the control parameters and solve for the state variables by forwarding in time using the initial conditions, and then solve for the adjoint equation using backward in time with the transversality conditions according to their differential equations in the optimality system (Lenhart and Workman, 2007). The simulation process continues until the convergence criterion performs.

To examine the impacts of several control strategies to mitigate the spread of the two diseases, we considered the following four scenarios.

- Scenario A (implementation of single control)
  - * Strategy 1: practicing only TB prevention methods ($u_1 \neq 0$, $u_2 = u_3 = u_4 = 0$).
  - – Strategy 2: practicing COVID-19 only prevention methods ($u_1 = 0$, $u_2 \neq 0$, $u_3 = u_4 = 0$).
  - – Strategy 3: practicing medical care for TB infected individuals ($u_1 = 0$, $u_2 = 0$, $u_3 \neq 0$, $u_4 = 0$).
  - – Strategy 4: applying the COVID-19 treatment measures ($u_1 = 0$, $u_2 = 0$, $u_3 = 0$, $u_4 \neq 0$).
- Scenario B (implementation of double controls)
  - – Strategy 5: applying both the COVID-19 and TB prevention methods ($u_1 \neq 0$, $u_2 \neq 0$, $u_3 = 0$, $u_4 = 0$).

- Strategy 6: applying the TB prevention methods and medical care for TB infections ($u_1 \neq 0, u_2 = 0, u_3 \neq 0, u_4 = 0$).
- Strategy 7: applying the TB prevention methods and COVID-19 treatment measures ($u_1 \neq 0, u_2 = 0, u_3 = 0, u_4 \neq 0$).
- Strategy 8: applying COVID-19 prevention methods and medical care for TB infections($u_1 = 0, u_2 \neq 0, u_3 \neq 0, u_4 = 0$).
- Strategy 9: practicing COVID-19 prevention methods and COVID-19 treatment measures ($u_1 = 0, u_2 \neq 0, u_3 = 0, u_4 \neq 0$).
- Strategy 10: implementing medical care for TB infections and applying COVID-19 treatment measures ($u_1 = 0, u_2 = 0, u_3 \neq 0, u_4 \neq 0$).

- Scenario C (implementation of triple controls)
  - Strategy 11: applying both the COVID-19 and TB prevention methods, and implementing medical care for TB infected individuals ($u_1 \neq 0$, $u_2 \neq 0$, $u_3 \neq 0$, $u_4 = 0$).
  - Strategy 12: applying both the COVID-19 and TB prevention methods, and practicing COVID-19 treatment measures ($u_1 \neq 0, u_2 \neq 0, u_3 = 0, u_4 \neq 0$).
  - Strategy 13: applying COVID-19 prevention methods, implementing medical care for TB infected individuals, and practicing COVID-19 treatment measures ($u_1 \neq 0, u_2 = 0, u_3 \neq 0, u_4 \neq 0$).
  - Strategy 14: applying COVID-19 prevention methods, implementing medical care for TB infected individuals, and practicing COVID-19 treatment measures ($u_1 = 0, u_2 \neq 0, u_3 \neq 0, u_4 \neq 0$).

- Scenario D (implementation of all controls)
  - Strategy 15: applying both the COVID-19 and TB prevention methods, implementing medical care for TB infected individuals, and practicing COVID-19 treatment measures ($u_1 \neq 0, u_2 \neq 0, u_3 \neq 0, u_4 \neq 0$).

Scenario A (implementation of single control)

The simulation results of infected and co-infected individuals via implementation of single control interventions are plotted in Figure 5.16. Figure 5.16a illustrates that TB infected individuals decrease notably compared to those without applying time dependent controls measures. We also note in Figure 5.16b that COVID-19 infected individuals in the presence of optimal control measures would lead to a significant decrease over time compared to those without applying the controls.

Prevention mechanisms of COVID-19 and treatments for both diseases are more effective as compared to TB prevention. This is because the treatment for TB and COVID-19 makes

the infected individuals recover from the infection. This effect is shown in Figure 5.16c. However, the combinations of both TB and COVID-19 prevention and treatment control strategies have a remarkable influence on the prevalence of coinfection. Moreover, when only TB preventive control is used the impact seems negligible at the beginning but one gets a significant effect after a while. This is due to prevention influences the spread of the disease after some time stages. In the beginning, the prevalence of coinfection shown in Figure 5.16c with and without TB prevention goes at the same level, but later, one can observe its impact. The corresponding control profiles are depicted in Figure 5.16d. It is clear from this figure that the profile of the control starts at its maximum values $u_i = 1$ and remains maximal for $(0 \leq t \leq 20)$ in each strategy. Then it gradually declined and drops to zero about the final time for strategies 2, 3, and 4. This suggests that to attain the expected outcomes, the control efforts need to be implemented initially at their maximum effort and then relaxed slowly until it comes to zero. The control profile for strategy 1 shows the control term should be kept at 1 for the entire simulation period.

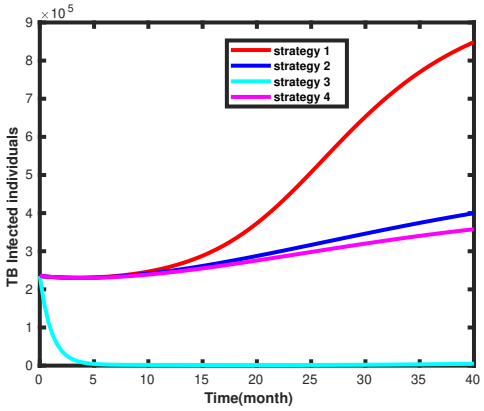

(a) Infected TB

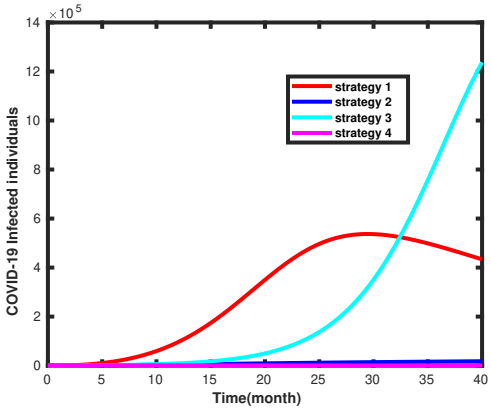

(b) Infected COVID-19

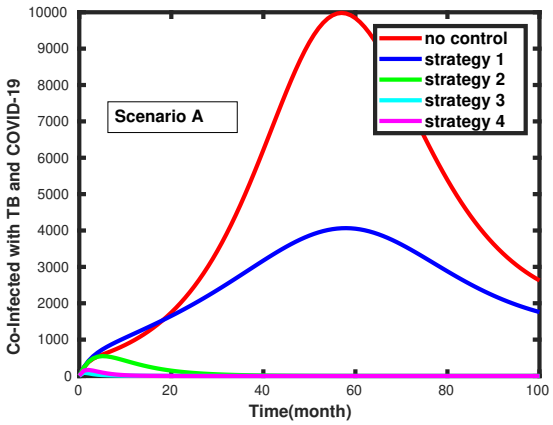

(c) Co-infected (I_{TC})

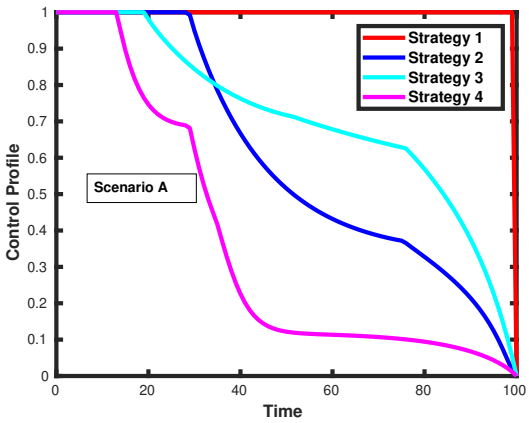

(d) Control profile

Figure 5.16: Solutions infected TB, infected COVID-19, and co-infected with TB and COVID-19 individuals with single control strategies.

Scenario B (implementation of double controls)

In this scenario, we considered combinations of two control functions. The simulation results are displayed in Figures 5.17a-5.17d. It reveals that the number of co-infected individuals significantly reduced as shown in these figures. Figure 5.17a shows that strategy 9 takes more time to reduce the number of TB infected individuals compared to strategy 6. On the contrary, Figure 5.17b presents that strategy 9 has a good gain compared to strategy 6 in declining the number of COVID-19 infected individuals. In Figures 5.17c and 5.17d, strategy 5 takes more time for reducing the number of co-infected individuals compared to strategy 10. We observe that the strategy with the highest number of co-infected individuals with the diseases are strategies 5 and 6 compared to strategies 8 and 10.

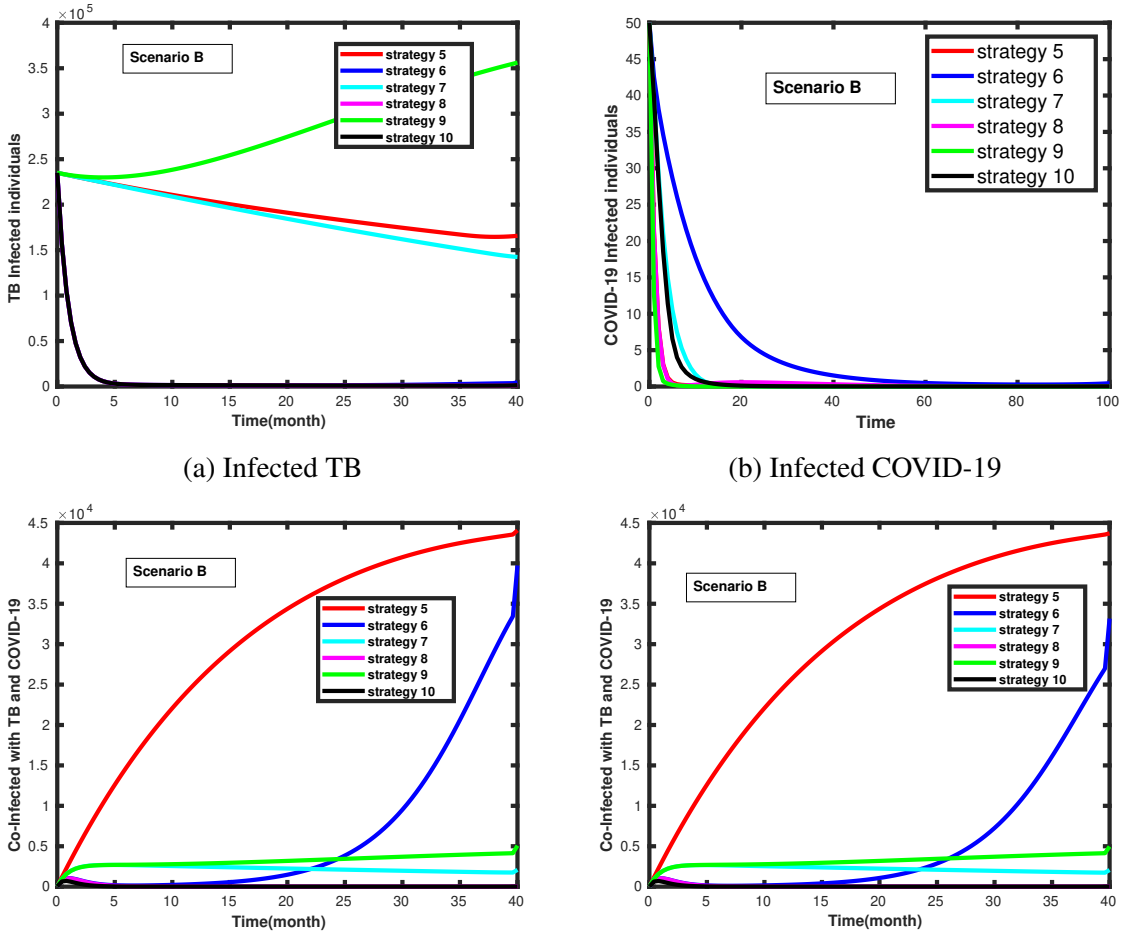

(a) Infected TB

(b) Infected COVID-19

(c) Co-infected ($L_{TC} + I_{TC}$)

(d) Co-infected (I_{TC})

Figure 5.17: The dynamics of infected TB, infected COVID-19, and the coinfection of TB and COVID-19 individuals, with applying two of the control strategies.

Scenario C (implementation of triple controls)

In Figure 5.18, we conducted numerical simulations considering the application of three control functions. In this case, one can observe that there is slight variation among the outcomes of strategies 11, 12 and 13 as shown in Figure 5.18a. Similarly, Figure 5.18b displays the variation with the effectiveness of strategies 12, 13, and 14 in combating the co-dynamics of TB and COVID-19. Hence, the simulation results confirm that the strategies

11 and 13 have relatively a good approach to halting the prevalence of TB and COVID-19 co-infection.

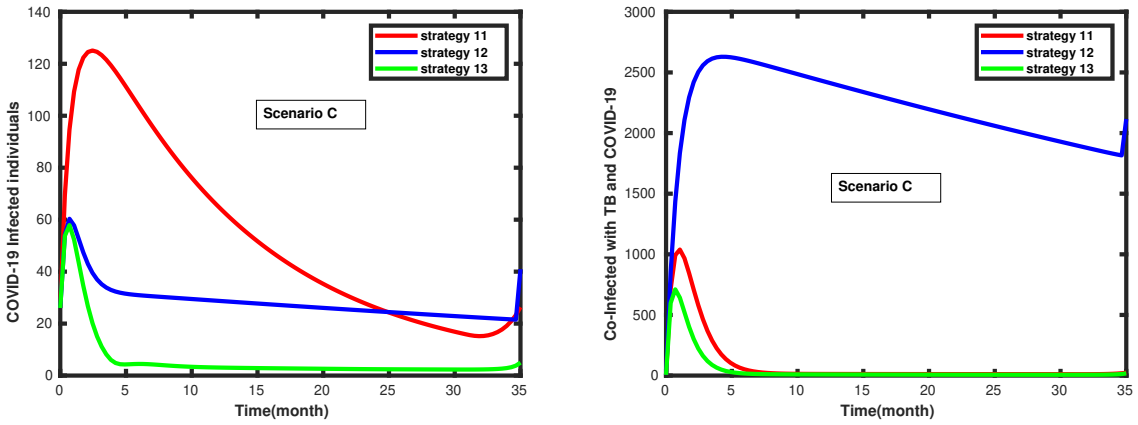

(a) Infected COVID-19

(b) Co-infected TB and COVID-19

Figure 5.18: The dynamics of infected infected COVID-19, and the coinfection of TB and COVID-19 individuals, with applying three control strategies.

Scenario D (implementation of quadruple (all) controls)

In this scenario, we compared the simulations of the target compartments with and without controls. We apply all controls at the same time and study their impact on the diseases. The simulation results revealed that the size of the co-infected population significantly reduced as shown in Figure 5.19. As it can be seen in Figures 5.19a-5.19d, the prevalence of both diseases significantly reduced.

We noticed in Figure 5.19a that the number of TB infected individuals vastly reduces when one applies simultaneously the four controls. Figure 5.19b also shows that the COVID-19 infected individuals can be eliminated within a short time when we simultaneously implement all control measures. In particular, Figure 5.19c shows the impact of strategy 15 on the co-dynamics of TB and COVID-19. Clearly, the number of co-infected individuals are drastically decreased which shows the effectiveness of the proposed strategy.

Figure 5.19d shows that numerous susceptible populations go to the infectious classes in the absence of controls. Besides, the number of recovered individuals is also increasing. However, applying the control measures decreases the susceptible population for being infected with the diseases, and hence the number of recovered populations also less compared to the first case.

The corresponding control profiles for strategy 15 are given in Figure 5.20. Initially, the profiles take the maximum amounts to be implemented, and nearly after 5^{th} time levels, the controls of u_1, and u_2 decrease gradually to the values of 0.2. After this time level, they stabilize and slowly drop to the zeroth level until the final implemented time. We have observed from the figure that the control profile for u_3, and u_4 takes the maximum value and decreases to a value of 0.9 on the 10^{th} time, and then gradually drops to its minimum value

till the final time level.

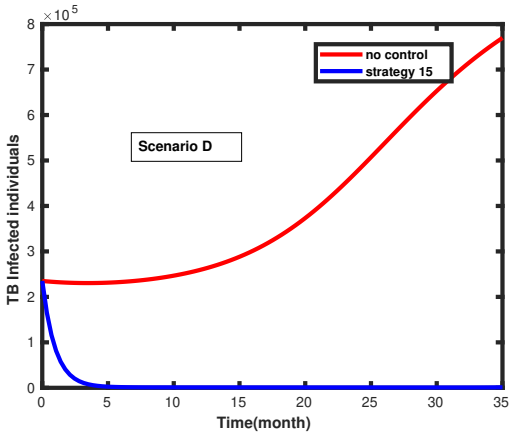

(a) Infected TB

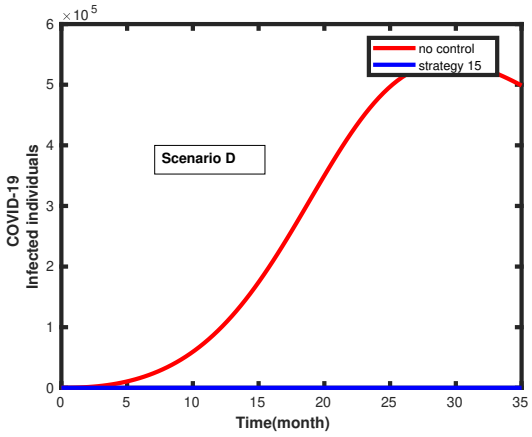

(b) Infected COVID-19

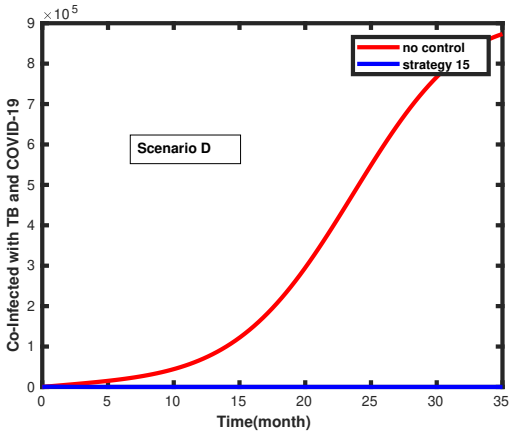

(c) Co-infected TB and COVID-19

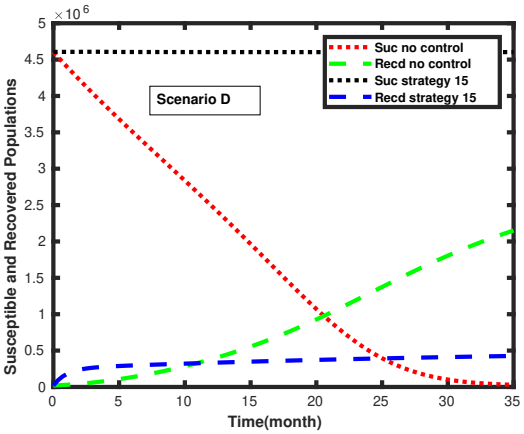

(d) Susceptible and Recovered

Figure 5.19: The dynamics of infected TB, infected COVID-19, and the coinfection of TB and COVID-19 individuals, with out extremal controls and with applying all the control strategies.

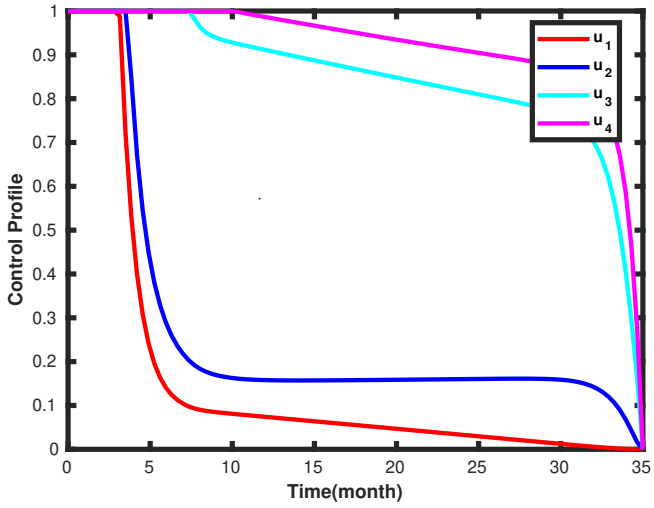

Figure 5.20: Associated controls profile for strategy 15 of the governing system.

CHAPTER 6

SUMMARY, CONCLUSION AND RECOMMENDATIONS

This dissertation provides theoretical support to mitigate the COVID-19 pandemic and reduce the burden of individuals co-infected with TB and COVID-19. We have developed two mathematical models with the help of existing and standard mathematical techniques. The details for the formulation of the models are presented in chapters 4, and 5. In this chapter, summary of our work, conclusions of the findings, and recommendations for further studies are discussed.

6.1 Summary and Conclusion

A deterministic models with non-linear ordinary differential equations for COVID-19, and the coinfection of TB and COVID-19 have been developed. The proposed models were analyzed both qualitatively and numerically. Furthermore, the coinfection model is extended to an optimal control problem. For the optimal control problem, we incorporated four time dependent control parameters into the modeling process.

First, we developed a Susceptible-Educated-Infected-Recovered-Death Mathematical model with the addition of environmental transmission with the virus for the transmission dynamics of COVID-19. The well-posedness of the model is examined by proving the existence, positivity, and boundedness of the solutions. The disease-free equilibrium point is computed. We performed a local and global stability analysis of the disease free equilibrium point, by finding the basic reproduction number of the model. The result show that the disease-free equilibrium point is locally and globally asymptotically stable if $R_0 < 1$ and unstable if $R_0 > 1$. The parameters are estimated using a combination of least square and Bayesian estimation techniques. We developed Matlab codes for the combination of the MH algorithm with the least square. The estimation results of the model parameters vary from country to country as the case of the spread of the virus varies accordingly. The sensitivity analysis of the countries shows that the infection rates β_1 (human to human) and β_2 (from the infected surfaces or environment to human) have high positive impacts on the spread of COVID-19. We determined that the reproduction number depends mostly on the infection rates, the threshold value of the force of infection for a population, the recovery rates, and the virus decay rate in the environment, which hurts the spread of the virus. We have also observed that high numbers of people with knowledge about the virus, who are practicing the prescribed self-protective measures, can slow down the outbreak. It has also been investigated

that increasing human behavioral changes toward self-protective measures are essential to stop the spreading of the virus.

Another mathematical model described by a system of ordinary differential equations have been formulated and analyzed. A study of nonlinear deterministic mathematical modeling for the coinfection of TB and COVID-19 is proposed to examine the possible spread of these diseases. The biological meaningfulness of the model is verified by showing the existence, uniqueness, positivity, and boundedness of solutions in a feasible region. Then, the equilibria are computed for the coinfection model and each sub-model's independently. The stability analysis of these equilibria is also presented with the help of the calculated respective basic reproduction numbers. The disease free equilibrium point of the model was calculated and its stability analysis was performed. The impacts of the two diseases are shown in our analysis, which results that there is a positive impact on the spread of the diseases. The analytical results in both sub-models reveal that the disease-free equilibrium points are stable if the basic reproduction numbers are less than one otherwise unstable. Furthermore, there exists a stable endemic equilibrium point for the basic reproduction numbers greater than one. Besides, the stability analysis of coinfection disease-free equilibrium point is investigated via the corresponding basic reproduction number. Different simulation cases were performed to supplement the analytical results and they are observed to be in good agreement. Furthermore, the simulation results reveal that an increase in the contact rate exacerbated the coinfection of both diseases, whereas a decrease in the effective contact rates and increase in recovery rates would minimize the spread of coinfection diseases.

To reduce the prevalence of the diseases, we extended the model to an optimal control problem with four control strategies in the form of prevention and treatment. Prevention mechanisms for COVID-19, treatment of infected individuals with TB, and medical care for infected individuals with COVID-19 are our control strategies. Prevention controls are applied to the susceptible and exposed classes, while the treatment mechanisms are applied to the infected and co-infected ones. The objective functional is established to minimize the diseased classes by considering fundamental biological goals. We proved the existence and uniqueness of the optimal control efforts and examined the control characterizations using Pontryagin's Minimum Principle. Furthermore, we numerically simulated our mathematical model using estimated and assumed parameter values, and suitable initial conditions. The numerical solution of the optimal control problem was solved with a forward-backward sweep method. Numerical simulations of the optimal control extended model indicate that the prevention and treatment interventions are effective in reducing the transmission for the coinfection of the diseases, so we may get maximum disease control that the control measures are applied. Therefore, it could be concluded that the comprehensive use of all four controls keeps handling a population from getting infections.

6.2 Recommendations

Recently, we have been concerned about the menace of the COVID-19 pandemic, TB, and their coinfection and means to find pathways to control and reduce their consequences. Here, we wish to make some recommendations, which, if taken into consideration, might bring some positive changes to minimize prevalence of the diseases. Individuals must develop their behavioral changes about COVID-19 by applying self-protection measures, and increase virus decay rate from the environment. These mechanisms will decline and stop the spread of the virus from the contaminated environment to uninfected individuals and from infected individuals to the surrounding. It is also essential to create awareness and disseminate information for societies to keep themselves from the virus, which can reduce the pandemic threshold of the infections.

The coinfection model had showed success in attempting to predict the causes of TB and COVID-19 transmission dynamics within a population. From our simulation results, we recommend that increasing simultaneous treatment and medical care, decreasing the effective contact rates, and increasing recovery rates of the two diseases, has a big contribution to minimize the spread of the two diseases in the community. Implementation of medical care for TB infections and applying COVID-19 treatment measures have good gain in declining the number of co-infected individuals with TB and COVID-19. A combined effort of applying COVID-19 prevention methods, implementing medical care for infected individuals with TB, and practicing COVID-19 treatment measures would have superb gain in declining the disease. Moreover, applying both the COVID-19 and TB prevention methods, implementing medical care for infected individuals with TB, and practicing COVID-19 treatment measures have excellent gain in reducing the prevalence of both diseases, and their coinfections within a short time period. We recommend for the health workers and policy makers, a decrease in contact between susceptible and infected individuals, create awareness about the disease and proper treatment will reduce the spread of the diseases from the community.

6.3 Future Work

The deterministic models that were developed in this dissertation can be extended for further study in divers ways. The following are recommended areas for future study.

As a first, it is open to extend the models to a delayed model by introducing time delays in the awareness level of individuals toward self-protection behavior changes, and the delay time in the latent period of the diseases. The incubation period and progression of the disease's symptoms may also require considering different time scales, and taking time-dependent contact frequency, time-dependent death and recovery rates.

To continue, our mathematical models can be extended to a fractional-order model to study the memory effects (which means the future state of the fractional operator of a given

function depends on the current state and the historical behavior of the state) of the biological systems, and some degrees and levels of memory and hereditary properties of through their processes. Cost effectiveness analysis for extended optimal control model will also be another interesting future study.

Furthermore, the consideration of the stochastic differential equations for the developed model is recommended to study the uncertainties and probabilities of the diseases trajectories and to recognize the random nature of the input components. Moreover, use of real coinfection data and estimation of the coinfection parameters for the developed model of the TB and COVID-19 coinfection may be an important part of future research.

REFERENCES

Ahmed, I., Goufo, E. F. D., Yusuf, A., Kumam, P., Chaipanya, P., and Nonlaopon, K. (2021). An epidemic prediction from analysis of a combined HIV-COVID-19 co-infection model via abc-fractional operator. *Alexandria Engineering Journal*, 60(3):2979–2995.

Alzahrani, E. and Khan, M. (2020). The co-dynamics of hepatitis e and HIV. *Filomat*, 34(14):4723–4745.

Asamoah, J. K. K., Okyere, E., Abidemi, A., Moore, S. E., Sun, G.-Q., Jin, Z., Acheampong, E., and Gordon, J. F. (2022). Optimal control and comprehensive cost-effectiveness analysis for COVID-19. *Results in Physics*, 33:105177.

Attiq, U. R., Ram, S., and Praveen, A. (2021). Modeling, analysis and prediction of new variants of COVID-19 and dengue co-infection on complex network. *Chaos, Solitons & Fractals*, page 111008.

Awoke, T. and Kassa, S. (2018). Optimal control strategy for TB-HIV/AIDS co-infection model in the presence of behaviour modification. *Processes*, 6(5):48.

Berge, T., Chapwanya, M., Lubuma, J. M.-S., and Terefe, Y. A. (2018). A mathematical model for ebola epidemic with self-protection measures. *Journal of Biological Systems*, 26(01):107–131.

Berhe, H. W., Makinde, O. D., and Theuri, D. M. (2019). Co-dynamics of measles and dysentery diarrhea diseases with optimal control and cost-effectiveness analysis. *Applied Mathematics and Computation*, 347:903–921.

Beyne, N. W., Sitota, A. L., Tegegn, B., and Bobobsha, K. (2021). The impact of COVID-19 on the tuberculosis control activities in addis ababa. *Pan African Medical Journal*, 38.

Biswas, M. H. A., , Paiva, L. T., and de Pinho, M. (2014). A SEIR model for control of infectious diseases with constraints. *Mathematical Biosciences and Engineering*, 11(4):761–784.

Brauer, F., Castillo-Chavez, C., and Castillo-Chavez, C. (2012). *Mathematical models in population biology and epidemiology*, volume 2. Springer.

Breierova, L. (1996). An introduction to sensitivity analysis. mit system dynamics in education project. *http://sysdyn. clexchange. org/sdep/Roadmaps/RM8/D-4526-2. pdf*.

Cao, J., Jiang, X., Zhao, B., et al. (2020). Mathematical modeling and epidemic prediction of covid-19 and its significance to epidemic prevention and control measures. *Journal of Biomedical Research & Innovation*, 1(1):1–19.

Castillo-Chavez, C., Feng, Z., and Huang, W. (2002). On the computation of R_0 and its role on. *Mathematical approaches for emerging and reemerging infectious diseases: an introduction*, 1:229.

Castillo-Chavez, C. and Song, B. (2004). Dynamical models of tuberculosis and their applications. *Mathematical Biosciences & Engineering*, 1(2):361.

Chen, Y., Wang, Y., Fleming, J., Yu, Y., Gu, Y., Liu, C., Fan, L., Wang, X., Cheng, M., Bi, L., and Liu, Y. (2020). Active or latent tuberculosis increases susceptibility to COVID-19 and disease severity.

Cilloni, L., Fu, H., Vesga, J. F., Dowdy, D., Pretorius, C., Ahmedov, S., Nair, S. A., Mosneaga, A., Masini, E., Sahu, S., and Arinaminpathy, N. (2020). The potential impact of the COVID-19 pandemic on the tuberculosis epidemic a modelling analysis. *EClinicalMedicine*, 28:100603.

Comella-del Barrio, P., De Souza-Galvão, M. L., Prat-Aymerich, C., and Domínguez, J. (2021). Impact of COVID-19 on tuberculosis control. *Archivos de bronconeumologia*, 57:5.

Deressa, C. T. and Duressa, G. F. (2021). Modeling and optimal control analysis of transmission dynamics of COVID-19: the case of ethiopia. *Alexandria Engineering Journal*, 60(1):719–732.

Dicker, R. C., Coronado, F., Koo, D., and Parrish, R. G. (2006). Principles of epidemiology in public health practice; an introduction to applied epidemiology and biostatistics.

Driessche, P. V. D. and Watmough, J. (2002). Reproduction numbers and sub-threshold endemic equilibria for compartmental models of disease transmission. *Mathematical Biosciences*, 180(1-2):29–48.

Ega, T. T., Dawed, M. Y., Gebremeskel, B. K., and Tegegn, T. T. (2020). Mathematical model for estimating unconfirmed cases of COVID-19 in ethiopia, and targeting sensitive parameters. *J. Math. Comput. Sci.*, 10(6):2853–2870.

Egonmwan, A. O. and Okuonghae, D. (2019). Mathematical analysis of a tuberculosis model with imperfect vaccine. *International Journal of Biomathematics*, 12(07):1950073.

Fatima, B. and Zaman, G. (2020). Co-infection of middle eastern respiratory syndrome coronavirus and pulmonary tuberculosis. *Chaos, Solitons & Fractals*, 140:110205.

Feldman, C. and Anderson, R. (2021). The role of co-infections and secondary infections in patients with COVID-19. *Pneumonia*, 13(1).

Fleming, W. H. and Rishel, R. W. (2012). *Deterministic and stochastic optimal control*, volume 1. Springer Science & Business Media.

Fund, T. G. (2021). Global fund results report reveals COVID-19 devastating impact on HIV, TB and malaria programs, results report, 08 September 2021. Technical report, The Global Fund.

Gaff, H. and Schaefer, E. (2009). Optimal control applied to vaccination and treatment strategies for various epidemiological models. *Mathematical Biosciences and Engineering*, 6(3):469–492.

Gao, D.-P. and Huang, N.-J. (2018). Optimal control analysis of a tuberculosis model. *Applied Mathematical Modelling*, 58:47–64.

Giordano, G., Blanchini, F., Bruno, R., Colaneri, P., Filippo, A. D., Matteo, A. D., and Colaneri, M. (2020). Modelling the COVID-19 epidemic and implementation of population-wide interventions in italy. *Nature Medicine*, 26(6):855–860.

Grigorieva, E. V., Khailov, E. N., and Korobeinikov, A. (2021). Optimal quarantine-related strategies for COVID-19 control models. *Studies in Applied Mathematics*.

Hattaf, K., Mohsen, A. A., Harraq, J., and Achtaich, N. (2021). Modeling the dynamics of COVID-19 with carrier effect and environmental contamination. *International Journal of Modeling, Simulation, and Scientific Computing*, 12(03):2150048.

Hattaf, K., Rachik, M., Saadi, S., Tabit, Y., and Yousfi, N. (2009). Optimal control of tuberculosis with exogenous reinfection. *Applied Mathematical Sciences*, 3(5):231–240.

Hezam, I. M., Foul, A., and Alrasheedi, A. (2021). A dynamic optimal control model for COVID-19 and cholera co-infection in yemen. *Advances in Difference Equations*, 2021(1):1–30.

Hirsch, M. W. and Smale, S. (1974). *Differential equations, dynamical systems, and linear algebra*. Academic press.

Holmdahl, I. and Buckee, C. (2020). Wrong but useful — what covid-19 epidemiologic models can and cannot tell us. *New England Journal of Medicine*, 383(4):303–305.

Jewell, N. P., Lewnard, J. A., and Jewell, B. L. (2020). Predictive mathematical models of the COVID-19 pandemic. *JAMA*, 323(19):1893.

J.H.University (2022). Johns Hopkins University coronavirus resource center. coronavirus cases-Ethiopia.

Kassa, S. M., Njagarah, J. B., and Terefe, Y. A. (2020). Analysis of the mitigation strategies for COVID-19: From mathematical modelling perspective. *Chaos, Solitons & Fractals*, 138:109968.

Kassa, S. M. and Ouhinou, A. (2011). Epidemiological models with prevalence dependent endogenous self-protection measure. *Mathematical Biosciences*, 229(1):41–49.

Kermack, W. . O. and McKendrick, A. G. (1927). A contribution to the mathematical theory of epidemics. page A115700–721.

Khurana, A. K. and Aggarwal, D. (2020). The (in)significance of TB and COVID-19 co-infection. *European Respiratory Journal*, 56(2):2002105.

Kifle, Z. S. and Obsu, L. L. (2022). Mathematical modeling for COVID-19 transmission dynamics: A case study in ethiopia. *Results in Physics*, 34:105191.

Last, J. M. (1993). Dictionary of epidemiology. *CMAJ: Canadian Medical Association Journal*, 149(4):400.

Ledzewicz, U. and Schättler, H. (2011). On optimal singular controls for a general sir-model with vaccination and treatment. *Conference Publications*, 2011(Special):981–990.

Lenhart, S. and Workman, J. T. (2007). *Optimal control applied to biological models*. Chapman and Hall/CRC.

Li, H., Liu, S.-M., Yu, X.-H., Tang, S.-L., and Tang, C.-K. (2020). Coronavirus disease 2019 (COVID-19): current status and future perspectives. *International Journal of Antimicrobial Agents*, 55(5):105951.

Liu, J. and Zhang, T. (2011). Global stability for a tuberculosis model. *Mathematical and Computer Modelling*, 54(1-2):836–845.

Liu, S., Li, Y., Bi, Y., and Huang, Q. (2017). Mixed vaccination strategy for the control of tuberculosis: A case study in china. *Mathematical Biosciences and Engineering*, 14(3):695–708.

Macrotrends. Life-expectancy of Ethiopia.

Mamo, D. K. (2020). Model the transmission dynamics of COVID-19 propagation with public health intervention. *Results in Applied Mathematics*, 7:100123.

Marimuthu, Y., Nagappa, B., Sharma, N., Basu, S., and Chopra, K. K. (2020). COVID-19 and tuberculosis: A mathematical model based forecasting in delhi, india. *Indian Journal of Tuberculosis*, 67(2):177–181.

Martcheva, M. (2015). *An introduction to mathematical epidemiology*, volume 61. Springer.

Mcquaid, C. F., Vassall, A., Cohen, T., Fiekert, K., White, R., et al. (2021). The impact of COVID-19 on tb: a review of the data. *The International Journal of Tuberculosis and Lung Disease*, 25(6):436–446.

Melese, Z. T. and Alemneh, H. T. (2021). Enhancing reservoir control in the co-dynamics of HIV-VL: from mathematical modeling perspective. *Advances in Difference Equations*, 2021(1).

Mohammed, H., Oljira, L., Roba, K. T., Yimer, G., Fekadu, A., and Manyazewal, T. (2020). Containment of COVID-19 in ethiopia and implications for tuberculosis care and research. *Infectious Diseases of Poverty*, 9(1):1–8.

Muscat, J. (2008). Ordinary differential equations.

Nana-Kyere, S., Boateng, F. A., Jonathan, P., Donkor, A., Hoggar, G. K., Titus, B. D., Kwarteng, D., and Adu, I. K. (2022a). Global analysis and optimal control model of COVID-19. *Computational and Mathematical Methods in Medicine*, 2022:1–20.

Nana-Kyere, S., Boateng, F. A., Jonathan, P., Donkor, A., Hoggar, G. K., Titus, B. D., Kwarteng, D., and Adu, I. K. (2022b). Global analysis and optimal control model of COVID-19. *Computational and Mathematical Methods in Medicine*, 2022.

Ndii, M. Z., Hadisoemarto, P., Agustian, D., and Supriatna, A. K. (2020). An analysis of COVID-19 transmission in indonesia and saudi arabia. *Commun. Biomath. Sci*, 3(1):19–27.

Obsu, L. L. and Balcha, S. F. (2020). Optimal control strategies for the transmission risk of COVID-19. *Journal of Biological Dynamics*, 14(1):590–607.

Okosun, K., Khan, M., Bonyah, E., and Okosun, O. (2019). Cholera-schistosomiasis coinfection dynamics. *Optimal Control Applications and Methods*, 40(4):703–727.

Okosun, K. and Makinde, O. (2014). A co-infection model of malaria and cholera diseases with optimal control. *Mathematical Biosciences*, 258:19–32.

Omame, A., Abbas, M., and Onyenegecha, C. (2021a). A fractional-order model for COVID-19 and tuberculosis co-infection using atangana–baleanu derivative. *Chaos, Solitons & Fractals*, 153:111486.

Omame, A., Isah, M. E., Abbas, M., Abdel-Aty, A.-H., and Onyenegecha, C. P. (2022a). A fractional order model for dual variants of COVID-19 and HIV co-infection via atangana-baleanu derivative. *Alexandria Engineering Journal*.

Omame, A., Nwajeri, U. K., Abbas, M., and Onyenegecha, C. P. (2022b). A fractional order control model for diabetes and COVID-19 co-dynamics with mittag-leffler function. *Alexandria Engineering Journal*.

Omame, A., Rwezaura, H., Diagne, M., Inyama, S., and Tchuenche, J. (2021b). Covid-19 and dengue co-infection in brazil: optimal control and cost-effectiveness analysis. *The European Physical Journal Plus*, 136(10):1–33.

Organization, W. H. (2020a). Key messages and actions for COVID-19 prevention and control in schools.

Organization, W. H. (2020b). Modes of transmission of virus causing COVID-19: implications for ipc precaution recommendations: scientific brief, 29 march 2020. Technical report, World Health Organization.

Organization, W. H. (2020c). World health organization (WHO) information note tuberculosis and covid-19.

Organization, W. H. (2021). Who information note: COVID-19: considerations for tuberculosis (tb) care, 5 may 2021. Technical report.

Organization, W. H. et al. (2020). Advice on the use of masks in the context of COVID-19: interim guidance, 5 june 2020. Technical report, World Health Organization.

Park, M., Cook, A. R., Lim, J. T., Sun, Y., and Dickens, B. L. (2020). A systematic review of COVID-19 epidemiology based on current evidence. *Journal of Clinical Medicine*, 9(4):967.

Peng, L., Yang, W., Zhang, D., Zhuge, C., and Hong, L. (2020). Epidemic analysis of COVID-19 in china by dynamical modeling.

Piret, J. and Boivin, G. (2021). Pandemics throughout history. *Frontiers in microbiology*, page 3594.

Pontryagin, L. S. (2018). *Mathematical theory of optimal processes*. Routledge.

Prevention, E. C. D. and Control (2021). Implications for the eu/eea on the spread of the sarscov-2 delta (b.1.617.2) variant of concern- 23 june 2021.ecdc: Stockholm.

Saltelli, A., Ratto, M., Andres, T., Campolongo, F., Cariboni, J., Gatelli, D., Saisana, M., and Tarantola, S. (2008). *Global sensitivity analysis: the primer*. John Wiley & Sons.

Sameni, R. (2020). Mathematical modeling of epidemic diseases; a case study of the COVID-19 coronavirus.

Schroers, B. J. (2011). *Ordinary differential equations: a practical guide*. Cambridge University Press.

Sharomi, O. and Malik, T. (2017). Optimal control in epidemiology. *Annals of Operations Research*, 251(1-2):55–71.

Shi, D., Ren, J., and Wang, C. (2020). Analysis of a fractional order mathematical model for tuberculosis with optimal control. *Journal of Nonlinear Functional Analysis*, 2020(1).

Siegenfeld, A. F., Taleb, N. N., and Bar-Yam, Y. (2020). Opinion: What models can and cannot tell us about COVID-19. *Proceedings of the National Academy of Sciences*, 117(28):16092–16095.

Silva, C. J., , and and, D. F. M. T. (2015). A TB-HIV/AIDS coinfection model and optimal control treatment. *Discrete & Continuous Dynamical Systems - A*, 35(9):4639–4663.

Silva, C. J., Cruz, C., Torres, D. F. M., Muñuzuri, A. P., Carballosa, A., Area, I., Nieto, J. J., Fonseca-Pinto, R., Passadouro, R., dos Santos, E. S., Abreu, W., and Mira, J. (2021). Optimal control of the COVID-19 pandemic: controlled sanitary deconfinement in portugal. *Scientific Reports*, 11(1).

Silva, C. J. and Torres, D. F. M. (2014). Modeling TB-HIV syndemic and treatment. *Journal of Applied Mathematics*, 2014:1–14.

Stop-TB-Partnership (2020). Tuberculosis situation in Ethiopia, 2010-2020.

Tadolini, M., García-García, J.-M., Blanc, F.-X., Borisov, S., Goletti, D., Motta, I., Codecasa, L. R., Tiberi, S., Sotgiu, G., and Migliori, G. B. (2020). On tuberculosis and covid-19 co-infection. *European Respiratory Journal*, 56(2):2002328.

Tchoumi, S., Diagne, M., Rwezaura, H., and Tchuenche, J. (2021). Malaria and COVID-19 co-dynamics: A mathematical model and optimal control. *Applied Mathematical Modelling*, 99:294–327.

Thieme, H. R. (2018). *Mathematics in population biology*. Princeton University Press.

Tilahun, G. T. (2019). Modeling co-dynamics of pneumonia and meningitis diseases. *Advances in Difference Equations*, 2019(1).

Tilahun, G. T., Makinde, O. D., and Malonza, D. (2018). Co-dynamics of pneumonia and typhoid fever diseases with cost effective optimal control analysis. *Applied Mathematics and Computation*, 316:438–459.

Trauer, J. M., Denholm, J. T., and McBryde, E. S. (2014). Construction of a mathematical model for tuberculosis transmission in highly endemic regions of the asia-pacific. *Journal of Theoretical Biology*, 358:74–84.

Treesatayapun, C. (2022). Epidemic model dynamics and fuzzy neural-network optimal control with impulsive traveling and migrating: Case study of COVID-19 vaccination. *Biomedical Signal Processing and Control*, 71:103227.

Tsay, C., Lejarza, F., Stadtherr, M. A., and Baldea, M. (2020). Modeling, state estimation, and optimal control for the US COVID-19 outbreak. *Scientific Reports*, 10(1).

Tuite, A. R., Fisman, D. N., and Greer, A. L. (2020). Mathematical modelling of COVID-19 transmission and mitigation strategies in the population of ontario, canada. *Canadian Medical Association Journal*, 192(19):E497–E505.

Ucakan, Y., Gulen, S., and Koklu, K. (2021). Analysing of tuberculosis in turkey through SIR, SEIR and bseir mathematical models. *Mathematical and Computer Modelling of Dynamical Systems*, 27(1):179–202.

Ullah, I., Ahmad, S., Al-Mdallal, Q., Khan, Z. A., Khan, H., and Khan, A. (2020). Stability analysis of a dynamical model of tuberculosis with incomplete treatment. *Advances in Difference Equations*, 2020(1).

Visca, D., Ong, C., Tiberi, S., Centis, R., D'Ambrosio, L., Chen, B., Mueller, J., Mueller, P., Duarte, R., Dalcolmo, M., Sotgiu, G., Migliori, G., and Goletti, D. (2021). Tuberculosis and COVID-19 interaction: A review of biological, clinical and public health effects. *Pulmonology*, 27(2):151–165.

Wang, A., MacNeil, A., and Maloney, S. (2021). Comparison and lessons learned from neglected tropical diseases and tuberculosis. *PLOS Global Public Health*, 1(10):e0000027.

WHO (2019). *Global tuberculosis report 2019*. World Health Organization.

Willis, B. L. (2005). Eigenvalues by row operations. *University of Nebraska at Kearney, Karney*.

Worldometers. https://www.worldometers.info/coronavirus/#countries. Accessed January to July, 2020.

Yang, Y., Tang, S., Ren, X., Zhao, H., and Guo, C. (2016). Global stability and optimal control for a tuberculosis model with vaccination and treatment. *Discrete and Continuous Dynamical Systems - Series B*, 21(3):1009–1022.

Zhao, S., Kuang, Y., Ben-Arieh, D., et al. (2015). Information dissemination and human behaviors in epidemics. In *IIE Annual Conference. Proceedings*, page 1907. Institute of Industrial and Systems Engineers (IISE).

APPENDIX A

PRELIMINARY ON MATHEMATICAL BACKGROUNDS

In this Appendix, we present some essential mathematical tools in the form of definitions, lemmas, propositions and theorems which are adapted from different literature. Since those are available in existing literature, we do not present any proof. We use those in our analysis as helping tools in our developments.

A.1 Basics of Dynamical Systems

A system of ordinary differential equations of the form

$$\frac{dx}{dt} = \dot{x} = f(t,x), \quad x(t_0) = x_0 \tag{A.1}$$

where x takes values in n-dimensional Euclidean space and t is time is said to be *autonomous* or time-invariant if f does not depend explicitly on t. Otherwise they are *non-autonomous*. The equation (A.1) is called an initial value problem.

A.1.1 Well-Posedness.

Definition A.1.1. *An initial-value problem* (A.1) *on* $t \in [\alpha, \beta]$, $x(\alpha) = x_0$, *is said to be well-posed when*

- *a solution exists*
- *the solution is unique*
- *the solution depends continuously on* x_0 .

Definition A.1.2. *(Invariant Regions). A region R is said to be positively invariant for a differential equation* $x' = f(x), x(0) = x_0$ *if whenever* x_0 *is a point in R, then the solution* $x(t,x_0)$ *of the initial value problem exists for all times* $t \geq 0$ *and lies in R,* $x(t,x_0) \in R$ *for all* $t \geq 0$. *Analogously, R is said to be negatively invariant for the initial value problem if whenever* x_0 *is a point in R, then the solution* $x(t,x_0)$ *of the initial value problem exists for all times* $t \leq 0$ *and lies in R,* $x(t,x_0) \in R$ *for all* $t \leq 0$. *A region R is said to be invariant if it is both positively and negatively invariant.*

Theorem A.1.1. *(Picard-Lipschitz) Fundamental Theorem of ODEs (Muscat, 2008)*
Given the initial value problem (A.1). if f is continuous in t and Lipschitz in x in a neighborhood of the initial point $t \in (t_0-h, t_0+h), \quad x \in (x_0-l, x_0+l)$, then the ODE has a unique solution on some (smaller) interval, $t \in (t_0-r, t_0+r)$, that depends continuously on x_0 .

Theorem A.1.2. *(Picard–Lindelöf Theorem (Schroers, 2011))*
Consider the intervals $I_t = [t_0-h, t_0+h]$ and $B_x = [x_0-l, x_0+l]$ for positive, real numbers h, l. Suppose that $f : I_t \times B_x \to R$ is continuous and that its partial derivative $\frac{\partial f}{\partial t} : I \times B \to R$ is also continuous. Then there is a $\delta > 0$ so that the initial value problem (A.1) has a unique solution in the interval $I_\delta = [t_0-\delta, t_0+\delta]$.

Proposition A.1.1. *Positivity of Solutions (Thieme, 2018)*
Consider a system of differential equations in $\mathbb{R}^n$,

$$x' = f(t,x),$$

$x(t) = (x_1(t), x_2(t), \ldots, x_n(t))$, $f(t) = (f_1(t), f_2(t), \ldots, f_n(t))$, where $f(t,x)$ is defined for all $t \geq 0, x \in \mathbb{R}^n$. Assume that f has the property that solutions of the initial value problems $x(t_0) = x^0$ are unique for $x^0 \in [0,\infty)^n, t_0 \geq 0$.
Furthermore assume that, for all $j = 1, 2, \ldots, n, t \geq 0$, we have
$f_j(t,x) \geq 0$ when ever $x \in [0,\infty)^n, x_j = 0, t \geq 0$.
Then $x(t) \in [0,\infty)^n$ for all $t \geq t_0 \geq 0$ for which it is defined, whenever $x(t_0) \in [0,\infty)^n$.

Definition A.1.3. *Lipschitz condition*
A vector-valued function $f(t,x)$ is said to satisfy a Lipschitz condition in a region R in (t,x)-space if, for some constant K (called the Lipschitz constant), we have $||f(t,x) - f(t,y)|| \leq k||x-y||$, whenever $(t,x) \in R$ and $(t,y) \in R$.

A.1.2 Equilibrium Points and Stability

Equilibrium Point

Definition A.1.4. *Let X be an open subset of R^n and $f : X \to R^n$ be continuous, $f(x) = (f_1(x), f_2(x), \ldots, f_n(x))$, $x = (x_1, x_2, \ldots, x_n) \in X$.*
Furthermore, assume that any solution

$$x' = f(x), \quad x(0) = x_0 \tag{A.2}$$

on an interval $(-\varepsilon, \varepsilon)$ is uniquely determined by x_0 .
A point $z \in X$ with $f(z) = 0$ is called a critical point or an equilibrium; and a point $y \in X$ with $f(y) \neq 0$ is called a regular point.

Definition A.1.5. *Consider a system of ordinary differential equations as given in* (A.2) *with* $x(t) \in R^n$ *and* $f : R^n \to R^n$ *is continuously differentiable. Let* x^* *be the equilibrium point of* (A.2).

(a) An equilibrium x^* *of* (A.2) *is called locally stable if and only if the following holds: For each* $\varepsilon > 0$*, there is some* $\delta > 0$ *such that* $||x(t) - x^*|| < \varepsilon$ *for* $t > 0$ *whenever* x *is a solution of* (A.2) *and* $||x(0) - x^*|| < \delta$.

(b) A locally stable equilibrium x^* *is called locally asymptotically stable if and only if there exists some* $\delta > 0$ *such that* $x(t) \to x^*$ *for* $t \to \infty$ *whenever* x *is a solution to* (A.2) *and* $||x(0) - x^*|| < \delta$.

(c) An equilibrium is called unstable if and only if it is not locally stable, i.e., if and only if the following holds.
There exists some $\varepsilon > 0$ *and a sequence* x_n *of solutions to* (A.2) *and a sequence* $t_n > 0$ *such that* $||x_n(0) - x^*|| \to 0$ *as* $n \to \infty$ *but* $||x(t_n) - x^*|| > \varepsilon$ *for all* $n \in N$.

Principle of Linearized Stability

It is important to find criteria which guarantee the stability or instability of equilibria. The most important one is the principle of linearized stability. As a result, we expand solutions to (A.2) around the equilibrium: $x(t) = x^* + y(t)$. Using the fact that f is continuously differentiable we obtain

$$y' = Df(x^*)y + \psi(y)y$$

with $\psi(y)$ being a matrix such that $\psi(y) \to 0$ for $y \to 0$, and Df (next denoted by J) denotes the derivative of f (called the Jacobean matrix). The variational matrix or Jacobian matrix of $f(x_1, x_2, \cdots, x_n)$ denoted by J is defined as follows:

$$J(x) = \begin{pmatrix} \frac{\partial f_1}{\partial x_1} & \frac{\partial f_1}{\partial x_2} & \cdots & \frac{\partial f_1}{\partial x_n} \\ \frac{\partial f_2}{\partial x_1} & \frac{\partial f_2}{\partial x_2} & \cdots & \frac{\partial f_2}{\partial x_n} \\ \vdots & \vdots & \ddots & \vdots \\ \frac{\partial f_n}{\partial x_1} & \frac{\partial f_n}{\partial x_2} & \cdots & \frac{\partial f_n}{\partial x_n} \end{pmatrix}$$

Lemma A.1.1. *(Hirsch and Smale, 1974)*

(a) The equilibrium x^* *is locally asymptotically stable if all eigenvalues of* $J(x^*)$ *have strictly negative real parts.*

(b) x^* *is unstable if at least one eigenvalue of* $J(x^*)$ *has a strictly positive real part.*

Invariance Principle

Definition A.1.6. *: A set M is invariant if and only if for all $x \in M, \phi(x,t) \in M$ for all t. A set is positively (negatively) invariant if for all $x \in M, \phi(x,t) \in M$ for all $t > 0 (t < 0)$.*

Theorem A.1.3. *Let $x_i = F_i(t, x_1, \cdots, x_n)$ for $i \in [1,n]$ be a system of n differential equations with initial conditions $x_i(t_0) = x_i^0$ for $i \in [1,n]$. If each of the functions $F_1, \cdots, F_n$ and the partial derivatives $\frac{\partial F_1}{\partial x_1}, \cdots, \frac{\partial F_1}{\partial x_n}, \cdots, \frac{\partial F_n}{\partial x_1}, , \cdots, \frac{\partial F_n}{\partial x_n}$ are continuous in $\mathbb{R}^{n+1}$ space, then there exists a unique solution $x_1 = \sigma_1(t), \cdots, x_n = \sigma_n(t)$ that satisfies the initial conditions.*

A.1.3 Characteristic Polynomials and Routh-Hurwitz

Definition A.1.7. *A matrix $A \in \mathbb{R}^{n \times n}$ is called Hurwitz or asymptotically stable, if and only if $\Re e(\lambda_i) < 0; \forall i = 1, 2 \cdots, n$. where λ_i's are the eigenvalues of the matrix A.*

If the system is of nth order, the characteristic polynomial can be taken in the general form

$$P(\lambda) = \lambda^n + a_1 \lambda^{n-1} + \cdots + a_{n-1}\lambda + a_n = 0$$

where $a_i, i = 0, 1, \ldots, n$ are all real and $a_n \neq 0$. We require conditions on the $a_i, i = 0, 1, \ldots, n$ such that the zeros of $P(\lambda)$ have negative real parts. The necessary and sufficient conditions for this to hold are the Routh-Hurwitz conditions. There are various equivalent forms of these, one of which is, together with $a_n > 0$,

$$D_1 = a_1 > 0, D_2 = \begin{vmatrix} a_1 & a_3 \\ 1 & a_2 \end{vmatrix} > 0, D_3 = \begin{vmatrix} a_1 & a_3 & a_5 \\ 1 & a_2 & a_4 \\ 0 & a_1 & a_3 \end{vmatrix} > 0,$$

$$D_k = \begin{vmatrix} a_1 & a_3 & \cdot & \cdot & \cdot & \cdot \\ 1 & a_2 & a_4 & \cdot & \cdot & \cdot \\ 0 & a_1 & a_3 & \cdot & \cdot & \cdot \\ 0 & 1 & a_2 & \cdot & \cdot & \cdot \\ \cdot & \cdot & \cdot & \cdot & \cdot & \cdot \\ 0 & 0 & \cdot & \cdot & \cdot & a_k \end{vmatrix} > 0, k = 1, 2, \cdots, n.$$

As an example, for the cubic equation

$$\lambda^3 + a_1\lambda^2 + a_2\lambda + a_3 = 0$$

the conditions for $\Re e\lambda < 0$ are $a_1 > 0$, $a_3 > 0$; $a_1 a_2 - a_3 > 0$. The Routh-Hurwitz Criteria for $n = 2, 3, 4$, and 5 is summarized as follows:

- $n = 2$: $a_1 > 0$ and $a_2 > 0$.

- $n = 3 : a_1 > 0, a_3 > 0$ and $a_1 a_2 > a_3$.
- $n = 4 : a_1 > 0$ and $a_2 > 0, a_4 > 0$ and $a_1 a_2 a_3 > {a_2}^2 + {a_1}^2 a_4$.
- $n = 5 : a_i > 0,\ i = 1, 2, 3, 4, 5,\ a_1 a_2 a_3 > {a_3}^2 + {a_1}^2 a_4$ and $(a_1 a_4 - a_5)(a_1 a_2 a_3 - {a_3}^2 - {a_1}^2 a_4) > a_5 (a_1 a_2 - a_3)^2 + a_1 a_2 a_5$.

A.2 Optimal Control Problems (OCP)

Optimal Control is the process of determining control and state trajectories for a dynamic system over a period of time in order to minimize/maximize a performance index.

A.2.1 Lagrange, Mayer and Bolza Formulations

There are three well known equivalent formulations to describe the OCP, which are Lagrange , Mayer and Bolza forms.

Definition A.2.1. *(Lagrange formulation:) An OCP in Lagrange form is given by*

$$\begin{aligned} \max_u J(x(t),u(t)) &= \int_{t_0}^{t_f} (f(t,x(t),u(t)))dt \\ S.t\ x'(t) &= g(t,x(t),u(t)) \\ x(t_0) &= x_0 \end{aligned} \tag{A.3}$$

Definition A.2.2. *(Bolza formulation): The Bolza formulation of the OCP can be defined as*

$$\begin{aligned} \max_u J(x(t),u(t)) &= \phi(t_0,x_0(t_0,t_f,x(t_f))) + \int_{t_0}^{t_f} (f(t,x(t),u(t)))dt \\ S.t\ x'(t) &= g(t,x(t),u(t)) \\ x(t_0) &= x_0 \end{aligned} \tag{A.4}$$

where ϕ is a continuously differentiable function.

Definition A.2.3. *(Mayer formulation): The Mayer formulation of the OCP can be defined as*

$$\begin{aligned} \max_u J(x(t),u(t)) &= \phi(t_0,x_0(t_0,t_f,x(t_f))) \\ S.t\ x'(t) &= g(t,x(t),u(t)) \\ x(t_0) &= x_0 \end{aligned} \tag{A.5}$$

A.2.2 Existence of an Optimal Control Pair.

We examine sufficient conditions for the existence of a solution to the Lagrangian form of the optimal control problem. Let us first state an existence theorem for optimal control available

at Theorem 4.1 in Chapter III of Fleming and Rishel (Fleming and Rishel, 2012).

Theorem A.2.1. *Consider a control problem with system equations*

$$x' = f(t, x(t), u(t)), t_0 \leq t \leq t_f \tag{A.6}$$

where the vector $x(t) \in \mathbb{R}^n$ denotes the system state and $u(t) \in U$ the control applied at time t. Let $\mathscr{F}'$ denote the class of all (x_0, u) such that u is a Lebesgue-integrable function on an interval $[t_0, t_f]$ with values in U and the solution of (A.6) satisfies the end conditions $e \in S$, where $e = (t_0, t_f, x(t_0), x(t_f))$ and S is a given subset of $\mathbb{R}^{2n+2}$. Suppose f is continuous; moreover, there exist positive constants C_1, C_2 such that

(i) $|f(t,x,u)| \leq C_1(1+|x|+|u|)$,

(ii) $|f(t,x',u) - f(t,x,u)| \leq C_2|x'-x|(1+|u|)$, *for all* $t \in \mathbb{R}^1, x, x' \in \mathbb{R}^n$, *and* $u \in U$.

Suppose that assumptions (i) and (ii) hold, that L (the Lagrangian) is continuous, and moreover that:

(a) $\mathscr{F}'$ *is not empty;*

(b) U *is closed;*

(c) S *is compact and* ϕ *is continuous on* S*; where* $\phi(t_0, t_1, x_0, X_f)$ *be a vector function* $\phi : \mathbb{R}^1 \times \mathbb{R}^1 \times \mathbb{R}^n \times \mathbb{R}^n \to \mathbb{R}^k$ *which is of class* C^1.

(d) $F(t,x)$ *is convex for each* $(t,x) \in \mathbb{R}^{n+1}$;

(e) $L(t,x,u) \geq g(u)$ *where* g *is continuous and* $|u|^{-1}g(u) \to +\infty$ *as* $|u| \to \infty$, $u \in U$.

Then there exist (x_0^*, u^*) *minimizing* $J(x_0, u)$ *on* $\mathscr{F}'$.

In the book it is proved that, the assumptions (i) and (ii) of Theorem A.2.1 are satisfied, if f is $\mathbb{C}^1$, implied by suitable bounds on partial derivatives of f and on $f(t,0,0)$. If u is compact, then the assumption (e) of Theorem A.2.1 holds vacuously.

Definition A.2.4. *Let $\mathscr{V}$ be a vector space. A set $\mathscr{K} \subset \mathscr{V}$ is convex if $u_1, u_2 \in \mathscr{K}$ and $0 \leq \theta \leq 1$ imply $(1-\theta)u_1 + \theta u_2 \in \mathscr{K}$.*

Definition A.2.5. *Let $\mathscr{K}$ be a convex set in a vector space and let $f : \mathscr{V} \to \mathbb{R}$ be a function. Then*

- *f is called convex if:*
  $\forall x_1, x_2 \in \mathscr{K}, \forall \theta \in [0,1]: \quad f(\theta x_1 + (1-\theta)x_2) \leq \theta f(x_1) + (1-\theta) f(x_2)$
  A differentiable function of one variable is convex on an interval if and only if its graph lies above all of its tangents.

- *f is called strictly convex if:*
  $\forall x_1 \neq x_2 \in \mathscr{K}, \forall \theta \in (0,1): \quad f(\theta x_1 + (1-\theta)x_2) < \theta f(x_1) + (1-\theta) f(x_2),$
- *A function f is said to be (strictly) concave if $-f$ is (strictly) convex.*

Theorem A.2.2. *Filippov–Cesari Existence Theorem. For all $(t,x) \in \mathbb{R}^{n+1}$, define the set*

$$N(t,x) = \{(g(x,u) + \xi, f(x,u)) : \xi \leq 0, u \in A\}$$

Suppose that

1. *$N(t,x)$ is convex for every (t,x).*
2. *A is compact.*
3. *There exists a constant $K > 0$ such that $||x(t)|| \leq K$ for all $t \in (0,T)$ and all admissible pairs (x,u).*

Then there exists an optimal pair$(x^*(t), u^*(t))$,where $u^*(t) \in A$.

A.2.3 Pontryagin's Maximum Principle (PMP)

The necessary first order optimality conditions were developed by Lev Pontryagin and his coworkers. Pontryagin introduced the idea of adjoint functions to append the differential equation to the objective functional. Adjoint functions have a similar purpose as Lagrange multipliers in multivariate calculus, which append constraints to the function of several variables to be maximized or minimized.
With out lose of generality we consider the OC problem in Lagrange form (A.3).

Definition A.2.6. *(Hamiltonian). The function*

$$H(t,x(t),u(t),\lambda(t)) = f(t,x(t),u(t)) + \lambda(t) g(t,x(t),u(t)) \tag{A.7}$$

is called the Hamiltonian function, and λ is the adjoint variable. Now we are formulate the PMP for problem for the Lagrange formulation (A.3).

Theorem A.2.3 (PMP)**.** *If u^* and x^* are optimal for problem (A.3), then there exists a piece wise differentiable ad-joint variable $\lambda(t)$ such that*

$$H(t,x^*(t),u(t),\lambda(t)) \leq H(t,x^*(t),u^*(t),\lambda(t))$$

for all controls u at each time t, where the Hamiltonian H is defined by

$$H = f(t,x,u) + \lambda g(t,x,u)$$

and

$$\begin{aligned} \lambda'(t) &= -\frac{\partial}{\partial x} H(t, x^*, u^*, \lambda) \\ \lambda(t_f) &= 0 \end{aligned} \tag{A.8}$$

The last condition of Theorem A.2.3, $\lambda(t_f) = 0$, is called the transversality condition, and is only used when the OC problem does not have the terminal value in the state variable, i.e., $x(t_f)$ is free. Theorem A.2.3 converts the problem of finding a control which maximizes the objective functional subject to the state ODE and initial condition, into the problem of optimizing the Hamiltonian point-wise. As a consequence, we have

$$\frac{\partial H}{\partial u} = 0, \tag{A.9}$$

where u is an open set, at u^* for each t, that is, the Hamiltonian has a critical point at u^*. Usually this is called the optimality condition.

Remark A.2.1. *If the Hamiltonian is linear in the control variable u, it can be difficult to calculate u^* from the optimality equation, since $\frac{\partial H}{\partial u}$ would not contain u.*

In addition, the following conditions hold:

- If $\frac{\partial^2 H}{\partial u^2} < 0$ at u^*, for each $t \in [0, t_f]$, then the OC problem is of the maximization type.
- If $\frac{\partial^2 H}{\partial u^2} > 0$, for each $t \in [0, t_f]$, then the OC problem is of the minimization type.

Theorem A.2.4. *Let the set of controls for problem (A.3) be Lebesgue integrable functions on $t_0 \le t \le t_f$ in $\mathbb{R}$. Suppose that $f(t,x,u)$ is concave in u, and there exist constants $C_1, C_2, C_3 > 0, C_4$, and $\beta > 1$ such that*

$$\begin{aligned} &g(t,x(t),u(t)) = \alpha(t,x(t)) + \beta(t,x(t))u(t), \\ &\|g(t,x(t),u(t))\| \le C_1(1 + |x(t)| + |u(t)|), \\ &|g(t,\hat{x}(t),u(t)) - g(t,x(t),u(t))| \le C_2|\hat{x}(t) - x(t)|(1 + |u(t)|), \\ &f(t,x(t),u(t)) \le C_3|u|^\beta - C_4 \end{aligned}$$

for all t with $t_0 \le t \le t_f$ in $\mathbb{R}$. Then there exists an optimal pair (x^*, u^*) maximizing J , with $J(x^*, u^*)$ finite.

Optimal Control with Bounded Controls

Definition A.2.7. *(OCPs with bounded controls). An OCP with bounded control, in Lagrange form, is:*

$$\begin{aligned} \max_u J(x(\cdot),u(\cdot)) &= \int_0^{t_f} (f(t,x(\cdot),u(\cdot)))dt, \\ S.t x'(t) &= g(t,x(t),u(t)), \\ x(t_0) &= x_0, \\ a \leq u(t) &\leq b \end{aligned} \tag{A.10}$$

where a and b are fixed real constants with $a < b$.

Proposition A.2.1. *(Necessary conditions). If $u^*(t)$ and $x^*(t)$ are optimal for problem (A.10), then there exists a piece wise differentiable adjoint variable $\lambda(t)$ such that*

$$H(t,x^*(t),u(t),\lambda(t)) \leq H(t,x^*(t),u^*(t),\lambda(t))$$

for all admissible controls u at each time t, where H is the Hamiltonian (A.7), and

$$\begin{aligned} \lambda'(t) &= -\frac{\partial H(t,x^*(t),u^*(t),\lambda(t)}{\partial x}, \quad \textit{(adjoint function)} \\ \lambda(t_f) &= 0 \quad \textit{(transversality condition)} \end{aligned} \tag{A.11}$$

We assume that H is a nonlinear differentiable function of u. We should adjust the optimal control as follows:

$$\begin{aligned} &f_u + \lambda g_u \leq 0 \quad \textit{at} \quad u^*(t), \textit{ which gives } u^*(t) = a \\ &f_u + \lambda g_u = 0 \ \textit{ at } \ u^*(t), \textit{ implies } a \leq u^*(t) \leq b \\ &f_u + \lambda g_u \geq 0 \ \textit{ at } \ u^*(t), \textit{ which gives } u^*(t) = b \end{aligned} \tag{A.12}$$

The other necessary conditions for the optimal control are:

$$\begin{aligned} &-\frac{\partial H}{\partial x} = \lambda' \quad \textit{i.e.,} \quad \lambda'(t) = -(f_x + g_x) \quad \textit{adjoint equation} \\ &\frac{\partial H}{\partial \lambda} = x' \quad \textit{i.e.,} \quad x'(t) = g \quad \textit{state equation.} \end{aligned} \tag{A.13}$$

By an adaptation of the PMP, the OCP must satisfy the optimality condition:

$$u^*(t) = \begin{cases} a & \textit{if } \frac{\partial H}{\partial u} < 0 \\ a < \bar{u} < b & \textit{if } \frac{\partial H}{\partial u} = 0 \\ b & \textit{if} \frac{\partial H}{\partial u} > 0 \end{cases} \tag{A.14}$$

i.e., the maximization is over all admissible controls, and u^* is obtained by the expression $\frac{\partial H}{\partial u} = 0$. In particular, the optimal control u^* maximizes H point wise with respect to $a \leq u \leq$

b.

Remark A.2.2. *If we have a minimization problem instead of maximization, then u^* is instead chosen to minimize H point-wise. This has the effect of reversing $<$ and $>$ in the first and third lines of the optimality condition* (A.14).

Remark A.2.3.

$$u^*(t) = \min\left(a, \max\left(b, \frac{\partial H}{\partial u}\right)\right)$$

Optimal Control of Several Variables

Definition A.2.8. *(OC with several variables and several controls). An OC with n state variables, m control variables can be written in the form*

$$\begin{aligned} &\int_{t_0}^{t_f} f(t, x_1(t), \cdots, x_n(t), u_1(t), \cdots, u_m(t))dt \to \max_{u, \cdots, u_m} \\ &S.t x_i'(t) = g_i(t, x_1(t), \cdots, x_n(t), u_1(t), \cdots, u_m(t)) \\ &x_i(t_0) = x_{i0},\ i = 1, 2, \cdots, n \end{aligned} \tag{A.15}$$

where the functions f, g_i are continuously differentiable in all variables.

To simplify the notation, we denote

$$X(t) = [x_1(t), \cdots, x_n(t)],\ U(t) = [u_1(t), \cdots, u_m(t)],\ X_0 = [x_{10}, \cdots, x_{n0}]$$

So, the problem (A.15) can be rewritten in a compact way as

$$\begin{aligned} &\max_U \int_{t_0}^{t_f} f(t, X(t), U(t)) \\ &S.t X'(t) = g_i(t, X(t), U(t)) \\ &X(t_0) = X_0, i = 1, 2, \cdots, n \end{aligned} \tag{A.16}$$

Using the same approach of the control with one variable, it is possible to derive generalized necessary conditions.

Proposition A.2.2. *(Necessary conditions). Let U^* be an optimal control functions and X^* be the vector of corresponding optimal state variables. With n states, we will need n adjoints, one for each state. There is a piece-wise differentiable vector-valued function $\lambda(t) = \lambda_1(t), \cdots, \lambda_n(t)$, where each λ_i is the adjoint variable corresponding to x_i, and the Hamiltonian is*

$$H(t, X, U) = f(t, X, U) + \sum_{i=1}^{n} \lambda_i(t) g_i(t, X, U).$$

It is possible to find the variables satisfying optimality, adjoint and transversality conditions in each vector component. Namely, X^* maximizes $H(t, X, U, \lambda)$ with respect to U at each t,

and U^*, X^* and λ satisfy

$$\lambda_j'(t) = -\frac{\partial H}{\partial x_j} \quad for \quad j = 1,2\cdots,n \quad (adjoint\ conditions)$$
$$\lambda_j(t_f) = 0 \quad for \quad j = 1,\cdots,n \quad (transversality\ conditions)$$
$$\frac{\partial H}{\partial u_k} = 0 \quad at \quad u_k^* \quad for \quad k = 1,\cdots,n \quad (optimality \quad condition)$$

Remark A.2.4. *Similarly to the previous section, if bounds are placed on a control variable, $a_k \le u_k \le b_k$ (for $k = 1,\cdots,m$), then the optimality condition is changed from $\frac{\partial H}{\partial u_k} = 0$ to*

$$u_k^*(t) = \begin{cases} a_k & \text{if } \frac{\partial H}{\partial u_k} < 0 \\ a_k < \frac{\partial H}{\partial u_k} < b_k & \text{if } \frac{\partial H}{\partial u_k} = 0 \\ b_k & \text{if} \frac{\partial H}{\partial u_k} > 0 \end{cases}$$

The following is an outline of steps in formulating optimal system of an optimal control problem.
(1) Formulate the Hamiltonian for the problem

$$H(t,x,u,\lambda) = f(t,x,u) + \lambda g(t,x,u)$$

(2) Write the adjoint differential equation, transversality condition and optimality condition. Now there are three unknowns, $u^*, x^*$and λ.

$$\lambda' = -\frac{\partial H}{\partial x} \Rightarrow \lambda' = -(f_x + \lambda g_x) \quad \text{(adjoint condition)}$$
$$\lambda(t_f) = 0 \text{(transversality condition)}$$
$$\frac{\partial H}{\partial u} = 0 \quad \text{at} \quad u = u^* \Rightarrow f_u(t,x,u) + \lambda g_u(t,x,u) = 0 \quad \text{(optimality condtion)}$$

(3) Solve for u^* in terms of x^* and λ.
(4) After finding the optimal states and adjoint, solve for the optimal control.

Theorem A.2.5 (Sufficient condition (the Mangasarian sufficiency theorem) for (global) optimality)**.** *For the basic optimal control problem*

$$\begin{aligned} \max_u J(x(\cdot),u(\cdot)) &= \int_0^{t_f} f(t,x,u)dt, \\ S.t\, x'(t) &= g(t,x,u), \\ x(t_0) &= x_0, \end{aligned} \tag{A.17}$$

where $f(t,x,u)$ and $g(t,x,u)$ are both continuously differentiable functions in their three arguments. If $f(t,x,u)$ and $g(t,x,u)$ are concave both with x and u, and $(\hat{x},\hat{u},\lambda)$ is a Pontryagin

extremal with $\lambda(t) \geq 0$*, then* $J(\hat{x},\hat{u} \geq J(x,u)$ *for any admissible pair* (x,u).

Remark A.2.5. *The sufficient condition Theorem for the maximization type OCP still holds true if we change the assumption of concavity of g into convexity and the hypothesis* $\lambda(t) \geq 0$ *into* $\lambda(t) \leq 0$.

A.3 Numerical Methods.

The numerical solutions of the deterministic model equations together with the initial conditions of the state system with out control is solved numerically by forward in time using the MATLAB built-in ODE45 routine. ODE45 solves same as a 4th order Runge-Kutta routine. The routine is as follows. Given a step size h and an ODE $x'(t) = f(t,x(t))$, the approximation of $x(t+h)$ given $x(t)$ is:

$$x(t+h) \approx x(t) + \frac{h}{6}(k_1 + 2k_2 + 2k_3 + k_4)$$

where,

$$\begin{aligned} k_1 &= f(t,x(t)), \\ k_2 &= f(t+\frac{h}{2}, x(t)+\frac{h}{2}k_1), \\ k_3 &= f(t+\frac{h}{2}, x(t)+\frac{h}{2}k_2), \\ k_4 &= f(t+h, x(t)+hk_3). \end{aligned}$$

The optimal control system is solved numerically using the forward-backward sweep numerical method (Lenhart and Workman, 2007). The method requires an initial value on the optimal controls u_i. The initial condition for the state variables is used to solve the state system forward in time using the Rung-kutta method of order four routine. Next, the adjoint system is solved using the transversality condition (A.8) and the approximated solution of the state system; by backward in time using the Rung-kutta method of order four routine. Then, the value of control variables are computed using the control characterization in (A.9), and the controls u_i are updated via a convex combination of previous and current values of the control characterization. The process continues until the state variables, adjoint and control values converge.

A rough outline of the algorithm is given below. Here, $\vec{x} = (x_1,...,x_N)$ and $\vec{\lambda} = (\lambda_1,...,\lambda_N)$ are the vector approximations for the state and adjoint. For the initial guess, $\vec{u} \equiv 0$ is almost always sufficient. In certain problems, where division by u occurs for example, a different initial guess must be used.

It is sufficient to require $\| \vec{u} - o\vec{l}du \| = \sum_{i=1}^{N} |u_i - oldu_i|$ to be small, where $\vec{u}$ is the vector is the of estimated values of the control during the current iteration, and $o\vec{l}du$ is vector of

Algorithm 2 Forward-Backward Sweep Method

Step 1. Make an initial guess for the control $\vec{u}$ over the interval.

Step 2. Using the initial condition $x_0 = x(t_0)$ and the values for $\vec{u}$, solve $\vec{x}$ forward in time according to its differential equation in the optimality system.

Step 3. Using the transversality condition $\lambda_N = \lambda(t_f) = 0$ and the values for $\vec{u}$ and $\vec{x}$, solve $\vec{\lambda}$ backward in time according to its differential equation in the optimality system.

Step 4. Update $\vec{u}$ by entering the new $\vec{x}$ and $\vec{\lambda}$ values into the characterization of the optimal control.

Step 5. Check convergence. If values of the variables in this iteration and the last iteration are negligibly close, output the current values as solutions. If values are not close, return to Step 2.

estimated values from the previous iteration. Here, $\| \, . \, \|$ refers to the $\mathscr{L}^1$ norm for vectors, i.e., the sum of the absolute value of the terms. Here, we use a slightly stricter convergence test. Namely, we will require the relative error to be negligibly small, i.e.,

$$\frac{\| \vec{u} - o\vec{l}du \|}{\| \vec{u} \|} \leq tol$$

where tol is the accepted tolerance.

APPENDIX B

OPERATIONAL DEFINITIONS

There are a number of concepts in epidemiology which are been related to infectious diseases that plays an important role in the construction of mathematical models. In this dissertation, some of the widely used epidemiological terms with their meanings are listed below.

- **Susceptible Individuals:** The classes of individuals who are healthy but can have contract with the disease at some future time. It is a member of a population who is at risk of becoming infected by a disease.

- **Exposed Individuals:** When a healthy individual who is vulnerable to contracting a disease makes a potentially disease-transmitting contact, that individual becomes exposed. Exposed individuals may or may not develop the disease. These individuals are typically not infectious for some disease (like tuberculosis) and infectious for some other disease (like HIV, COVID-19‘). In mathematical models, we often assume that all exposed individuals eventually develop the disease. The time from infection to when the host is able to transmit the infectious agent to another individual is defined as the latent period (Martcheva, 2015).

- **Infected and Infectious Individuals:** If the pathogen establishes itself in an exposed individual, then that individual becomes infected. Infected individuals who can transmit the disease are called infectious. Infected individuals may not be infectious during the entire time of being infected (Martcheva, 2015).

- **Recovered Individuals:** denotes the number of individuals who have been infected and then removed from the possibility of being infected again or of spreading infection. Removal is carried out through isolation from the rest of the population, through immunization against infection, through recovery from the disease with full immunity against reinfection, or through death caused by the disease. These characterizations of removed members are different from an epidemiological perspective but are often equivalent from a modeling point of view that takes into account only the state of an individual with respect to the disease (Brauer et al., 2012).

- **Incubation Period:** The incubation period is the period between exposure to an infectious agent and the onset of symptoms of the disease. In infectious diseases, the incubation period is the time required for the infectious agent to multiply to a threshold necessary to produce symptoms or laboratory evidence of infection. The incubation

period does not necessarily coincide with the latent period. For instance, in influenza, individuals become infectious approximately one day before they exhibit visible flu symptoms (Martcheva, 2015). Incubation time is the time interval between initial contact with an infectious agent and appearance of the first sign or symptom of disease in question. Latent Period is the period between exposure and the onset of the period of communicability, which may be shorter or longer than incubation period.

- **Incidence and Prevalence:** Incidence is the number of individuals who become infected during a specified interval of time. The prevalence of a disease is the number of people who have the disease at a specific time (Martcheva, 2015). Prevalence is the number of disease cases present in a particular population at a given time, whereas incidence is the number of new cases that develop during a specified time period.

- **Force of infection:** is the rate at which susceptible individuals acquire an infectious disease.

- **Coinfection:** Co-infection is the simultaneous infection of a host by multiple pathogen species. In virology, co-infection includes simultaneous infection of a single cell by two or more virus particles. An example is the co-infection of liver cells with hepatitis B virus and hepatitis D virus, which can arise incrementally by initial infection followed by super-infection.

- **Immunity:** The condition of being immune, protected against an infectious disease conferred either by an immune response generated by immunization or previous infection (Last, 1993).

- **Communicability:** Period of communicability (infectious period) is the time during which an infectious agent may be transferred directly or indirectly from an infected person to another person, from an infected animal to humans, or from an infected person to animals (Last, 1993).

- **Epidemic:** refers to a sudden increase in the number of cases of a disease above what is normally expected in that population in a specified area (Dicker et al., 2006).

- **Outbreak:** carries the same definition of epidemic, but is often used for a more limited geographic area.

- **Pandemic:** refers to an epidemic that has spread over several countries or continents, usually affecting a large number of people.

- **Endemic:** refers to the constant presence and usual prevalence of a disease in a population within a geographic area (Dicker et al., 2006).

APPENDIX C

MATLAB CODES

%This function solves the COVID-19 mathematical mode
%By: Kassahun G. and Tatek G.
%A first paper on Mathematical modeling of COVID-19 with self protection behavior changes considering indirect transmission
%Adama Science and Technology University, Department of Applied Mathematics
% 2021/22 A.Y

```
function dx=covid19modf(t,x)
global a m et d g xi p b1 b2 l0 k L;
n=2;
l=b1*x(3)/(x(1)+x(2)+x(3)+x(4)+x(5))+b2*x(6)/(k+x(6));
e=l.^n/(l0^n+l.^n);
dx=zeros(6,1);
dx(1)=L-(l+a*e+m)*x(1);
dx(2)=a*e*x(1)-(m+(1-et)*l)*x(2);
dx(3)=l*x(1)+(1-et)*l*x(2)-(m+d+g)*x(3);
dx(4)=g*x(3)-m*x(4);
dx(5)=d*x(3)-m*x(5);
dx(6)=xi*x(3)-p*x(6);
end
```

%This function estimates the COVID-19 mathematical mode parameters using
%A modified least square and Bayesian estimation techniques with Ethiopian COVID-19 data
%By: Kassahun G. and Tatek G.

```
function [theta,ssr]=modtatkaspareth(nn);
global a m et d g xi p b1 b2 l0 k L;
%%%Data for the simulation purpose
ED = xlsread('Ethiopian-dailylydata-2020.xlsx');
totalcases=ED(:,1)';totaldeath=ED(:,3)';recover=ED(:,4)';
%%%
xx1=totalcases-totaldeath-recover;%%%active case
xx2=totaldeath;
```

```
xx3=recover;
t=1:length(xx1);
length(xx1);
%figure(1)
%plot(t,xx1,t,xx2,t,xx3)
n=nn;
theta=zeros(12,n);
ssr=zeros(12,n);
theta0=[0.682 0.0481 0.07 0.0023  0.065 0.0064...
 0.978 0.146 0.0032 0.459 590 19595];
theta(:,1)=theta0;
x0=[1000000 5 1 0 0 0];
%L=theta(1,1);
a=theta(1,1); m=theta(2,1); et=theta(3,1);
d=theta(4,1); g=theta(5,1); xi=theta(6,1); p=theta(7,1);
b1=theta(8,1); b2=theta(9,1); l0=theta(10,1);k=theta(11,1);
L=theta(12,1);
%   opt = odeset ("AbsTol",[1*10^(-7) 1*10^(-7) 1*10^(-7) 1*10^(-7) 1*10^(-7)...
%       1*10^(-7)], "RelTol", 1e-6);
[t,x]=ode45('covid19modfc4',t,x0);
%hold on
%plot(t,x(:,1),t,x(:,2))
ssr(:,1)=sum((xx1-x(:,3)').^2)+sum((xx2-x(:,5)').^2)+sum((xx3-x(:,4)').^2);
for i=2:n
for j=1:12
thep=theta(:,i-1);
if(j==11||j==12)
thep(j)=theta(j,i-1)-5+2*(5)*rand(1);
if(thep(j)<0)
while(thep(j)<0)
thep(j)=theta(j,i-1)-5+2*(5)*rand(1);
end
end
else
thep(j)=theta(j,i-1)-0.01+2*(0.01)*rand(1);
if(thep(j)<0)
while(thep(j)<0)
thep(j)=theta(j,i-1)-0.01+2*(0.01)*rand(1);
end
```

```
end
end
if(j~=11&&j~=12&&thep(j)>1)
%   while(thep(j)>1)
%   thep(j)=theta(j,i-1)-0.1+2*(0.1)*rand(1);
thep(j)=0.01+2*(0.01)*rand(1);
% endwhile
end
%global L a m et d g ep xi p b1 b2 k l0;
a=thep(1);m=thep(2); et=thep(3); d=thep(4);
g=thep(5); xi=thep(6); p=thep(7);b1=thep(8);
b2=thep(9);l0=thep(10);k=thep(11); L=thep(12);
% L=m*(x0(1)+x0(2)+x0(3)+x0(4)+x0(5));
[t,x]=ode45('covid19modfc4',t,x0);
% hold on
% plot(t,x(:,1),t,x(:,2))
ssri=sum((xx1-x(:,3)').^2)+sum((xx2-x(:,5)').^2)+sum((xx3-x(:,4)').^2);
%AIC=nn*(log(ssri./nn))+2*(15+1);%Akaike information criterion
if(ssri<ssr(j,i-1))
theta(j,i)=thep(j);
ssr(j,i)=ssri;
else
theta(j,i)=theta(j,i-1);
ssr(j,i)=ssr(j,i-1);
end
end
if(rem(i,200)==0)
disp(i)
theta(:,i)
figure(i+1)
plot(t,xx1,t,x(:,3),'linewidth',1.6)
title ("Infected");
legend('real','estimated')
xlabel('time in days')
ylabel('Population size')
figure(i+2)
plot(t,xx3,t,x(:,4),'linewidth',1.6)
title ("Recovered")
legend('real','estimated')
```

```
xlabel('time in days')
ylabel('Population size')
figure(i+3)
plot(t,xx2,t,x(:,5),'linewidth',1.6)
title ("Death");
legend('real','estimated')
xlabel('time in days')
ylabel('Population size')
end
end
figure(1)
plot(t,x(:,1),t,x(:,2),t,x(:,3),t,x(:,4),t,x(:,5),'linewidth',1.6)%t,x(:,1),
legend('Susceptible','Educated','Infected','Recovered','Death')
xlabel('time in days')
ylabel('Population size')
title ("All Population");
figure(2)
plot(t,x(:,2),'linewidth',3)
title ("Exposed");
figure(3)
plot(t,xx1,t,x(:,3),'linewidth',3)
title ("Infected");
legend('real','estimated')
xlabel('time in days')
ylabel('Population size')
set(gca,'linewidth',3)
figure(4)
plot(t,xx3,t,x(:,4),'linewidth',3)
title ("Recovered")
legend('real','estimated')
xlabel('time in days')
ylabel('Population size')
set(gca,'linewidth',3)
figure(5)
plot(t,xx2,t,x(:,5),'linewidth',3)
title ("Death");
legend('real','estimated')
xlabel('time in days')
ylabel('Population size')
```

```
set(gca,'linewidth',3)
figure(6)
plot(t,x(:,6),'linewidth',1.6)
title ("Contaminated Material");
end
```

%This function solves the coinfection of COVID-19 and TB mathematical model
%By: Kassahun G.
%A second paper on Mathematical modeling of TB and COVID-19 coinfection
%Adama Science and Technology University, Department of Applied Mathematics
% 2021/22 A.Y

```
function dx=mod_tb_cov(t,x)
global L b1 b2 m vp dc dt th g ps a et s e n tu dtc p w r;
pp=0.4;q=0.3;mm=0.5;nn=0.3;
N=x(1)+x(2)+x(3)+x(4)+x(5)+x(6)+x(7)+x(8);
lt=b1*(x(3)+x(7))/N;
lc=b2*(x(4)+x(5)+x(6)+x(7))/N;
dx=zeros(8,1);
dx(1)=L-(lt+lc+m)*x(1);
dx(2)=lt*x(1)-(m+a+et*lc+w)*x(2);
dx(3)=a*x(2)+q*s*x(6)+nn*tu*x(7)-(m+dt+th+g)*x(3);
dx(4)=lc*x(1)-(m+e*lt+vp+p)*x(4);
dx(5)=vp*x(4)+pp*s*x(6)+mm*tu*x(7)-(m+dc+n+ps)*x(5);
dx(6)=et*lc*x(2)+e*lt*x(4)-(m+dc+r+s)*x(6);
dx(7)=r*x(6)+th*x(3)+n*x(5)-(m+dtc+tu)*x(7);
dx(8)=w*x(2)+g*x(3)+p*x(4)+ps*x(5)+(1-(pp+q))*s*x(6)+(1-(mm+nn))*tu*x(7)-m*x(8);
end
```

%This Matlab script simulates the TB and COVID-19 coinfection model using %A runge kutta method of order 4 (ode45) Matlab routine with estimated Ethiopian data %By: Kassahun G.

```
function HKHG=mod_tb_cov_odew45
global L b1 b2 m vp dc dt th g ps a et s e n tu dtc p w r;
m=0.0012;L=6193;th=0.01229;s=1.3523;n=0.0199;tu=0.0422;r=1.1148;
et=1.01;e=1.06;dtc=0.001;
%%%%%Fitted parameters
b1=11.5/12;w=0.01/12;dt=0.001/12;a=0.0973/12;g=0.01/12;
b2=0.33238;vp=1.57141;dc=0.009;ps=0.05;p=0.1;
x0=[4605410 300000 235000 96 26 25 6 20000];
```

```
tsp=[0,40];
[t,x]=ode45('mod_tb_cov',tsp,x0);
plot(t,x(:,1),'g',t,x(:,2),'b',t,x(:,3),'r',t,x(:,4),'m',t,x(:,5),'c'...
,t,x(:,6),'k',t,x(:,7),'y',t,x(:,8),'linewidth',3)
legend('Susciptible','Latent-TB','Infected-TB','Exposed-C19','Infected-C19'...
,'Latent-TBC19','Infected-TBC19','Recoverd')
title ("All Populations")
xlabel('Time (month)')
ylabel('Population size')
set(gca,'linewidth',3)
%semilogy(t,x(:,2))
end
```